Dissecting Complex Mechanisms of Calcium Influx

in a Simple Wound System

By

Erica Kristine Shannon

Dissertation

Submitted to the Faculty of the

Graduate School of Vanderbilt University

in partial fulfillment of the requirements

for the degree of

DOCTOR OF PHILOSOPHY

in

Cell and Developmental Biology

September 30, 2017

Nashville, Tennessee

Approved:

Andrea Page-McCaw, Ph.D.

Irina Kaverina, Ph.D.

Jeffrey Davidson, Ph.D.

M. Shane Hutson, Ph.D.

Ian Macara, Ph.D.

ACKNOWLEDGEMENTS

TABLE OF CONTENTS

LIST OF FIGURES

INTRODUCTION AND OVERVIEW

Epithelial tissue makes up the largest organ in the human body, our skin. Indeed, it lines all of our surfaces which come into contact with the environment. Epithelia is a sheet-like structure composed of interconnected cells. These apical-basal polarized cells sit atop a basement membrane (BM) and can form stratified layers or remain as a single sheet. This tissue has many important functions. For example, epithelial tissues regulate and exchange nutrients and chemicals with underlying tissues, secrete hormones into the vascular system, and secrete mucus and sweat[1,2]. A particularly important function of epithelial tissue is to serve as a physical barrier between the organism and the environment[2,3]. Cell-cell adhesions and other structural components pull cells together to create an impermeable wall. The wall is sealed by tight junctions which form close adhesions between adjacent cells and serve as highly selective gates between the extracellular environment and underlying tissue[4]. Despite how it sounds, this is not a passive job and epithelia are not inert tissues. Penetrating pathogens, sharp objects, burns, radiation, desiccation, and harsh chemicals are just a few external threats can that compromise the epithelial barrier and reduce the fitness of an organism[5]. To mitigate further damage and prevent microorganism entry, a normally quiescent epithelia must quickly and dynamically respond to these threats.

The fastest response to an epithelial wound is the calcium wave[6]. A calcium wave forms when cells in an epithelia increase cytosolic levels of calcium in a sequential, wave-like fashion[7]. Around wounds, calcium increases in the cells within seconds of wounding[8-10]. Calcium ions are potent signaling molecules, and their concentration in cells is heavily regulated[11]. In the cytosol, calcium concentrations are very low ($\sim 10^{-7}$ M). In contrast, calcium concentrations can be high in the extracellular space ($\sim 10^{-3}$ M) and organelles, including the endoplasmic reticulum (ER), mitochondria, and Golgi[1,11]. Calcium can enter the cytosol through gap junctions, ion channels in the plasma or ER membrane, and directly through membrane tears.

Once inside the cell, the calcium wave is a master regulator of wound healing. At wounds, calcium drives the production and release of paracrine signals including ROS[12] and eicosanoids[13,14] to upregulate the immune response. Seconds to minutes after wounding, calcium dynamics are spatially and temporally correlated with cytoskeletal dynamics and drive rapid actomyosin remodeling by activating actin-filament severing

enzymes and actin nucleators[8,15]. Calcium activates RhoA and Cdc42 at wound sites which are necessary for actomyosin purse-string based wound closure[10,16-20]. Furthermore, calcium influx has been observed to activate downstream transcriptional responses[21,22]. Blocking the calcium wave at wounds results in excessive apoptosis[23], reduces rates of re-epithelization[22,24-27], inhibits wound healing[28,29], and can result in death of the organism[20].

So, what regulates a master regulator? What are the upstream factors driving and mediating calcium dynamics around wounds? There is not a consensus within the wound healing field regarding calcium wave initiation and propagation. In fact, there is extensive variability and some findings even seem to be mutually exclusive. Unfortunately, these contradictions and the lack of clarity may undermine the field's efforts to understand the calcium wave. Some studies report the calcium wave is initiated by ER stores of calcium[20,30-32], other studies report initiation requires extracellular calcium[9,21,23,24,33], and still others report that *both* extracellular and intracellular calcium play a role in wave initiation[12,34,35]. Calcium wave propagation can occur intracellularly, by which calcium or IP3 diffuses through gap junctions[12,21,31,34,36,37], or extracellularly, by which a diffusible ligand activates receptors on the cell surface as it spreads[25,30,32,34,37,38]. There is variability in the literature about whether the calcium wave oscillates[9,12,31,36] or not[23,24,34,35]. Some studies also suggest a role for tissue mechanics in wave initiation and propagation[8,10,20,31,38-42]. All of these studies are informative and add to our understanding of wound-induced calcium dynamics. Despite this, only one complete mechanism for calcium influx and propagation has surfaced; in cell culture models ATP is released from damaged cells and activates receptors on the cell surface as it diffuses away from the wound[30,32,38,42]. Interestingly, this has still not brought a consensus to the field as it is not fully validated by other cell culture experiments[34,35] and is not consistent with data from *in vivo* models[8,12,20,21,43]. If not ATP, what initiates and propagates the calcium wave *in vivo*?

We decided to approach this question by analyzing calcium wave initiation and propagation kinetics at wounds in the *Drosophila* notum. We chose the *Drosophila* notum as an *in vivo* wounding model for three important reasons. First, the genetic tractability of the organism is well established and allowed us to perform complex manipulations of the tissue. Second, the epithelial architecture in the notum is simple, yet conserved. The diploid, cuboidal cell monolayer sits atop a basement membrane and exhibits apical-basal polarity[44]. Finally, and perhaps most importantly, this tissue is easily accessible and can

be live imaged over long periods of time because the animal remains still during pupariation. A collaboration with the Hutson Lab (Department of Physics, Vanderbilt University) allowed us to administer wounds using laser ablation techniques. True laser ablation occurs over a nanosecond time scale. A custom light path added to a scanning confocal microscope allowed us to wound without interrupting our imaging scans. This was a significant advantage to our studies because we could begin analyzing calcium expansion kinetics milliseconds after wounding.

With this tool kit, we made novel observations. We found that calcium increases in cells within the first 2 milliseconds of wounding. Our studies reveal this immediate calcium influx is a result of single cell damage, or micro-tears, on the plasma membrane. This micro-tear induced calcium influx expands to neighboring cells via gap junctions. Approximately 45 seconds after wounding, a second, wound-induced calcium expansion event occurs. This expansion event is distinct from the micro-tear induced expansion as it correlates with damage on a tissue-wide level and does not require gap junctions. By applying computational methods to the second expansion in collaboration with the Hutson lab, we found that an unknown signal induces calcium influx as it diffuses away from the wound with a diffusion constant between 7 and 30 μm^2/s. Our results indicate this unknown signal is a ligand that drives IP3 mediated calcium influx through a Gαq-bound GPCR. The parameters we have identified here allow us to significantly narrow down the potential mechanisms for calcium wave initiation and propagation.

Ultimately, our results can be used to make sense of the variability found in the literature and show these various findings are not mutually exclusive. We demonstrate that multiple types of damage occur at the same epithelial wound. Pulsed laser ablation is a common wounding method, but many biologists are not aware that an associated cavitation bubble can create a more complex damage profile than simple ablation. We report that the distinct types of damage associated with this complex wound profile result in multiple mechanisms of calcium influx and propagation. Micro-tears drive direct calcium entry from outside of the cell and direct calcium diffusion through gap junctions. At the same wound, we propose that a ligand found in cell lysate diffuses extracellularly and activates receptors on neighboring cell surfaces. This results in a gap-junction-independent wave propagation and release from either ER stores (if the ligand binds a GPCR) or extracellular space (if the ligand binds an ion channel). In light of our observations, the variability of mechanisms driving calcium dynamics in previous literature

seems to stem from the fact wound healing models are well suited to study one type of damage and therefore only one aspect of the calcium wave. When the models do not recapitulate the same type of damage, they observe different mechanisms of calcium entry and report contradictory results.   For example, cell culture scratch assays generate cell lysate but, beyond the row of cells touching the scratch, do not generate micro-tears[34,35]. *In vivo* models which study calcium wave upon the addition of cell lysate do not generate any micro-tears either. These models are ideal for investigating a lysate-driven, wound-induced wave but will not provide information on calcium dynamics as a result of single cell damage. *In vivo* models typically use laser ablation to study calcium dynamics around wounds and laser ablation results in extensive microtearing. If investigators do not create large enough ablation wounds, they may not generate a wound-induced wave and will only report on micro-tear induced calcium expansions.

      We have developed a comprehensive wounding system in an accessible model organism. Importantly, our wounding system creates a complex damage profile that allows us to study multiple mechanisms of calcium influx at the same wound. Our observations unite and make sense of previous findings from other models. Moreover, because this model more fully captures the extent of calcium dynamics at wounds, it can be used to study how cells regulate, integrate, and interpret this potent wound response.

      The first chapter of this dissertation will discuss the state of the wound healing field in more detail. It will explore other early wound signals aside from calcium and potential mechanisms driving calcium dynamics at wounds. The second chapter maps out the mechanism for micro-tear induced influx at wounds and presents a computational analysis of both of the calcium expansion events we describe. The mechanism behind the second, wound-induced expansion of calcium is explored in the third chapter. Our findings add value to the wound healing field and inspire new questions, all of which will be discussed in the Summary and Implications and the Future Directions. Finally, the end of the document contains appendices with data and information supplemental to the dissertation.

CHAPTER 1

A REVIEW OF EARLY DAMAGE SIGNALS AND WOUND RESPONSES WITH
AN EMPHASIS ON CALCIUM DYNAMICS AT WOUNDS

General wound healing

If a breach occurs, cells within the epithelium are rallied to migrate and proliferate in order to rapidly repair the barrier. In mammals, a cut on differentiated skin initiates a complex wound healing cascade. When blood vessels are broken, fibrin and extracellular matrix (ECM) proteins form a clot which plugs the breach. This clot occludes extracellular microorganisms and provides an essential framework for migrating inflammatory cells[45-48]. The inflammatory cells – neutrophils, monocytes, lymphocytes – defend against contamination and phagocytose debris at the wound site. Neutrophils detect EGF, PDGF, TGF-β, and other molecules released by the clot and arrive within minutes of damage[49-52]. In addition to combating bacterial infection they transcriptionally upregulate the release of pro-inflammatory cytokines such as IL-α, IL-β, and TNF-α which recruit more inflammatory cells and activate local fibroblasts and keratinocytes[53]. Hours after wounding, epithelial cells receive a plethora of environmental cues which transform their transcriptional profile from a quiescent state to a highly dynamic, mobile state. For example, JNK signaling in keratinocytes on the leading edge of the wound leads to transcriptional upregulation of Matrix Metalloproteases (MMPs), which remodel the BM and enable cell migration into the wound bed[54,55]. Cell proliferation also begins hours after wounding and is an important feature of the wound response[56-59]. Surviving hair follicles contribute to the proliferating pool of cells that support re-epithelialization[59-62]. After the breach is covered, fibroblasts secrete BM components and the tissue undergoes a period of remodeling for days after wounding[54,63,64].

In differentiated tissue, a clot provides a temporary barrier during the hours between wounding and the onset of re-epithelization. Interestingly, there is no lag time in embryonic tissue; re-epithelization begins right away[48,65-68]. Instead of invading the wound via slow lamellipodial crawling, re-epithelialization in embryos occurs much faster as it is driven by cell shape changes, intercalation, and the formation of an actomyosin purse-string[65,68-70]. An exception to this is the mouse cornea, which has also been observed to form an actin purse-string[71]. This is not the only key fundamental difference between

embryonic and adult wound healing. Researchers have also found that there are significantly fewer inflammatory cues present in embryonic wounds, and as a result, there is little to no scar formation[48,68,72,73]. Understanding the finer mechanisms of wound healing has already led to important clinical advancements[74]. Wound healing research encompasses the fields of migration, differentiation, development, and cell-signaling. It is not surprising that information learned in wound healing studies can also contribute to cancer science and our general understanding of cell biology[75-82].

Early damage signals and wound responses

Changes in cell behavior driven by gene expression do not occur immediately after wounding, some changes may take hours or days[54,63,83]. So while cells are redirecting their transcriptional profile they must also be adapting to their immediate environment. Studies showing epithelial wound responses within minutes of damage have been important in identifying early, non-transcriptional damage signals and wound responses.

DAMPs and ATP

Cells within a tissue can respond to lysis of their neighbors by using a myriad of cell surface receptors to detect Damage Associated Molecular Patterns, known as DAMPs[13,84,85]. DAMPs can be metabolites, RNA's and DNA's, peptides, and even whole proteins and can come from invading pathogens or be endogenous in nature[84,86-88]. They can result from revealed cryptic sites or can be intercellular molecules released into the extracellular space[89-93]. Both High-mobility group box protein-1 (HMGB1), a chromatin binding protein, and Heat Shock Proteins are well characterized DAMPs.   HMGB1 is passively released from dying cells and actively secreted from immune cells[94,95]. In addition to activating the immune system[89,90,96], HMGB1 can induce cytoskeletal re-arrangements and chemotaxis[94]. Heat Shock Proteins (HSPs) activate NF-κB transcription factors in macrophages[84,97] and induce migration in cell culture models[98].

ATP is a well-studied DAMP that plays an important role in some wound healing models. The release of ATP from cells around a wound can be visualized with a biochemical, luciferase-based assay[38]. It can be actively released[99-102], or passively released during necrosis[85,89,100]. Once outside the cell, ATP binds and activates purinergic (P2) receptors: P2X (ionotropic, ligand-gated channels) and P2Y (metabotropic, G-Protein Coupled Receptors)[101,103,104]. Calcium release is a downstream result of P2 receptor activation, and will be discussed in following sections. ATP signaling through P2X7

channels has been shown to induce an immune response in macrophage cell culture by stimulating the direct release of the IL-6 cytokine[105]. Potentiated ATP release at wound sites in zebrafish led to potentiated epithelial cell migration[106]. *In vitro* studies have made great progress in mapping out the mechanism of ATP induced cell motility. In cornea cell culture, activation of the P2Y2 receptor is important for wound closure[32,107]. P2Y receptor activation results leads to proteolytic shedding of HB-EGF and EGFR activation[108]. This process is mediated via DUOX, a NADPH Oxidase homologue that produces H_2O_2, which oxidizes extracellular proteases in an ATP-dependent manner[109-111]. In parallel, ATP activates EGFR through phospholipase D2[112].

Hydrogen Peroxide (H_2O_2)

Waves of H_2O_2 have been observed within seconds of wounding in zebrafish tail fin wounding assays[113]. As a small molecule, H_2O_2 can readily diffuse away from a wound and directly into nearby cells without the assistance of a membrane channel. H_2O_2 and other ROS can be produced by oxidative stress in damaged and dying cells[114,115]. It can also be produced in the leading edge of migrating cells[115,116]. Work in *Drosophila* embryos has shown that H_2O_2 is produced in a field of cells by DUOX, a calcium sensitive transmembrane protein[12]. H_2O_2 can drive platelet aggregation by stimulating platelet activation[117,118]. It can also stimulate inflammation by recruiting immune cells and activating signal transduction cascades[12,113,119-121]. In both zebrafish and *Drosophila*, H_2O_2 gradients serve as a chemotaxis signal for immune cells[12,113]. H_2O_2 can facilitate the release of immune factors, like the DAMP, HMGB1[122]. Furthermore, H_2O_2 plays a role in cell migration and therefore promotes re-epithelialization[123-125]. Through different post-translational modifications, H_2O_2 regulates proteins upstream of Rho activity[126]. ROS can also regulate the activity of MMPs[127,128], which are important for re-epithelialization[83].

Calcium

Intercellular calcium transients in cells around wounds were first observed in cell culture scratch assays 20 years ago[34]. When these calcium transients spread uniformly across a tissue, they are termed a calcium wave. Cell culture scratch assays have since been a useful tool in characterizing wound-induced calcium waves. Typically, a fast calcium wave that lasts a few minutes after wounding is observed in cell culture scratch assays[23,24,34,35,129]. The speed of wave propagation ranges from 4.6 to 49.3 µm/s[25,34,35]. A second, slower calcium wave has been observed to propagate through the tissue an hour

after wounding only in bovine epithelial cells[24]. Investigators have shown that calcium waves depend on extracellular calcium[21,23-25,30,34] and intracellular stores[30,34], depending on which cell culture line used. In cases where extracellular calcium is important, dye influx assays show that the cell membranes, at least in cells not immediately adjacent to the scratch, are intact[24,34,35,130]. This suggests calcium is not entering through membrane damage and a transmembrane receptor or channel is important for wave formation. The propagation of these waves seems to be dependent on extracellular diffusion of a ligand, as the wave expansion was biased by directional flow and/or could spread across breaks in the cell monolayer[34,35,131].

The development of genetically encoded calcium indicators, like GCaMP, has allowed these studies to advance *in vivo*. A strong advantage of *in vivo* research is that experiments can be performed in the context of development and in the full scope of tissue architecture. Calcium waves *in vivo* also occur within seconds of wounding[6,8,10,12,20,29,113,132]. *In vivo* calcium waves propagate much more slowly, at rates ranging from 0.4 to 6.9 μm/s[12,31,43]. Wave oscillations, where the calcium wave fades and re-appears, have also been observed in different wounding models[9,12,133]. Certain *in vivo* model systems allow investigators to apply chemical inhibitors and other drugs to the tissue. By quenching extracellular calcium stores with cell-impermeable EDTA and depleting internal stores with Thapsagargin, investigators have found extracellular calcium and intracellular calcium stores are important for the calcium wave[9,12,33].

Both studies *in culture* and *in vivo* have established calcium as a master regulator of wound healing. Intracellular calcium is a ubiquitous second messenger[1,11,134,135]. Aside from initiating transcriptional activators that drive delayed responses[21,22], the calcium wave results in immediate changes in cell behavior. Inhibiting this wound-induced calcium wave has negative effects on wound closure[8,20,22,24,28,29]. Work in the *Drosophila* embryo indicated that calcium can recruit inflammatory cells by activating redox signaling via DUOX[12]. Pro-inflammatory calcium signaling seems to be mediated through phospholipase A_2 activation in zebrafish[14] and through mitochondrial ROS in worms[136]. Calcium may also be contributing to the inflammatory response by inducing the secretion of paracrine signals[137,138]. The calcium wave also has a direct protective effect on epithelial cells around a wound; cell-culture assays have shown that calcium transients inhibit apoptosis while inducing proliferation[23]. However, proliferation is not always beneficial. In stab wounds of the rat brain calcium activated JNK signaling and

8

downstream transcriptional responses to drive abnormal astrocyte proliferation, astrogliosis, and scarring[21]. In epithelia, JNK signaling is required for efficient wound healing[64,75,83,139,140]. If calcium also activates JNK signaling in epithelia, it would likely have positive effects. Lastly, the regulation of cytoskeleton at wounds by calcium influx is conserved across the model organisms[8,20,33,40]. In the *Xenopus* embryo, intracellular calcium levels drive Rho and Cdc42 activity at wounds, which are important in re-epithelization[10]. These actin dynamics are essential for wound healing. Upon wounding the cytoskeleton must adopt a dynamic, migratory structure. It is possible that calcium is a key factor in this switch. Indeed, investigators have recently described a phenomenon they term Calcium Activated Reset (CaAR) where an influx of calcium leads to the disassembly of cortical actin and the formation of dynamic actin filaments[15]. Consistent with these findings, other research proposes that intracellular calcium activates a calcium sensitive actin severing protein, Gelsoin, and permits actomyosin flow towards the wound bed[8].

Mechanisms of calcium release and propagation at wounds

A particularly high priority within the field is understanding the details regarding the initiation and propagation of calcium at wounds[6,85]. Calcium is regularly used in cells as a ubiquitous second messenger and has important functions outside of the context of wound healing[11,134,135,141,142]. Abnormal calcium signaling can have pathological effects[143-146]. How do cells regulate this potent second messenger? How do cells determine whether calcium-influx is a result of a wound or other normal cellular process? To answer these questions, we need to explore mechanisms of calcium wave initiation and propagation. Despite years of research, there is not a common consensus among the field.

ATP

ATP is a ligand for P2X and P2Y receptors. The P2X receptor is a ligand gated calcium channel that permits direct calcium entry into the cytoplasm[101-104]. The P2Y receptor is a GPCR which initiates a signaling cascade and results in calcium release from intercellular stores[32,101]. In cell culture scratch assays, ATP is known to be an initiator of the wound-induced calcium wave[30,32,34,35,38,129,147-149]. Assays used to demonstrate ATPs role in calcium influx at wounds includes over-expression of ATP degrading enzymes[30,32,38], addition of purified ATP homologues to induce calcium influx or sensitize cells[30,32,150], and treatment with P2 receptor antagonists[32,38]. Once calcium is inside the

cell, ATP can stimulate gap junction opening and allow calcium to diffuse to neighboring cells[151]. It has been suggested that ATP diffusion also accounts for the propagation of the calcium wave away from the wound margin[42]. Extracellular enzymes degrade ATP and limit its diffusion; it functions mainly in a paracrine manner[101,106,152-154]. Therefore, it is unlikely that ATP diffusion alone can account for the long range propagation of calcium waves observed at wounds[13]. However, intracellular calcium has been shown to stimulate release of ATP[100,155,156]. If calcium and ATP are involved in a positive feedback loop, it is feasible for ATP to participate in the propagation of a long distance calcium wave.

Tissue mechanics and mechanically gated channels

Changes in tissue mechanics have been shown to regulate cell behaviors, such as migration, gene expression, and differentiation[157-159]. The distribution of mechanical forces across a tissue changes upon wounding[160]. This has led many investigators to ask, do changes in tissue mechanics upon wounding drive wound healing programs? Generally, changes in tension are transduced by mechanosensitive proteins which undergo conformational changes in response to the changes in their environment. These proteins could be stretch activated ion channels that open when the tension in the lipid membrane changes[161-163]. Or they could be cytoskeleton-associated proteins that activate in response to relaxation or contraction of the cytoskeleton[164-168].

There is growing evidence in the literature that tissue mechanics can drive calcium influx, especially in the context of wounding. When cells in culture are grown on a flexible membrane and that membrane is stretched, ATP is released from cells and activates purinergic calcium channels[38,42,169]. This mechanism has also been observed in *Xenopus* oocytes[170]. Other cell culture models find that stretch induced calcium waves are a direct function of stretch activated calcium channels[41,162,171]. Experiments *in vivo* have followed up on this mechanism. When a putative mechanosensitive channel in the worm is knocked down, a wound-induced calcium wave no longer occurs[20]. In flies, TRPM knockdown doesn't completely impair the wave or alter wave kinetics, but it reduces the intensity GCaMP fluorescence upon calcium influx[8,12]. There are other indications that tissue mechanics are necessary for wave propagation. In *Xenopus* oocytes the calcium wave propagates asymmetrically and seems to favor cell borders[40]. The authors postulate that the mechanical properties of cell edges creates favorable conditions for calcium influx or propagation. A cortical actin ring is usually associated with cell edges[172]. When cortical actomyosin components are knocked down or inhibited, the calcium wave is also

perturbed[8]. Recently, direct mechanical manipulations of the tissue have allowed the field to draw stronger conclusions regarding the role of mechanics in calcium wave propagation. Calcium waves occur when *in vivo* and *ex vivo* wing discs are mechanically prodded[31]. These findings were confirmed when wing discs were mechanically compressed in a highly reproducible manner using an engineered microfluidics device[39]. Interestingly, the precision of this device allowed the investigators to conclude that calcium waves were initiated upon the release of compression. Both labs that performed mechanical manipulations of tissue found that cell lysate was required for wave activity.

Direct calcium entry through membrane damage

Concentrations of calcium are low in the cytosol ($\sim 10^{-7}$ M) and very high in the extracellular environment ($\sim 10^{-3}$ M)[1]. A breach in the plasma membrane allows these high concentrations of calcium to flood into the cell[173,174]. Pathogens, shear stresses, and heat are just a few things that can compromise lipid membranes[175-181]. Calcium influx is well studied in the context of single cell wound healing. In fact, intracellular calcium is important for plasma membrane resealing[182-186]. Plasma membrane damage (we term this damage "micro-tears") occurs in cells surrounding puncture wounds[187,188]. Micro-tears also occur around laser ablation wounds. True laser ablation events are associated with a cavitation bubble, which is a hot gas bubble that expands and contracts around the wound[189]. This bubble imparts shear stresses on cells which damage the plasma membrane and permit calcium influx[190-193]. Shear stresses between 0.035 Pa s and 0.1 Pa s have been shown to permeabilize cells in culture while shear stresses over 0.1 Pa s result in cell necrosis[176]. Investigators have used the cavitation bubble as a tool when intentionally permeabilizing cells to drive the influx of ions, therapeutics, or other molecules[194-199].

IP3 and calcium induced calcium release

Research outside of the context of wounding can also be helpful to understanding calcium wave initiation and propagation. Calcium concentrations are highly regulated in cells because calcium is a potent second messenger[1,11,134]. One way a cell can keep calcium concentrations low is by actively pumping calcium into the ER[200]. Once calcium is in the ER the cell can regulate its release through ER ion channels. Common channels are the IP3 Receptor (IP3R) and the Ryanodine Receptor (RyR)[201]. The IP3R opens when inositol tri-phospate (IP3) binds the IP3 binding domain on the cytosolic surface[202].

High cytosolic calcium levels can lower the threshold for IP3R activation[203,204], but IP3 is still required to open the channel[205,206]. Unlike the IPR3, calcium alone can activate RyRs resulting in mobilization of ER stores[207,208]. Both IP3 and calcium can diffuse through gap junctions and trigger additional IP3 calcium release in neighboring cells, propagating a calcium wave[209]. Interestingly, some reports show that calcium can activate phospholipase C to trigger the production of IP3[210,211], which would further enable wave propagation. When the ER is depleted of calcium, a calcium sensitive protein embedded in the ER membrane, STIM1, couples with a plasma membrane ion channel, Orai1, to induce sustained extracellular calcium influx[212]. The added extracellular calcium influx further increases calcium concentrations inside the cell.

CHAPTER 2

MULTIPLE MECHANISMS DRIVE CALCIUM
DYNAMICS AROUND LASER-INDUCED EPITHELIAL WOUNDS

This chapter has been adapted from Shannon, E., Stevens, A., Edrington, W., Yunhua, Z.,
Jayasinghe, A. K., Page-McCaw, A., Hutson, M. S. Multiple mechanisms drive calcium dynamics
around laser-induced epithelial wounds. *Biophysical journal* (in press).

Introduction

Epithelial wound healing is a multi-stage process. Cells must detect the presence
of a wound, migrate and proliferate in a coordinated fashion to close the defect, and then
successfully re-establish tissue-wide epithelial architecture[13,63,83,213,214]. An important early
feature of the wound response is a rapid rise in cytosolic calcium. This rise initially occurs
in cells near the wound margin and then spreads to more distant cells[8,12,20,23,34,35] to act as
a potent signal that regulates several cellular responses around wounds: JNK signaling
[21]; Rho GTPase activity [33]; and remodeling of the actin cytoskeleton[8,15,20,33]. Nonetheless,
it is not yet clear how wound-induced calcium signals are initiated *in vivo*. In cell-culture
wounding models, calcium signals are generated downstream of a diffusible ligand
released by damaged cells into the extracellular space[24,30,32]. *In vivo* studies suggest
another model, in which wound-induced changes in tissue tension open stretch-activated
calcium channels or activate other mechanosensitive proteins[6]. In support of this
hypothesis, calcium waves can be generated in *Drosophila* wing discs by applying
mechanical pressure[31] and are perturbed in both *C. elegans* and *Drosophila* wounding
models after knocking out the putative stretch-activated calcium channel TRPM[8,12,20].
Importantly, the diffusible-ligand and altered-mechanics hypotheses are not mutually
exclusive: both could be upstream initiators of wound-induced calcium signals *in vivo*,
each acting through specific regulated receptors or channels.

Here, we use pulsed laser ablation to create repeatable and controllable wounds in
epithelial tissues in *Drosophila* larvae and pupae, and carefully measure the dynamics of
the induced calcium response in surrounding cells over time scales from milliseconds to
hundreds of seconds. We observe a complex spatiotemporal response with multiple
phases: initial calcium influx beginning within milliseconds at discrete loci as far as 70 µm
from the wound site; a rapid, intercellular expansion of calcium away from these loci; and

13

a second, slower expansion of high cytosolic calcium to additional cells as far as 150 μm from the wound. We show that the initial influx and subsequent expansion phases can be described by different diffusive processes – suggesting different expansion mechanisms – and can be linked to different aspects of cellular damage around laser-induced wounds.

Although laser energy can be precisely focused to remove single cells or even sub-cellular elements[215,216], additional cells near and far from the primary wound are affected through several mechanisms. The lasers typically used to investigate the mechanics of morphogenesis and wound healing *in vivo* are pulsed[160,217-219], with femtosecond to nanosecond pulsewidths, and ablate tissue via plasma formation[178,189,220]. The plasma directly destroys macromolecules within the laser focus (radius < 1 μm), but recombination of the plasma leaves the targeted location extremely hot, leading to the vaporization of water and expansion of a cavitation bubble[189]. The bubbles associated with laser ablation vary with pulsewidth and fluence[178,189,220]; those measured for near-threshold *in vivo* ablation using ns-pulse lasers have lifetimes on the order of microseconds and inferred maximum radii of 10 to 100 μm[178,221]. In cell-culture studies, the rapid expansion and collapse of cavitation bubbles generates shear stresses that can lyse cells close to the ablation site, creating a primary wound, and can transiently permeabilize cells farther away[176,177,222] – a process known as optoporation.

Here, we show that two mechanisms of laser-induced damage, a tissue-level primary wound and cellular micro-tears, each drive distinct calcium signaling dynamics. By imaging calcium dynamics with unprecedented time resolution, we show that calcium directly enters permeabilized cells 20-100 μm from the ablation site within milliseconds. This influx initiates a first calcium wave. In some cases, a second wave further expands the region of high cytosolic calcium, but the second wave is delayed by 30-60 s and its occurrence depends on the size of the primary wound. Through kinematic modeling of the calcium influx and expansion waves, we have identified parameters of the wave spread that narrow and inform the search for upstream mechanisms. Our findings have implications both specific to laser ablation and applicable to more general types of wounding. First, the precision lysis of laser ablation may be accompanied by cavitation bubble effects akin to a wider crush injury. Second, our general finding of two-phase initiation of calcium signaling is likely to be important for tissues sensing a wide range of traumatic damage.

Materials and Methods

Fly Lines

   pnr-Gal4 (Fly Base ID: FBst0025758) was used to drive expression of *UAS-GCaMP3* (Fly Base ID: FBst0032236), *UAS-GCaMP6m* (Fly Base ID: FBst0042748), *UAS-Arclight* (Fly Base ID: FBst0051056), *UAS-Inx2 RNAi #1* (Fly Base ID: FBst0029306), *UAS-Inx2 RNAi #2* (Fly Base ID: FBst0474063), and *UAS-Inx3 RNAi* (Fly Base ID: FBst0060112) in the notum. *tubP-Gal4* (Fly Base ID: FBst0005138) was used to drive expression of GCaMP6m in the wing disc. *shg-tdTomato* (Fly Base ID: FBst0058789) and *Ubi-p63E-shg.GFP* (Fly Base ID: FBst0307577) were used to visualize cell borders. *Vkg-GFP[454]* (Fly Base ID: FBti0153267) was used to visualize cell architecture in wing disc experiments with propidium iodide. *w[1118]* was used as wild type.

Mounting pupae

   White prepupae expressing *pnr-Gal4* and *UAS-GCaMP3, UAS-GCaMP6m* or *UAS-Arclight* were identified and aged for 12-18 hours After Puparium Formation (APF). For imaging, a pupa was placed on a piece of double-sided tape (Scotch brand, catalog #665), ventral side down, and its anterior pupal case was removed with fine tipped forceps to reveal the notum epithelium. The entire piece of double-sided tape was gently lifted from the dissecting stage with the pupae still attached and adhered to a 45 mm x 50 mm coverslip (no. 1.5, Fisherbrand, 12-544F) so that the pupal nota were laid against the coverslip, with the pupae between the coverslip and the tape layer. It was not necessary to adhere all edges of the double-sided tape to the coverslip, only the edge at the anterior of the pupae. Then, an oxygen permeable membrane (YSI, standard membrane kit, cat# 1329882) was applied over the pupae and secured to the coverslip with additional double-sided tape so pupae would not become dehydrated.

Mounting wing discs

   For wounding experiments in the wing disc, *tubP-Gal4* was used to drive the expression of *UAS-GCaMP6m*. Wing discs were dissected from 3rd instar larvae in a drop of PBS (137 mM NaCl, 2.7 mM KCl, 10 mM Na_2HPO_4, 2 mM KH_2PO_4, pH 7.4) and immediately mounted on coverslips for imaging and ablation. Cell-Tak Adhesive (Corning, catalog #354240) was used to adhere wing discs to 45 mm x 50 mm coverslips (no. 1.5, Fisherbrand, 12-544F). 7 ug of Cell-Tak was used to coat a surface area of 20 mm x 20 mm using the manufacturer's protocol. Because Cell-Tak was used, external forces were not applied to wing discs through mounting and imaging. A pap pen (RPI, catalog #50-

550-221) was used to trace a hydrophobic barrier around the wing discs on the coverslip. Two wing discs were mounted on one coverslip. For calcium-free conditions, wing discs were mounted in a drop of PBS. For 2 mM calcium conditions, wing discs were mounted in a solution for which 200 mM $CaCl_2$ at pH 7.0, was diluted to 2 mM in PBS.

Laser ablation and live imaging

Laser ablation and live imaging were performed using a Zeiss LSM410 raster-scanning inverted confocal microscope with a 40X 1.3 NA oil-immersion objective. Scans were performed either every 2.14 seconds or every 3.0 seconds. Laser ablation used single pulses of the 3rd harmonic (355 nm) of a Q-switched Nd:YAG laser (5 ns pulsewidth, Continuum Minilite II, Santa Clara, CA). Laser pulse energies ranged from 0.5 µJ to 10 µJ, depending on the experiment. A separate computer-controlled mirror and custom ImageJ plug-in were used to aim and operate the ablation laser so that ablation could be performed without any interruption to live imaging. For kymograph experiments, line scans with a scan rate of 2.09 ms were taken at the wound site. Line scan data was assembled into kymographs using ImageJ.

Cavitation experiments

Pupae were selected and pupal cases were removed as described above. PBS was used to release pupae from double-sided tape. Fly glue, made of double-sided tape (Scotch brand, catalog #665) dissolved with heptane, was used to adhere each pupa to the coverslip so its entire dorsal side was touching the glass. A pap pen (RPI, catalog #50-550-221) was used to trace a hydrophobic barrier around the pupae on the coverslip. Immediately prior to imaging, approximately 500 µl of distilled water was slowly dropped on top of the pupae on the coverslip so that the pupae were under a bubble of water. For wing disc cavitation experiments, discs were mounted as described above, in approximately 500 µl PBS or PBS with 2 mM calcium.

A small hydrophone (Onda, 0.5 mm aperture, <20 ns rise time, 2.24 V/MPa sensitivity), was mounted to the confocal stage and lowered into the bubble of water approximately 1 mm away from the focus of the laser. Hydrophone data were displayed on an oscilloscope. Samples were imaged and wounded as described above while the hydrophone measured the expansion and collapse of each cavitation bubble via their associated acoustic transients. Each cavitation bubble's maximum radius was calculated from its lifetime[221].

Cavitation bubble imaging

Drosophila embryos were collected approximately 2 hours after egg laying and aged at 18°C until germ band retraction. Prior to mounting, the chorion was removed using a 50% bleach solution. Fly glue, made as described above, was used to adhere each embryo to the coverslip. Embryos were immersed under a bubble of distilled water and the needle hydrophone was lowered into the solution as described above.

A second optical path was added to the Zeiss LSM410 microscope to image cavitation bubbles formed during ablation. This high-speed bright-field imaging system is built around a high-sensitivity CCD camera (Photometrics CoolSNAP EZ, Tucson, AZ; 1392×1040-pixel 12-bit sensor, >60% quantum efficiency in the range 450 to 650 nm) and a pulsed diode laser (Coherent Cube, Santa Clara, CA; λ = 660 nm, maximum average power = 61 mW). The diode laser serves as a flash illumination source with a controllable pulse duration. The camera is triggered before ablation, and the illumination laser is used as a strobe light with an accurately adjustable delay. Signals for triggering the camera, the ablation laser's Q-switch, and the diode laser pulse (rise and fall) are controlled by a digital delay generator (Stanford Research Systems DG645, Sunny Vale, CA) using the ablation laser's flash-lamp sync as the master timing signal. The accuracy of the illumination pulse delay is limited by the approximately 2-ns jitter inherent to the electronics controlling the ablation laser. This system can image cavitation bubbles in liquid with illumination pulse durations as short as 7 ns. For imaging in fly embryos, longer pulses (~0.5 µs) are needed to obtain sufficient contrast. Note that images formed by the bright-field imaging system lack all depth information. Each is essentially a picture of the shadows cast by structures in the ~200-µm thick embryo.

To protect the photomultiplier tubes in the confocal system from inadvertent exposure to the illumination laser, the dichroic normally used to reflect collected fluorescence is removed during high-speed imaging. It can be reinserted to take confocal images of the embryos within a few seconds of ablation.

FM 1-43 and Propidium Iodide (PI) dye analysis in wing discs

Wing discs were mounted as described above and FM 1-43 dye (ThermoFisher catalog# T35356), diluted in PBS to a final concentration of 5 µg/ml, was added immediately prior to imaging. To limit pre-wounding dye internalization via endocytosis, wounding experiments were performed and completed within 10 minutes of adding FM 1-43 dye. Since the kinetics of dye influx via micro-tears and its associated increase in dye-

labeled membrane fluorescence are slower than GCaMP6m kinetics, measurements of the region of dye influx were taken from images collected 60 seconds after ablation. Despite this delay, we did not observe any spreading of increased dye fluorescence to neighboring cells. Simultaneous cavitation measurements were performed as described above.

PI (ThermoFisher #P3566) was diluted in PBS to a final concentration of 20 µg/ml. Wing discs were mounted as described above and dye was added immediately prior to imaging. Because PI does not fluoresce until after wounding, a fluorescent marker was needed to identify the correct focal plane for laser ablation. Therefore, we used wing discs expressing *Vkg-GFP[454]* in a wild type background to fluorescently label the basement membrane. Measurements of the region of dye influx were taken from images collected approximately 5 minutes after ablation.

Image processing and analysis

Quantitative data was extracted from images and kymographs of GCaMP fluorescence via routines implemented in Mathematica (Wolfram Inc., Champaign, IL).

To identify the initial Ca^{2+}-influx sites in kymographs, the signal front was first defined as the earliest time at which the GCaMP signal exceeded the mean pre-wounding signal plus two standard deviations. Each signal front was then smoothed using a 3rd-degree 17-point Savitzky-Golay filter to remove noise and the positions of its local minima were identified as the initial sites of Ca^{2+} influx.

To analyze the diffusion of calcium from these influx sites, all available kymographs were examined to identify sites whose kymograph peaks were symmetric, remained below saturation, and were spatially isolated for some time. These criteria identified 25 individual peaks that were separated from other regions of calcium influx for at least 43 ms and remained below saturation for at least 21 ms (all 25 peaks are shown in Supplemental Fig. S3). These peaks were cropped in ImageJ to widths on the order of 10 µm and lengths on the order of 50 ms and then fit to a diffusion model for $t > 0$:

$$\phi(x,t; \alpha, q, x_0, y_0, \phi_0) = Min\left[1, \frac{q}{4\pi^{3/2}\alpha r}\Gamma\left(\frac{1}{2}, \frac{r^2}{4\alpha t}\right) + \phi_0\right] \qquad \text{Eqn. S1}$$

where $\Gamma(a, p) = \int_p^\infty u^{a-1}e^{-u}du$ is the incomplete gamma function. The model assumes a single point source where calcium enters the cytosol at a constant rate q and diffuses with a diffusion constant α from a location that is at position x_0 along the kymograph line and a distance y_0 from this line. Therefore, $r^2 = (x - x_0)^2 + y_0^2$ is the squared distance from a

18

position *x* on the kymograph line to the source location. Equation S1 was obtained by integrating the equation of diffusion from an initial point source concentration, $\phi(x, t') = (4\pi\alpha t)^{-3/2}\exp(-\frac{r^2}{4\alpha t'})$, over time from 0 to t, followed by a variable substitution $u = \frac{r^2}{4\alpha t}$. Due to the spatial symmetry of this model, there is no loss in generality in assuming the point source and the kymograph line are in the x-y plane and along the x-axis respectively.

This model further assumes that image intensity values are a linear function of calcium concentration, allowing for a constant non-zero intensity baseline ϕ_0, until image intensity saturates at a relative intensity value of 1. The fitted parameters were α, q, x_0, y_0, and ϕ_0 as defined above. Note that on the time scales analyzed, the calcium signals have not yet spread completely through individual epithelial cells; therefore, three-dimensional diffusion was considered instead of two-dimensional diffusion.

To analyze longer term spread of calcium signals from full-frame time-lapse images, the ImageJ Radial Profile Angle Plot plug-in was used on each image to determine the average GCaMP intensity profile as a function of distance from the center of the wound. A custom MATLAB script was then used to determine the distance from the wound at which the intensity dropped to half its maximum. This distance corresponds to the radius of the radially-averaged calcium wave and plotting it for each video frame yields a graph of calcium signal expansion over time. Sections of these signal expansion curves were fit to 2D diffusion models (Eqn 1 in Results) using nonlinear regression in Mathematica.

Results

Fast Ca^{2+} signal dynamics from 2 ms to 2 s.

To investigate mechanisms of calcium release upon wounding, we analyzed calcium dynamics in the *Drosophila* pupal notum (following procedures in Antunes et. al.[8]). At 12-18 h APF, the notum is a continuous epithelial monolayer of diploid cuboidal cells which exhibit apicobasal polarity and sit atop a basement membrane[44]. Pupae were wounded via laser ablation while imaged live simultaneously. Half of wounded pupae survive laser ablation and later eclose (data not shown and Antunes et. al.[8]). Wound-induced calcium waves were visualized with a genetically encoded, intracellular GCaMP3 reporter[223].

Prior to ablation, cytosolic calcium remained at low basal levels (Figure 1A, t = -2 s), with single cells occasionally exhibiting transient calcium increases. In the first frame (< 2 s) after ablation, a dramatic increase in cytosolic calcium was observed as bright GCaMP fluorescence both in cells along the wound margin and in surrounding cells up to seven cell diameters away (~ 50 μm) (Figure 1A). To analyze this initial response with improved temporal resolution, we performed line scans passing through the wound to increase our sampling rate to 2.1 ms/scan. For these experiments, we also employed a GCaMP6m calcium indicator since it has faster kinetics with an increased signal-to-noise ratio[224,225]. These line scans were assembled into kymographs, an example of which is shown in Figure 1B (additional examples shown in Figure 2). Within milliseconds after ablation, calcium entered the cytoplasm and increased GCaMP6m fluorescence in multiple cells up to ~50 μm away from the ablated region. We call this rapid increase of intracellular calcium the "initial response".

Few biological signals could propagate away from the wound site quickly enough to drive this spatially-distributed initial Ca^{2+} response. For example, the kymograph in Figure 1B and Figure 2 shows rises in intracellular Ca^{2+} that begin within 5 ms for cells up to 50 μm from the wound. To reach this far this fast, any ablation-induced diffusible signal would need a diffusion constant α ~1.3 x 10^5 μm^2/s, estimated from $(\Delta x)^2/4\Delta t$. This estimated diffusion constant is 2-3 orders of magnitude faster than that of a small molecule like ATP (3.5 x 10^2 μm^2/s), or of small ions (0.8 to 2.0 x 10^3 μm^2/s), or of even the self-diffusion of water (2.3 x 10^3 μm^2/s). Thus, a diffusible signal cannot trigger the initial rapid response.

The initial Ca^{2+} response is driven by cavitation.

Pulsed laser ablation generates a plasma that completely destroys macromolecules in a nearly diffraction limited region (< 1 μm diameter) and generates a rapidly expanding cavitation bubble with high shear stresses that lyse cells in a variably broader region. Importantly, the region of macromolecular destruction and region of lysis are both much smaller than the initial GCaMP response region we observe. The cavitation bubble is short-lived but it can expand hundreds of microns beyond the region of lysed cells[176,177,221]. To investigate whether the initial Ca^{2+} response could be driven by cavitation, we simultaneously measured initial Ca^{2+} response radii and cavitation bubble radii.

20
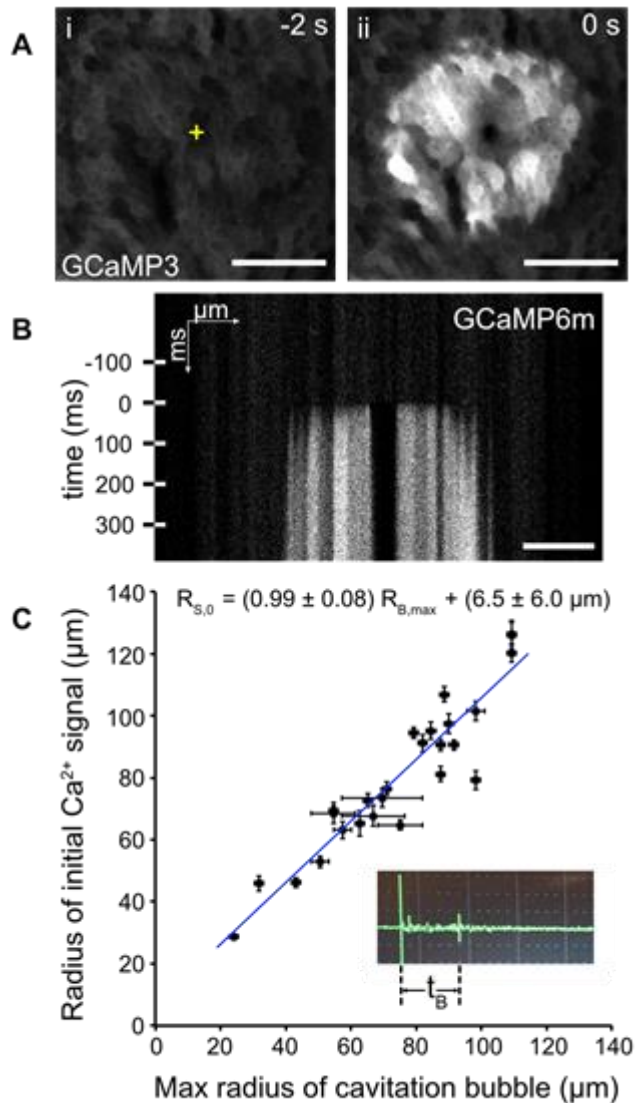
Figure 1: The initial calcium influx matches the radius of the cavitation bubble.
A) Confocal images of the calcium reporter GCaMP3 in the pupal notum. Basal levels of cytosolic calcium are low before wounding (i), but rise rapidly after laser-ablation (ii). The rapid rise occurs in cells within 5-7 rows from the ablation site (crosshairs in i, central dark area in ii). Scale bar is 50 µm. **B)** Confocal kymograph of GCaMP6m. Fluorescence is low before wounding (kymograph lines above t = 0 ms), but rises within milliseconds of laser ablation in cells distant from the wound site (central dark area for $t > 0$ ms). Scale bar is 50 µm. **C)** The radius of the Ca^{2+} signal ($R_{S,0}$) corresponds to the maximum radius of the laser-induced cavitation bubble ($R_{B,max}$). Linear regression yields a best fit with a slope of 0.99 (solid line; equation; $R^2 = 0.87$). Each data point corresponds to a single wound with initial Ca^{2+} signal radii measured from full frame confocal images (< 3 s after ablation) and bubble radii calculated from bubble lifetimes (t_B) measured via hydrophone (inset). Horizontal error bars represent estimated uncertainty in identifying the bubble collapse peak; vertical error bars are standard deviations of four radius measurements.
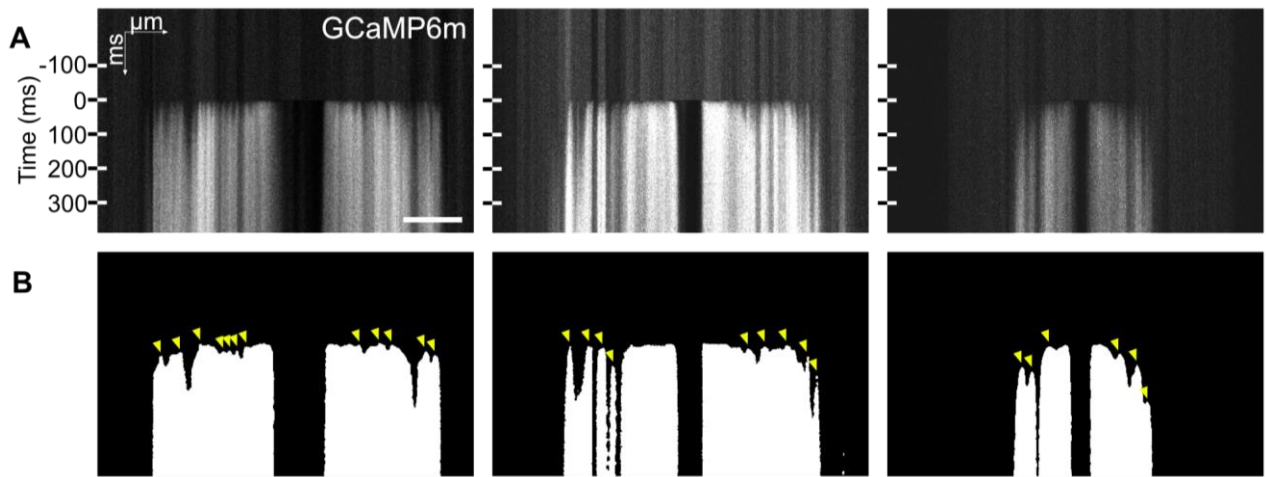
Figure 2: Kymographs show that increases in cytosolic calcium begin milliseconds after ablation, even tens of microns from the wound site.
GCaMP6m was expressed in the *pnr* domain using the *Gal4-UAS* system. Three separate samples are shown. Line scans were taken over the point of ablation and assembled into kymographs using ImageJ. **A)** Kymographs show that intracellular calcium levels rise within a few ms at distances at least 50 microns away from the wound. **B)** Identification of the initiation of calcium fluorescence in each pixel column (see Methods). Yellow arrowheads indicate calcium influx loci, or peaks. Scale bar is 50 µm.

We estimated cavitation bubble radii using a hydrophone to detect the acoustic transients associated with bubble expansion and collapse. For water at standard temperature and pressure, maximum bubble radii ($R_{B,max}$) are theoretically related to cavitation bubble lifetimes (t_B) according to $R_{B,max} \approx (5.46 \text{ µm/µs}) \, t_B$ [221]. Validation of hydrophone measurements based on this relationship is provided by direct flash imaging of bubbles in *Drosophila* embryos as shown in Figure 3. For each experiment in pupae, we also collected full-frame confocal images of GCaMP6m fluorescence to record the initial Ca^{2+} response radius. With laser pulse energy intentionally varied to create both large and small cavitation bubbles, we found that cavitation radius matched the radius of initial response radius ($R_{S,0}$) with a slope very close to one: the best linear fit to the relationship was $R_{S,0} = (0.99 \pm 0.08)R_{B,max} + (6.5 \pm 6.0 \text{ µm})$ (Figure 1C). Our initial response measurements are an overestimate as the calcium region can expand by as much as 17.6 ± 7.0 µm (mean radius ± s.d.) between the time of ablation and the capture of images used to determine the radius of calcium influx (<2 s). Correcting for this overestimate would reveal a trend line that runs very close to the origin. We conclude that the cavitation bubble is tightly linked to the extent of the initial calcium response, and we explore the mechanism below.

22

Amnioserosa-1   Amnioserosa-2   Epidermis

A Before wounding

B Cavitation bubble

C After wounding

D Acoustic trace
Q-switch
Expansion
Collapse
1 µs

E
Observed cavitation bubble radius (µm)
Calculated cavitation bubble radius from hydrophone (µm)
● single point
● two points
● line
● circle

F
i Q-switch   Expansion   1 µs
ii Q-switch   Expansion
iii Q-switch

23
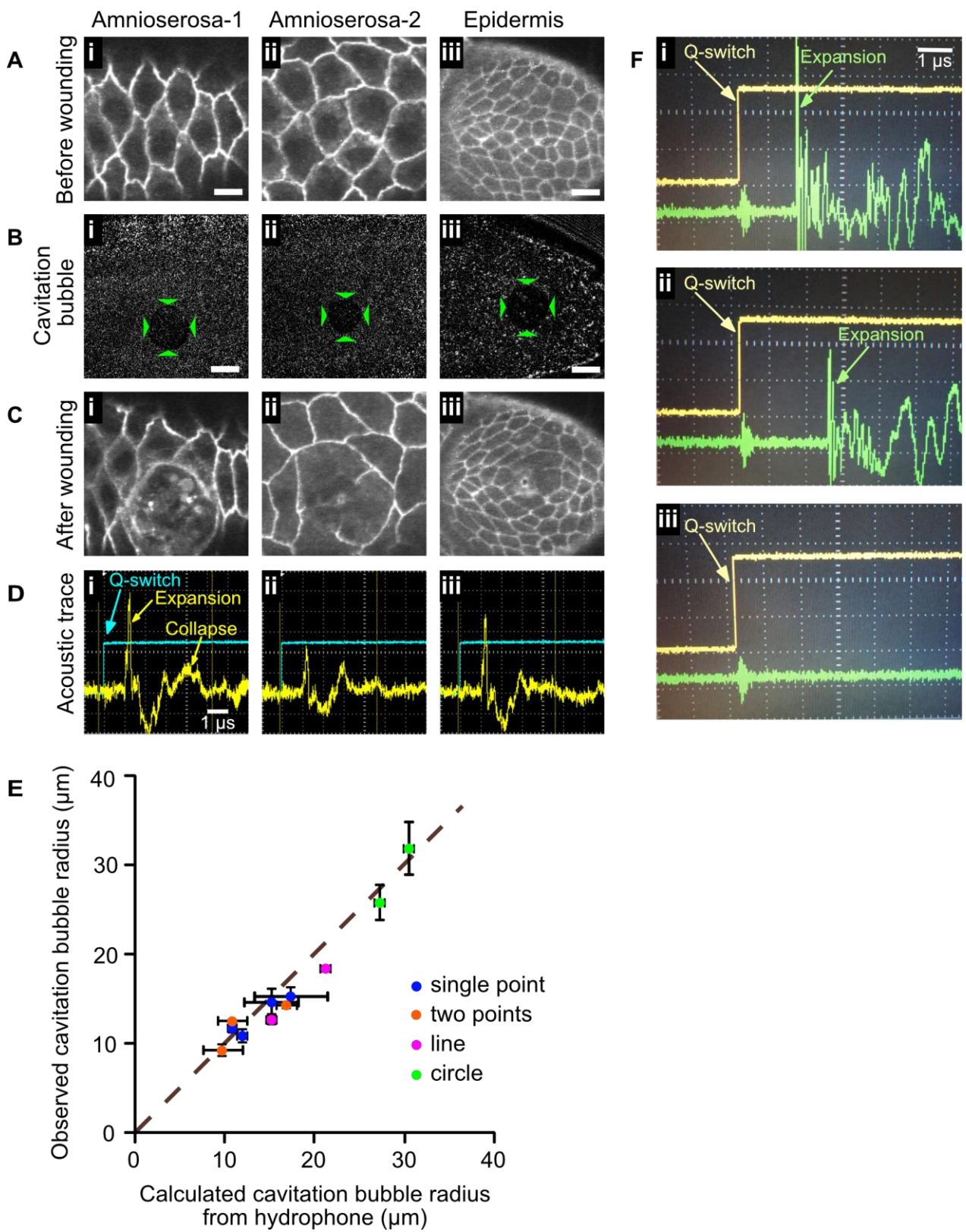
Figure 3: Acoustic data from a hydrophone can be used to measure cavitation bubble radii.
We validate the use of acoustic hydrophone data to measure laser-induced cavitation bubble radii in *Drosophila* embryos by comparison with direct bubble imaging. Three separate examples (i-iii) are shown in panels A-D: i-ii are from ablation of amnioserosa, a squamous epithelial tissue; iii is from ablation of columnar epithelial cells in the germband. **A)** Cell borders are visualized before laser wounding via confocal images of embryos expressing *Ubi-p63E-shg.GFP*. **B)** The cavitation bubble formed upon laser wounding (delineated by green arrowheads) is imaged by high-speed bright-field imaging. **C)** Recoil of the cells observed in post-ablation confocal images indicates that a wound has been made that is much smaller than the cavitation bubble. **D)** Acoustic traces from a hydrophone, overlaid with the ablation laser's Q-switch sync signal, show peaks corresponding to the initial rapid expansion and later rapid collapse of the cavitation bubble. The time between these peaks is used to calculate the maximum size of the bubble. All scale bars for A-D are 20 μm. **E)** Comparison of cavitation bubble radii calculated from hydrophone measurements with those observed by direct imaging. Root-mean-square deviation from an exact match (brown dashed line) is ~12% even when considering multiple laser ablation patterns: single points, two points, lines, or circles. When cavitation bubbles were ellipsoidal, e.g., for two-point and line ablations, the reported radius is the geometric mean of the bubble's semi-major and semi-minor axes. The shape of the bubble did not affect our ability to assess cavitation radius with the hydrophone. Horizontal error bars represent propagation of uncertainly from our determination of bubble collapse times. Vertical error bars are the standard deviation among four radius measurements (for circular bubbles) or propagation of uncertainty in the ellipse parameters used to estimate the equivalent radius (for ellipsoidal bubbles). **F)** Control experiments for hydrophone measurements: (i) when the hydrophone is located ~2.5 mm from the point of ablation, the first acoustic transient associated with bubble expansion is detected ~1.6 μs after the laser pulse, an appropriate time given the speed of sound in water (1,480 m/s); (ii) moving the hydrophone tip to 3.5 mm from the point of ablation appropriately delays the arrival of the first acoustic transient to 2.4 μs after ablation; (iii) allowing the laser to fire, but blocking the light from reaching the sample eliminates the acoustic transients associated with cavitation. In all cases, a small signal is present immediately after the laser fires and is likely attributable to electromagnetic interference from the capacitors that discharge in the ablation laser as its Q-switch is triggered.

The initial response begins at discrete loci.

Within milliseconds of ablation, kymographs of GCaMP6m fluorescence show the contemporaneous appearance of multiple high-Ca^{2+} loci (Figure 4A, arrowheads). This pattern cannot be due to Ca^{2+} flow from the wound margin through neighboring cells but instead indicates Ca^{2+} entering the cytosol at multiple distinct locations around the wound. To quantify the spatial distribution of these Ca^{2+}-influx loci, we first identified each kymograph's signal front – i.e., the time points when the fluorescence signal in each kymograph column first exceeded the unwounded background by two standard deviations (Figure 4A, solid white line). Considering this signal front as a function $t_{front}(x)$, we

identified influx loci as its local minima, which appear as peaks because of the inverted time axis of our kymographs (Figure 4A, arrowheads). Although Ca^{2+}-influx loci far from the wound appear as spatially distinct peaks, those close to the wound blend together into a wide band of high fluorescence. For this wide band of unresolved fluorescence near the wound, each pixel was counted as a Ca^{2+}-influx site.
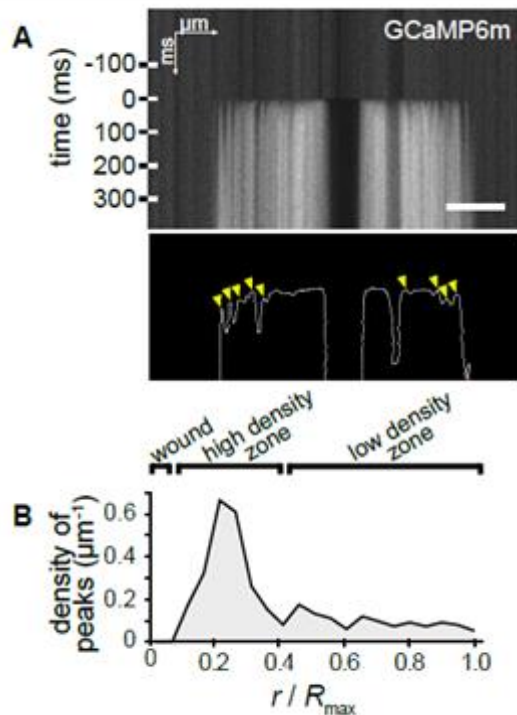
Figure 4: Early calcium influx appears at discrete loci.
A) Confocal kymograph of GCaMP6m showing discrete sites of cytosolic calcium entry in cells distant from the wound. These sites are marked by yellow arrowheads and were identified as local maxima along the signal front (outline in lower panel). Scale bar is 50 μm. **B)** Density of Ca^{2+}-signal initiation sites as a function of relative distance from the wound center. Data were compiled from 25 kymographs with distances normalized to each kymograph's maximum signal radius (R_{max}). Broad regions near the wound with rapid Ca^{2+} rise, but no discernable peaks, were treated as having one initiation site per kymograph pixel. Brackets above the plot demarcate different zones of initiation site density.

We plotted the radial density of influx sites around primary wounds by compiling data from 25 kymographs and normalizing peak locations to each kymograph's maximum signal radius (R_{max}). Figure 4B shows the primary wound plus two distinct zones of Ca^{2+}-influx site density: a high-density zone corresponding to the fast, unresolved band of high signal (0.1 $R_{max} < r < 0.4\ R_{max}$); and a zone of lower density corresponding to the region of

distinct kymograph peaks ($0.4\ R_{max} < r < R_{max}$). Although the density in this latter region is ~ 1 site per 10 µm, which is close to one per cell, the Ca^{2+}-influx sites do not fall in a regular pattern with respect to cell borders.
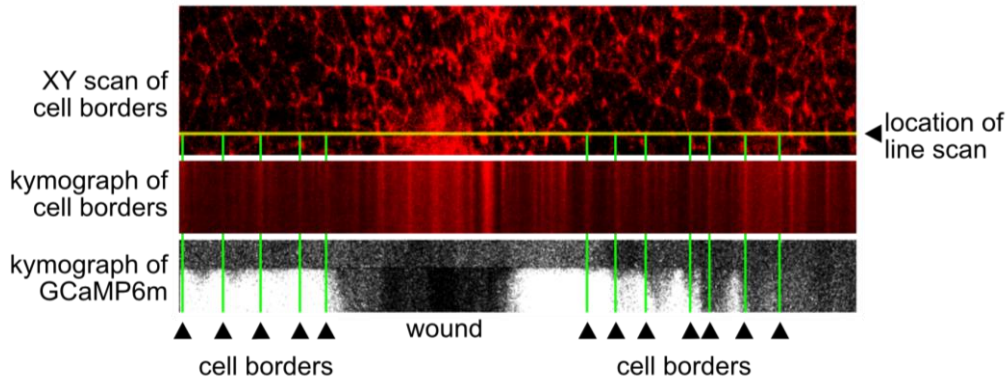
Figure 5: Ca^{2+} entry points appear randomly spaced with respect to cell borders.
The top panel shows an XY scan of *shg-tdTomato* (E-cadherin) used to label cell borders before ablation. The middle panel shows a kymograph of cell borders scanned along the yellow line before ablation. Because *shg-tdTomato* is present both at cell borders and in intracellular punctae, the determination of true cell borders (marked with green lines) required both the kymograph and the XY scan, registered for alignment. The bottom panel shows a kymograph of GCaMP6m upon wounding, with the cell borders shown as green lines from the top panel. Local maxima in the kymograph correspond to calcium entry points. The calcium entry points do not align with cell borders in any regular pattern.

The spatially distinct kymograph peaks show that Ca^{2+} enters the cytoplasm of cells around the wound at discrete loci and then spreads rapidly (Figure 6A). To quantify this spread, we individually fit 25 peaks to a three-dimensional diffusion model – i.e., the expected time-dependent signal along a sampled line due to diffusion from a point source of constant Ca^{2+} influx. An example fit for one peak is shown in Figure 6B, with selected temporal and spatial slices used to show overlays of the data and fit (Figure 6C and Figure 6D). The complete set of kymograph peak fits is available as Appendix A. From this complete set of fits, the interquartile range of estimated diffusion constants was 76 to 220 µm^2/s, with a median of 120 µm^2/s (Figure 6E). This range lies between the diffusion constants of cytosolically buffered Ca^{2+} (13 µm^2/s) and free Ca^{2+} (220 µm^2/s)[226]. The breadth of the fitted diffusion-constant distribution can be attributed to a combination of expected random error, systematic errors based on using an infinitesimal point source equation that would slightly overestimate the diffusion constants from finite-sized influx sites, and cell-to-cell variations in the degree to which Ca^{2+}-influx levels saturate cytoplasmic and GCaMP6 buffering capacity.
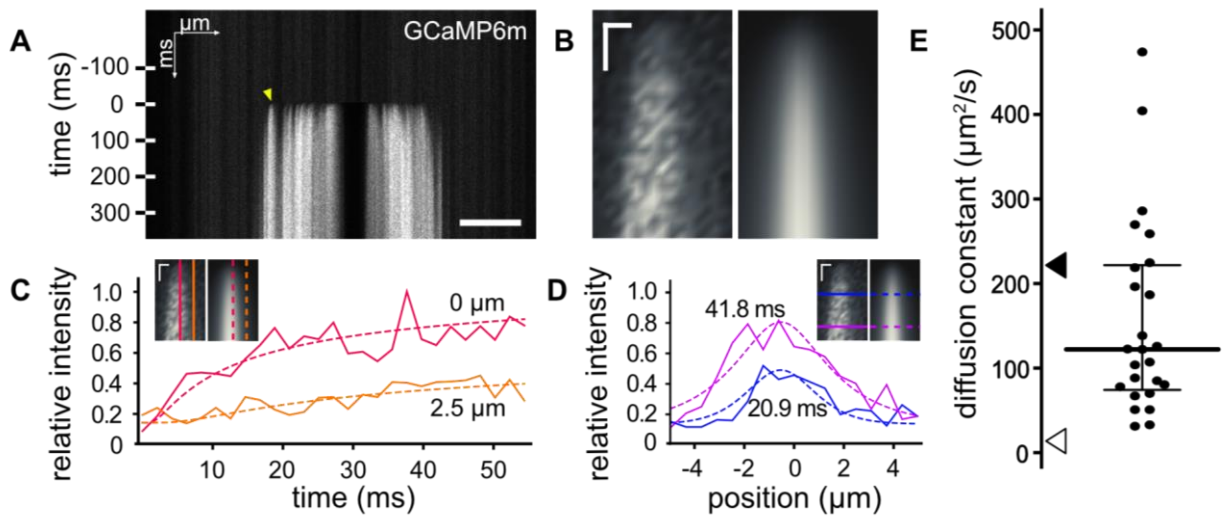
Figure 6: Intracellular calcium diffuses from discrete loci at rates that appear to overcome cytosolic buffering capacity.
A) Kymograph of GCaMP6m fluorescence upon wounding. A single peak (yellow arrowhead) is examined in more detail in B-D. Scale bar is 50 μm. **B)** End view of an isolated kymograph peak (left) and the best fit of that peak to a diffusion model (right; see main text for details). Scale bar is 2 μm horizontal and 10 ms vertical. **C)** Intensity versus time for two marked columns cutting through the selected kymograph section (at 0 and 2.5 μm from the center of the peak). **D)** Intensity versus position for two marked rows cutting through the selected kymograph section (at 20.9 and 41.8 ms after laser ablation). **E)** Box and whiskers plot of the diffusion constants from best fits of 25 isolated peaks. Bars show median and interquartile range. Arrowheads indicate diffusion constants of free calcium (black, 220 μm^2/s) and cytosolically buffered calcium (white, 13 μm^2/s) as measured by Allbritton *et. al.*[226].

The cavitation bubble creates plasma membrane micro-tears.

Our results thus far show that Ca^{2+} enters the cytoplasm from discrete loci spread throughout the maximum extent of the cavitation bubble. Previous reports show that cavitation bubbles induce cellular damage[227,228] and this cellular damage is associated with rises in intracellular calcium[190-193]. Plasma membrane micro-tears would provide a simple direct mechanism for the inflow of calcium into the cytoplasm from its high concentration in the extracellular space (~10^{-3} M extracellularly vs ~10^{-7} M in cytoplasm). We thus tested for ablation-induced micro-tears in three types of assays described below: depolarization, dye internalization, and altered extracellular calcium.
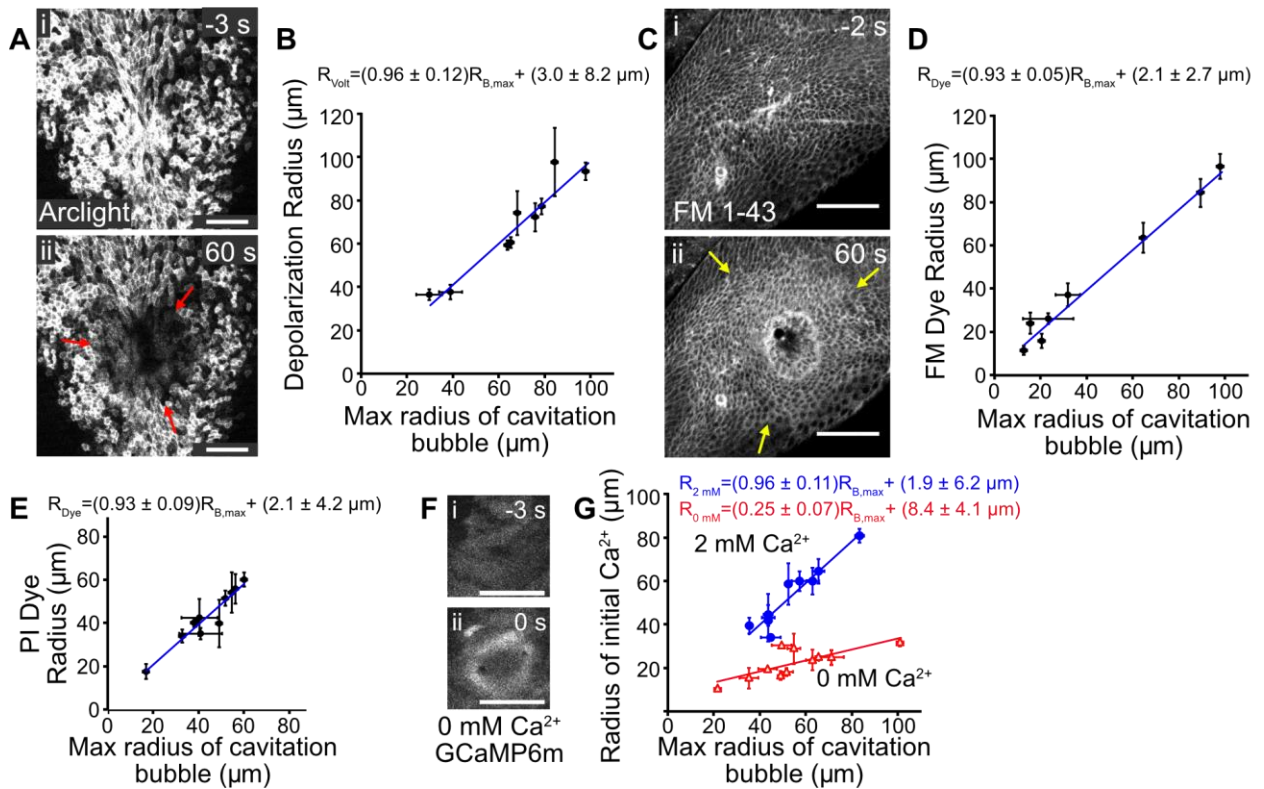
Figure 7: The cavitation bubble creates micro-tears in plasma membrane.
A) Arclight fluorescence in the notum is high before wounding (i) and decreases around the wound afterwards, indicating depolarization (ii). The margin of depolarization is marked by red arrows. **B)** The radius of depolarization (R_{Volt}) corresponds to the maximum radius of the laser-induced cavitation bubble ($R_{B,max}$) with a best fit slope of nearly 1 (solid line; equation; $R^2 = 0.91$). R_{Volt} was measured from confocal images taken on the first frame (< 3 s) after ablation. **C)** Fluorescent labeling of an *ex vivo* wing disc with FM 1-43 is modest before wounding (i), and increases around the wound afterwards, indicating a region of increased cell permeability and dye influx (ii). The outer margin of dye influx is marked by yellow arrows. Scale bar = 50 μm. **D)** The radius of dye influx (R_{Dye}) also corresponds to $R_{B,max}$ with a best fit slope of nearly 1 (solid line; equation; $R^2 = 0.98$). The radius of dye influx was measured from confocal images taken 60 seconds after ablation. **E)** Again, the radius of dye influx (R_{PI}) corresponds to $R_{B,max}$ with a best fit slope of nearly 1 (solid line; equation; $R^2 = 0.92$). The radius of dye influx was measured from confocal images taken approximately 5 minutes after ablation. **F)** Wing discs expressing GCaMP6m were ablated *ex vivo* in calcium-free media. Fluorescence is low before wounding (i) and only increases afterwards in cells close to the wound (ii). Scale bar is 50 μm. **G)** The radius of the initial wound-induced calcium rise in calcium-free media ($R_{0\,mM}$) is significantly smaller than $R_{B,max}$, with a best fit slope of 0.25 (red, open triangles; $R^2 = 0.60$). In contrast, when wing discs are wounded in 2 mM calcium, the initial wound-induced calcium radius ($R_{2\,mM}$) corresponds to $R_{B,max}$ with a best fit slope of nearly 1 (blue, closed circles; $R^2 = 0.90$). Best-fit equations shown above graph. Horizontal error bars represent estimated uncertainty in identifying the collapse peak; vertical error bars are standard deviations of four radius measurements.

28

First, we measured electrical depolarization. Epithelial cells maintain an electrical potential or voltage difference across their plasma membranes and micro-tears would allow the free movement of Na^+, Cl^- and K^+ ions to eliminate this membrane potential and thus depolarize the cells. Ca^{2+} would also cross the plasma membrane, but Ca^{2+} ions do not contribute significantly to establishing or depolarizing the electrical potential[229]. We visualized cavitation-induced changes in membrane potential using a genetically encoded voltage indicator, Arclight, whose fluorescence decreases upon depolarization[230,231]. Although Arclight kinetics are slower than those of GCaMP6m, we observed a slight decrease in fluorescence in the first frame upon wounding in a region centered around the wound, and this decrease became more pronounced over the next 30 to 60 s (Figure 7A). As shown above for the initial Ca^{2+} signal, the radius of the depolarized region also matched the radius of cavitation (Figure 7B) – linking both to the maximum extent of the cavitation bubble. Over the course of ten minutes, damaged but un-lysed cells within the cavitation footprint repolarized, indicating that cells survive micro-tear damage (Figure 8).

Next, we used two robust and well characterized micro-tear assays based on two cell-impermeable fluorophores, the lipophilic dye, FM 1-43[173,184,232-237], and the DNA intercalating agent, propidium iodide (PI)[238-241]. FM 1-43 fluoresces only when bound to lipid membranes. Prior to wounding, dye binds only the outer leaflet of the cells' plasma membranes. If wounding generates micro-tears, dye can then enter cells and label the inner leaflet of the plasma membrane, increasing its fluorescence intensity. We could not conduct these experiments in *Drosophila* pupae because they have an impermeable waxy cuticle that prevents dye from accessing notum cells and membranes. We thus used *Drosophila* wing discs, larval precursors of the pupal notum and wing that can be cultured *ex vivo*. We laser-wounded wing discs submerged in FM 1-43 while simultaneously imaging fluorescence and tracking cavitation with a hydrophone. After laser ablation, plasma membrane fluorescence increased, indicating inner-leaflet labeling and the presence of micro-tears in a circular region around the wound (Figure 7C). The radius of increased fluorescence matched the maximum radius of the cavitation bubble (Figure 7D) and did not expand with time**.** High-magnification imaging shows FM 1-43 preferentially labeling the plasma membrane with little labeling of endocytic vesicles, suggesting a route of entry that bypasses endocytosis (Figure 9). This route could be micro-tears, but since FM 1-43 has been observed to pass through some plasma membrane channels[242,243], we performed a similar experiment using the fluorophore PI. Upon laser ablation, the radius of

29

PI positive cells also matched the radius of cavitation (Figure 7E). These results showing the internalization of two different fluorophores suggests a non-specific route of dye entry.
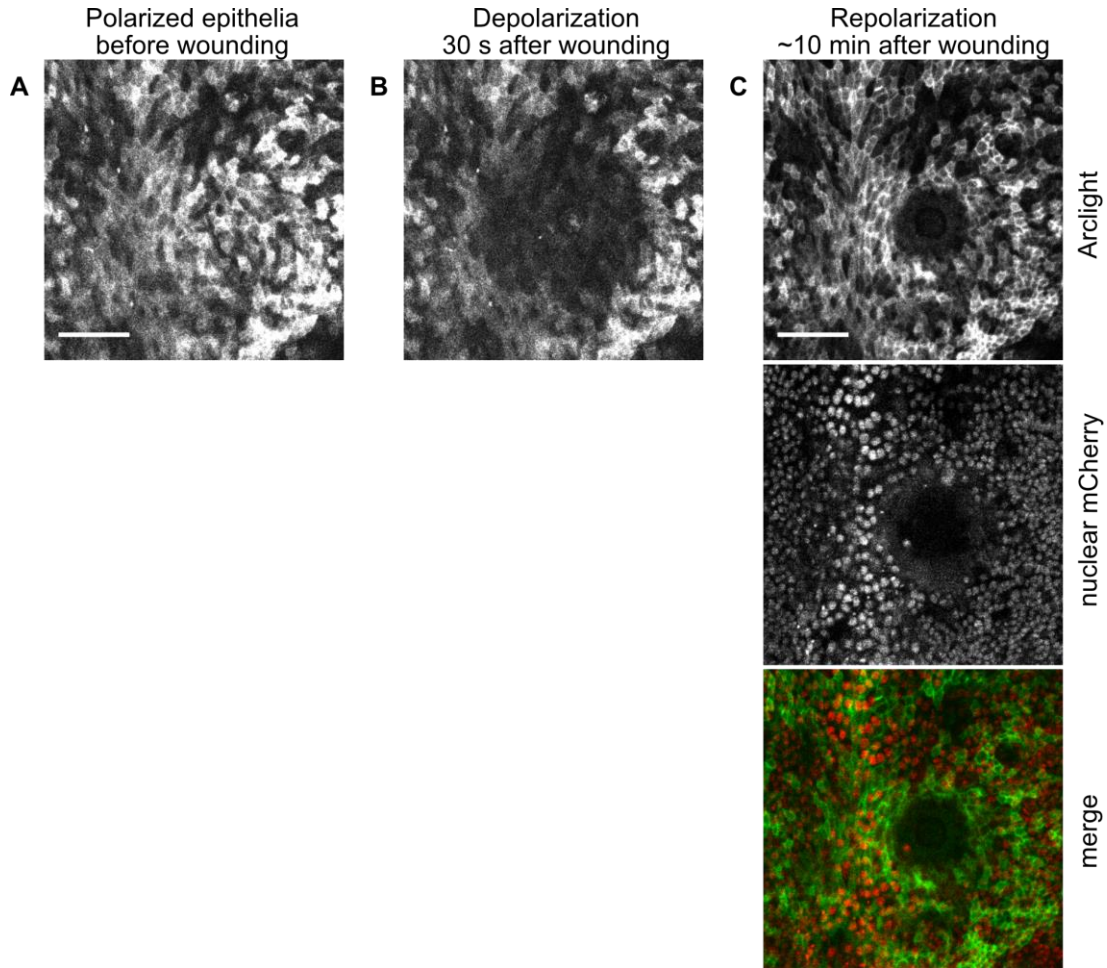
Figure 8: Cells in the cavitation footprint repolarize after wounding.
Panels show confocal images of electrical depolarization and repolarization over time after laser wounding of epithelial cells of the *Drosophila* notum. Cells express *pnr>Arclight* as a reporter of membrane electrical polarization. **A)** Fluorescence intensity is high 10 seconds before wounding. **B)** Fluorescence decreases after ablation, indicating depolarization in a region corresponding to the cavitation bubble footprint. **C)** Approximately 10 minutes after wounding, cells in the affected area repolarize (Arclight), indicating their ability to survive micro-tear damage. The only area that remains dark is the primary wound itself, as indicated by the lack of nuclear-mCherry staining (nuclear mCherry panel and merge). Scale bar is 50 µm.
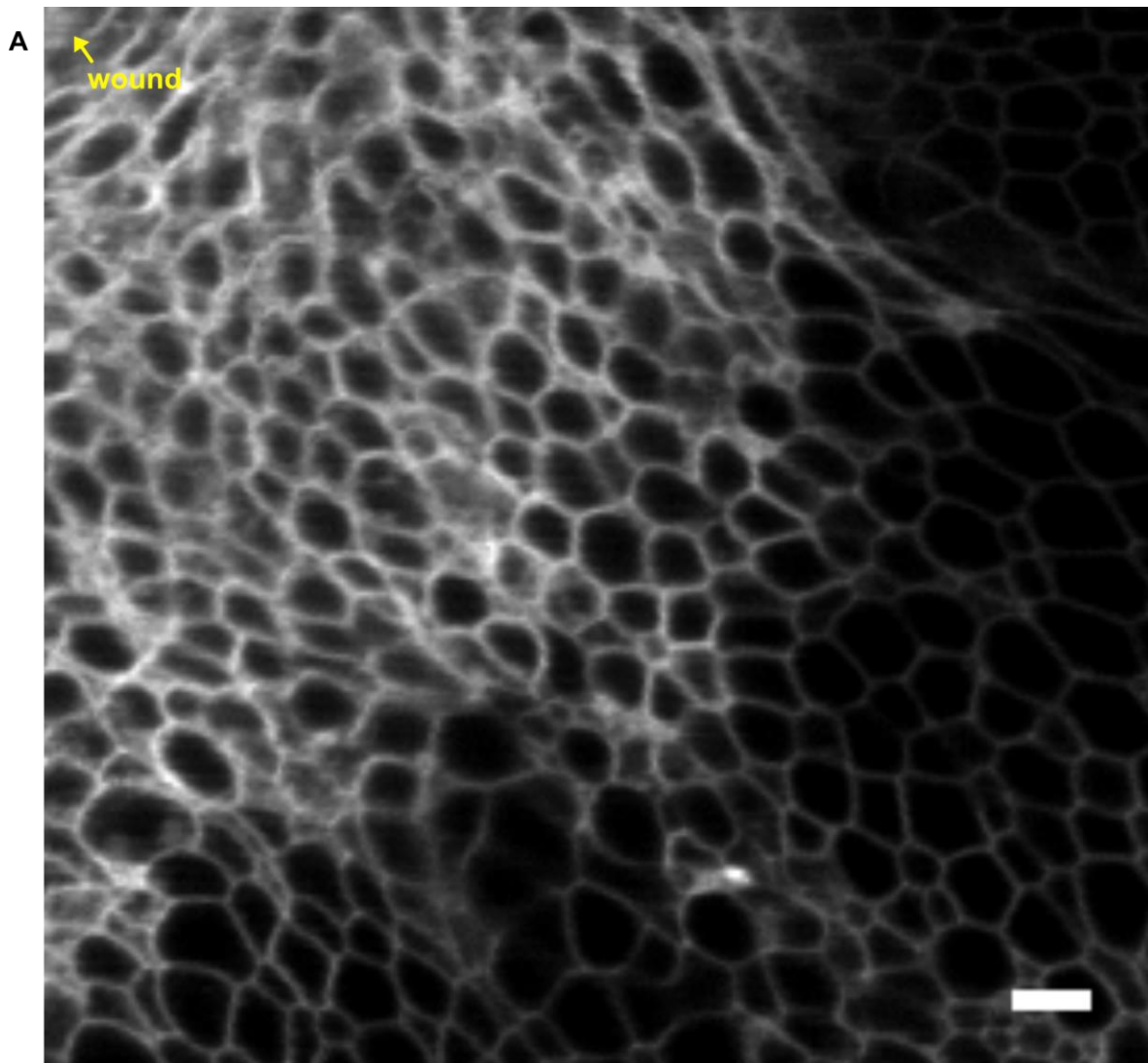
Micro-tear induced dye influx upon wounding labels plasma membranes of cells
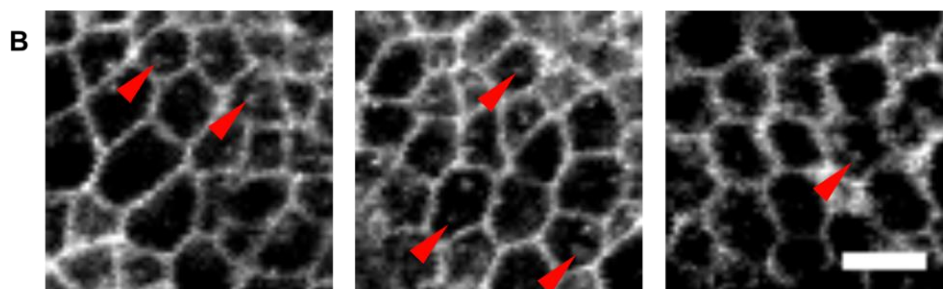
Endocytosis of dye appears as puncta in cells

Figure 9: Micro-tear induced dye influx labels plasma membranes.
FM 1-43 fluoresces upon binding lipid membranes. Prior to wounding, FM 1-43 cannot enter cells and labels the outer leaflet of the plasma membrane only. When micro-tears occur, FM 1-43 will enter cells and is expected to label the inner leaflet of the plasma

membrane, increasing its fluorescent intensity for cells with micro-tears. **A)** A high-resolution image of the apical cell surface of a wounded, wild-type wing disc taken within 10 minutes of dye application shows that FM 1-43 fluorescent intensity does increase for plasma membranes within the cavitation footprint. No dye-labeled endocytic vesicles are observed, confirming dye entry via micro-tears rather than endocytosis. Scale bar is 5 µm. The primary wound is out of frame, up and to the left of the image. **B)** Three example images of dye uptake by endocytosis in an unwounded wing discs in two wild-type flies. Tissue was incubated in FM 1-43 for 30 minutes to allow normal endocytic processes to internalize dye in endocytic vesicles (red arrowheads). Such puncta are not observed in the cavitation footprint after wounding in (A). Scale bar is 5 µm.

Third, we removed extracellular Ca^{2+} and measured the effects on wound-induced Ca^{2+} signals. We could not alter extracellular calcium concentrations *in vivo* in the notum, so we ablated wing discs *ex vivo* as above, but in media with or without calcium. Wounding in the presence of physiological $[Ca^{2+}]$ (2 mM) resulted in a calcium influx radius that matched the cavitation radius (Figure 7F). Wounding in calcium-free media did not eliminate cytosolic calcium influx, but the radius of this influx was just ~ 1/4 the cavitation radius (Figure 7E and Figure 7F). We conclude that *in vivo,* most of the cavitation-induced calcium influx is derived from an extracellular pool. Interestingly, the small region of calcium influx observed in calcium-free media has similar dimensions to the zone of high influx-site density identified in kymographs *in vivo* in the notum (Figure 4B). We discuss this connection and possible explanations in the Discussion. Nonetheless, the strongly reduced extent of initial calcium signals in calcium-free media, in concert with the cavitation-linked changes in membrane potential and dye permeability shown above, combine to strongly support the hypothesis that most of the initial calcium influx comes through cavitation-induced micro-tears in the cells' plasma membranes.

Additional wound-induced Ca^{2+} signaling on timescales of seconds to minutes.

After the initial influx, the region of high intracellular Ca^{2+} around the wound typically undergoes two stages of radially symmetric expansion. The first stage follows directly from the micro-tears generated in the footprint of the cavitation bubble and expands the high-Ca^{2+} region radially outward ~20 µm over a period of 15-20 seconds (Figure 10A, i-ii). This first expansion is eliminated by expressing RNAi against the *Drosophila* gap junction proteins *Inx2* or *Inx3* (Figure 10C and D), demonstrating signal propagation via gap junctions, consistent with some previous findings on other calcium waves[12,31]. The signal diffusing through gap junctions could simply be the leakage of Ca^{2+} from damaged to undamaged cells; alternatively, the first expansion could be mediated by

IP3, similar to calcium waves in wing discs and in other wounding systems[20,31,36]. Cytoplasmic calcium buffering makes direct Ca^{2+} transport through gap junctions less common than IP3 transport[244], but the estimated diffusion constants in Figure 6E suggests the presence of saturating concentrations of Ca^{2+} that could overcome cytoplasmic buffering and thus flow directly through gap junctions. After the brief expansion, this high-Ca^{2+} region then shrinks modestly before a second expansion becomes evident 40 to 200 s after ablation (Figure 10A, iii-iv). The second expansion is typically larger than the first and does not rely on gap junctions (Figure 10C and Figure 10D). After the second expansion, the high-Ca^{2+} region begins to shrink radially while sending off localized flares (Figure 10A, v-viii).

To further analyze the expansion of Ca^{2+} signals over time, we condensed each movie to a graph representing the expansion of the calcium wave with respect to time. This condensation involves radial averaging to identify the average edge of the calcium wave, and is thus most appropriate for analyzing time periods in which the high-Ca^{2+} region is radially symmetric – e.g., during the first and second expansions, but not once flaring commences. A collection of Ca^{2+} signal radius graphs for 24 laser ablation experiments is shown in Figure 10B. All of these experiments have a first signal expansion, but the presence of a second expansion depends on the presence and size of the primary wound. Large wounds (> 35-µm diameter, blue) always exhibited a second expansion, and intermediate wounds (15-35 µm, green) sometimes did, but small wounds (< 15-µm diameter, magenta) either had no second expansion or an atypical weak one. Furthermore, some samples exhibited a first expansion but no visible wound, likely due to slight mistargeting of the laser pulse, and never exhibited a second expansion. Thus, while the first expansion is tightly linked to cavitation-induced micro-tears, the second requires some cells to be damaged beyond repair and becomes more likely as the primary wound size increases.
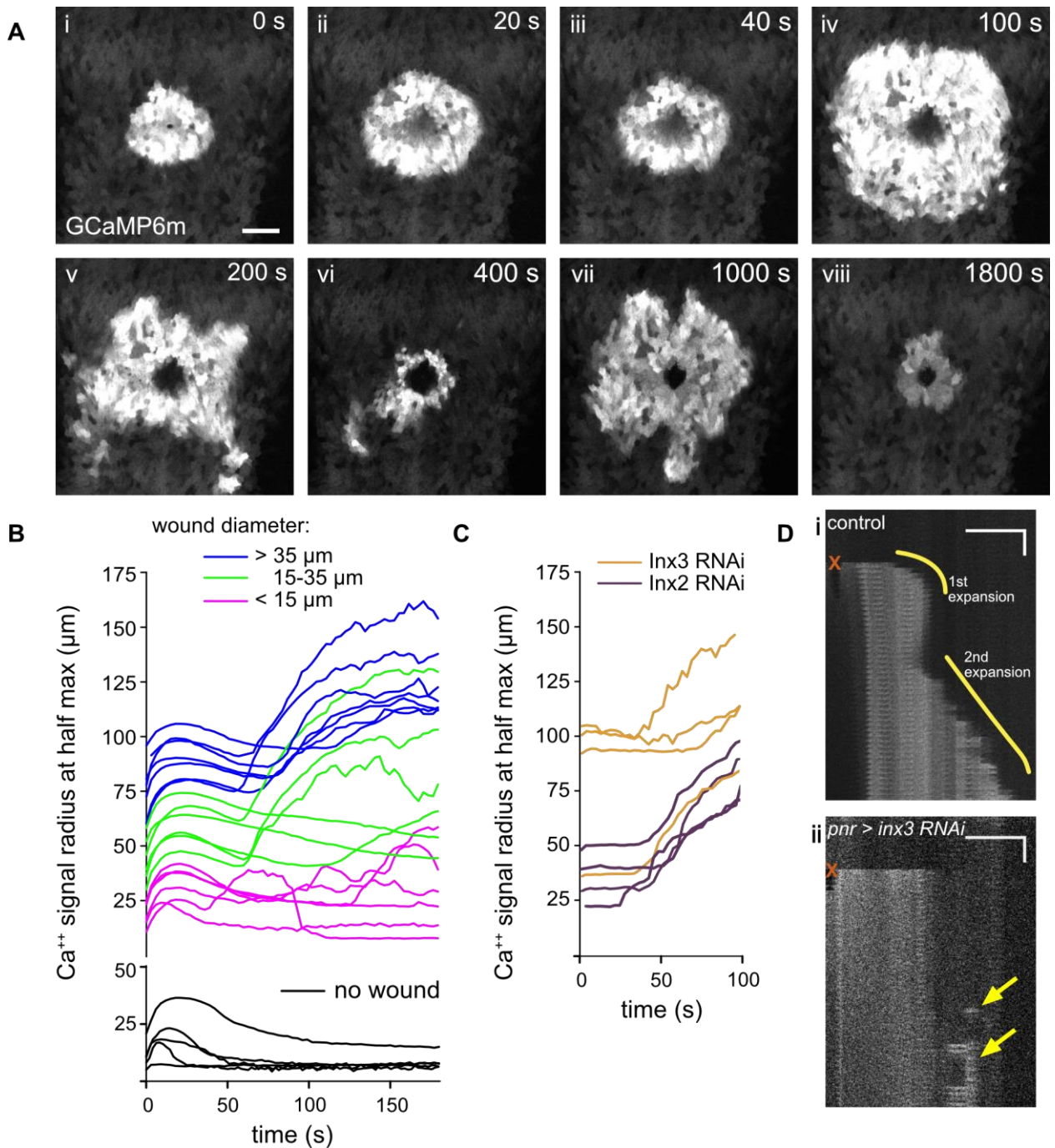
Figure 10: Two wound-induced calcium signal expansions occur on different timescales via different mechanisms.
A) Stills of *in vivo* live imaging of GCaMP6m in the notum. In the first frame after laser ablation, an increase of cytosolic calcium is observed in a ~5-7 cell radius around the wound (i). Seconds after wounding, the region of increased fluorescence expands to adjacent cells (ii) before contracting slightly (iii). The region of increased fluorescence then expands concentrically again (iv) before breaking into propagating, anisotropic calcium flares (v- viii). The flares continue initiating for >30 min after wounding while the

34

central region cyclically expands and contracts. Scale bar is 50 μm. **B)** The radial expansion of calcium signaling is plotted over time for 24 samples: each line represents a different sample with radii reported from the wound center. The initial region expands briefly in all samples before contracting. A second expansion may then occur and does so more frequently in larger wounds. No second expansion occurs when no wound is present. **C)** The radial expansion of calcium signaling over time for samples expressing either *Inx2* or *Inx3* RNAi in the *pnr* domain. A similar pattern was seen with a second *Inx2 RNAi* construct (data shown in Figure 16). Knocking down gap junctions blocks the first expansion but not the second. **D)** Kymographs showing the expansion of calcium signals over time for control (i) and *Inx3* knockdown samples (ii). The curved and straight yellow lines in controls indicate the normal shape of the first and second expansion. In *Inx3* knockdowns, the first expansion is absent; the second is perturbed but still occurs. Wound location and time are indicated by X, horizontal scale bar is 50 μm and vertical scale bar is 15 s.

We fit each expansion of the Ca^{2+} signal radius to a two-dimensional diffusion model to assess the kinematics and to begin to elucidate the signals driving each stage. This model assumes that some unknown signal X is released at a specific time (t_0) over a distributed area, given by an axisymmetric 2D Gaussian with $1/e^2$ radius σ_0 and total signal amount M. This signal diffuses with diffusion constant α and triggers a Ca^{2+} influx wherever the local concentration exceeds a threshold C_{th}. We acknowledge that the source likely is more complicated than a 2D Gaussian, but details of the distribution shape beyond its root-mean-square radius ($\sqrt{2}\sigma_0$) have no discernable effects over the time scales of our measurements. With this model, the time-dependent radius of the high-Ca^{2+} region (R_S) is thus given by

$$R_S^2 = 2\sigma^2 \ln\left[\frac{1}{2\pi\sigma^2(C_{th}/M)}\right] \quad \text{with} \quad \sigma^2 = \sigma_0^2 + 2\alpha(t - t_0) \qquad \text{Eqn 1.}$$

We fit models of this form to each expansion independently. The intervening and final shrinkage phases were not fit to this model because they involve additional mechanisms and timescales governing the return to baseline Ca^{2+} levels. The model fit the first expansion well with t_0 set to the time of laser ablation. This left three fit parameters: σ_0, α and C_{th}/M. The second expansion could not be fit well with $t_0 = 0$, so we instead set t_0 equal to the time at which each second expansion became apparent. Example fits are shown in Figure 11A, with the first expansions highlighted in red and the second in blue. The complete set of fits is shown in Appendix A, Figure 22. Note that the fitted equation has a degeneracy with respect to σ_0 and t_0, i.e., broadly distributed sources releasing a

signal at late times would be equivalent to narrowly distributed sources releasing the same signal earlier. This becomes a particular issue when fitting the second expansion because choosing earlier values for t_0 would lead to equivalent fits with smaller values for σ_0. Considering this degeneracy, fits to the second expansion have been back propagated (dashed lines in Figure 11A) to indicate that the driving signal could have been released before the second expansion became apparent. Notably, the back propagations do not go all the way back to $t = 0$. They instead intersect the time axis at a median time of 47 s (interquartile range of 29 to 61 s), strongly suggesting that the unknown signal driving the second expansion is either released tens of seconds after ablation or has a delay introduced by cellular signal transduction.

The best fit parameters for both expansions are compiled in the box-and-whiskers plots of Figure 11B. The $1/e^2$ radii of the initial signal distributions are comparable (24 versus 22 μm, assuming the second expansion starts when it first becomes apparent). On the other hand, the second expansion yields significantly smaller values for both the diffusion constant of the signal – median values for α of 53 versus 20 μm^2/s ($P = 1.5 \times 10^{-5}$; Mann-Whitney U test) – as well as for the relative signal threshold – median values for C_{th}/M of 2×10^{-5} μm^{-2} versus 6×10^{-6} μm^{-2} ($P = 7 \times 10^{-8}$). These results suggest that each expansion is driven by a different diffusive signal.

Interestingly, the diffusion constants for both the first and second expansion increase with wound size (Figure 11C). In fact, for large wounds, the diffusion constant of the first expansion approaches the value for free diffusion of calcium. These observations suggest a model in which larger wounds release more of both signals and thus yield larger effective diffusion constants by overcoming more of the buffering or binding capacity of the environment.
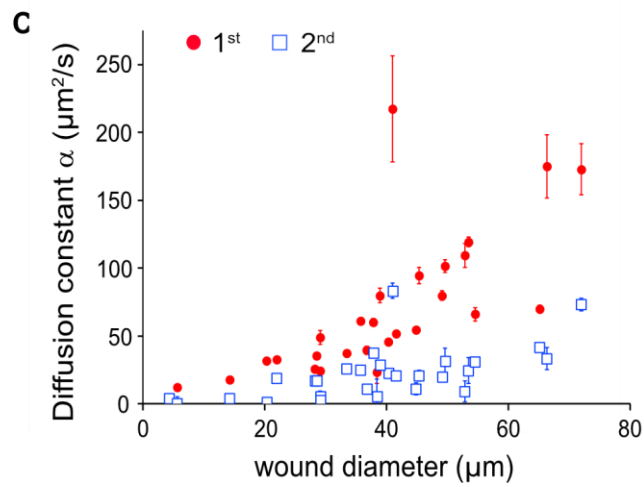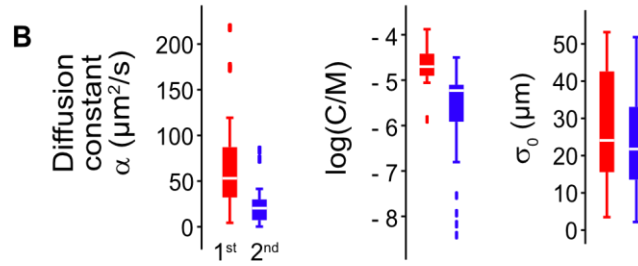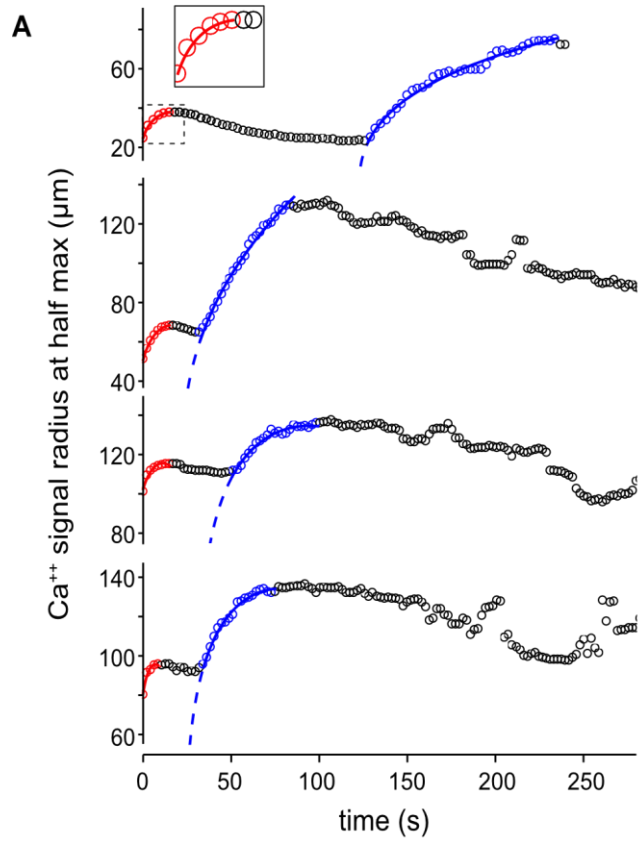
Figure 11: Parameterization shows distinct characteristics for each expansion.
A) Four examples showing the expansion of calcium over time. The initial and secondary expansions are highlighted in red and blue respectively. The solid lines show diffusional fits to each expansion; the dashed blue lines show back-projections of fits to the second expansion. The inset shows an expanded view of the fit to the data from the outlined region. The complete set of analyzed curves (N = 28) is shown in Appendix A, Figure 22. As a measure of goodness-of-fit, the standard errors of the regression for the four fitted first expansions were (from top to bottom) 0.19 µm, 0.18 µm, 0.95 µm, 1.04 µm and for the four fitted second expansions were (from top to bottom) 1.62 µm, 1.76 µm, 1.21 µm, 1.30 µm. **B)** Box-and-whiskers plots of the best-fit parameters for all first and second expansions: α is the diffusion constant; C/M is the ratio of the signal threshold to the amount released; and σ_0 is the $1/e^2$ radius of initial signal distribution. Median and interquartile range are displayed. **C)** Variability among the fitted diffusion constants for each expansion is partially explained by a dependence on the wound diameter.

Discussion

When a pulsed laser creates wounds in the epithelium of the *Drosophila* pupal notum, these wounds trigger a complex series of calcium signaling dynamics: a rapid influx into nearby surviving cells that matches the footprint of the laser-induced cavitation bubble; followed by a spreading of the high-cytosolic-calcium region via two sequential and concentric waves. These dynamics and a model that explains them are summarized in Figure 12.

The initial calcium influx occurs at hundreds of distinct loci and spreads throughout the affected cells in < 0.1 s. It spreads intracellularly with diffusion constants near that of free calcium, suggesting that high concentrations of calcium are flooding the cells and overcoming cytosolic buffering capacity. We propose that each locus corresponds to a cavitation-induced, plasma membrane micro-tear that allows calcium influx from the extracellular environment. In support of this model, cells in the cavitation footprint also become electrically depolarized and permeable to dye entry. Further, wounding in calcium-free media strongly reduces the extent of the initial rise in cytosolic calcium. These results could also be explained by cavitation-induced shear stresses opening mechanosensitive channels rather than micro-tears; however, the variety of observed effects implies a non-specific route of entry. We thus consider micro-tears more likely.
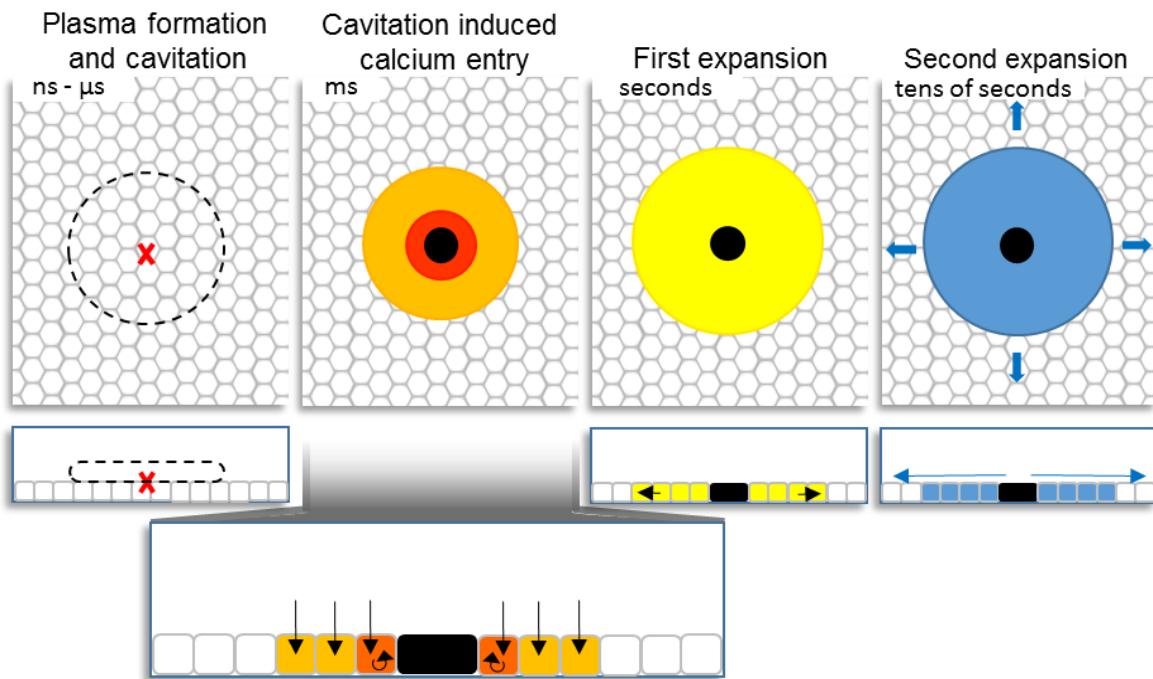
Figure 12: Summary of calcium signal dynamics after laser wounding.
Plasma formation and cavitation: Pulsed laser ablation generates a localized plasma at the laser focus (X), which then recombines and leads to expansion of a cavitation bubble (dashed black outline denotes maximum bubble radius).

Cavitation induced calcium entry: The cavitation bubble expands, damaging cells as it spreads. Close to the point of ablation, cavitation-induced shear stresses lyse cells, creating the primary wound (black). Cells close to the primary wound undergo extensive damage (dark orange). Micro-tears on the plasma membrane and in organelle membranes result in calcium influx from the extracellular space *and* internal stores milliseconds after wounding (black arrows). The shear forces applied to cells are attenuated as the cavitation bubble expands and slows. Cells far from the wound (light orange) exhibit plasma membrane micro-tear damage which allows calcium entry from the extracellular space (black arrows). Cells that were not lysed to create the primary wound survive cavitation damage.

First expansion: Seconds after wounding high concentrations of calcium that just entered the cells spreads intracellularly through gap junctions (black arrows) to neighbors (yellow).

Second expansion: After wounding a delayed second expansion of calcium spreads to cells distant from the wound (blue). This expansion is driven by extracellular ligand diffusion (blue arrows) but gap junctions may still have some role in generating a smooth wave front. Modeling of the second expansion shows it is characteristically different from the first expansion.

Membrane permeabilization is known to occur when laser-induced cavitation bubbles are used to get DNA, drugs or micro-particles into cultured cells via a process known as optoporation[194-199]. The shear stress associated with cavitation-bubble expansion and collapse can induce zones of acute cell lysis, cell necrosis, and membrane disruption[176,177]. We note similar zones of damage in our studies, observed as a primary wound surrounded by regions with a high and then low density of calcium influx sites (Figure 4B). This suggests more severe cellular damage close to the wound, which may be linked to the limited region of cytosolic calcium influx observed after wounding in calcium-free media. In fact, the radius of this limited region and the radius of high-density damage identified in kymographs represent similar fractions of the cavitation bubble radius (0.25 and 0.3 respectively). In this region proximal to the wound, the cavitation bubble and its shear stresses may generate additional micro-tears in organelle membranes that release calcium from the ER, mitochondria and Golgi or may trigger mechanosensitive GPCR-induced release of calcium from these same intracellular stores[245].

After the initial influx, the high-calcium region expands via two sequential waves. The first wave spreads with a diffusion constant of 32 to 87 μm^2/s. These rates still exceed that of cytosolically buffered calcium and suggest a simple model for the first wave based on the diffusion of excess calcium into neighboring cells through gap junctions. Indeed, variations in how well the excess calcium is buffered could explain this wave's wide range of fitted diffusion constants. Furthermore, this expansion is short-lived and short-ranged, which would be predicted as the calcium concentration decreases as it spreads and would thus be well buffered further from the wound. Although we favor this model in which the first expansion is caused by the direct diffusion of calcium to neighboring cells, the diffusion of IP3 has been identified as important for signal expansion in other wounding systems[20,31,36] and remains an alternative possibility.

The second wave begins ~45 seconds after wounding, but is not always present. The second wave occurs more frequently following larger wounds, suggesting its critical dependence on the extent of primary wound-induced damage. Interestingly, the second wave has a delayed start (at least 29 to 61 s after ablation) which may represent a delayed release of signal or time required for cells to transduce the signal into a calcium response. The second wave spreads with a diffusion constant of 7 to 30 μm^2/s, much slower than the first wave. This suggests distinct signals driving the two expansions, but further experiments are needed to identify the second wave's time delay and spread

mechanism. After the second expansion, the high-calcium region begins sending off asymmetric directional flares, likely representing waves of calcium-induced calcium release moving throughout the tissue. Each flare lasts tens of seconds, but new ones continue starting for more than 30 minutes after wounding. These flares are similar to calcium oscillations reported after epithelial wounds in zebrafish[9,133] and fly embryos[12].

Previous studies have identified two models for wound-induced calcium wave initiation: mechanosensitive calcium channels[8,12,20,31,133,245] and extracellular diffusible ligands[30,32,35,129,132,246]. In cell culture models, the driving signal for the calcium wave propagates extracellularly and very fast, with speeds ranging from 4.6 to 49.3 µm/s[25,35]. This is much faster than the speeds of calcium signal spread in our *in vivo* experiments: the median speeds were 2.9 and 1.7 µm/s for the initial portions of the first and second expansions, and these slowed in a diffusive manner. These rates are more similar to other *in vivo* wound healing models in which calcium signals propagate via gap junctions and spread at rates of 0.4 to 6.9 µm/s[12,31]. Signal propagation via extracellular ligand diffusion may occur in the *Drosophila* notum during the second wave, as this expansion is not dependent on gap junctions, but the ligand would have to diffuse much more slowly than those identified in cell culture models.

Once calcium enters a cell, regardless of how, it is a master regulator of wound healing. Calcium regulates Rho[16,33,40] and the actin cytoskeleton[8,15], activates JNK signaling[21], prevents apoptosis[23], and increases hydrogen peroxide and inflammation around wounds[12]. Calcium waves alert cells to the presence of a wound and permit the activation of healing programs[133]. Given the variety of types of wounds that may need to be healed, multiple mechanisms may have evolved to initiate calcium signaling cascades. Our study of laser wounding has identified at least three different mechanisms. The first calcium response is extracellular calcium entering the cytosol through plasma membrane micro-tears. Although this effect is driven here by laser-induced cavitation bubbles, similar cellular and tissue damage are inflicted simultaneously during puncture wounds[187,188]. In fact, pulsed-laser ablation is similar to a localized puncture accompanied by a wider crush injury. In either case, the calcium influx through micro-tears is in effect a single-cell response to cell-level damage; it becomes a tissue-level response as high cytosolic calcium spreads to neighboring cells by diffusion through gap junctions. This so-called first wave thus involves a second distinct mechanism by which surrounding undamaged cells experience a rise in cytosolic calcium. Importantly, this expansion of a single-cell

41

wound signal to neighboring cells suggests a continuum between single-cell and tissue-level wound responses.

Finally, if the region of ablated cells is large enough, a delayed signal initiates another wave of cytosolic calcium increases, which we term the second expansion. The unknown signal driving this wave represents a third mechanism governing calcium increases after wounding. Because this third mechanism occurs only after a discontinuity or hole appears in the epithelium, and not simply after cellular micro-tear damage, this signal may arise from cell mechanics or cell lysate or dying cells around the primary wound margin. It is noteworthy that separate, but overlapping calcium signals emanate from the wounded region due to both cell-level damage and tissue-level damage, albeit by different mechanisms. Our results suggest the interesting possibility that signaling from many types of damage may converge on increasing cytosolic calcium levels to regulate both single-cell and multicellular wound-healing programs.

Conclusions

Wounds created via laser ablation contain single-cell damage and tissue damage, similar to naturally occurring puncture or crush wounds. Each damage mechanism drives its own calcium signal dynamics. Single-cell damage arises from cavitation-induced, plasma membrane micro-tears and results in direct calcium influx from the extracellular environment followed by diffusive expansion into neighboring cells. Tissue damage in the form of a primary wound at the ablation site results in a delayed calcium wave that expands well beyond the cavitation bubble footprint. This second wave occurs more frequently following larger wounds. Our kinematic analysis narrows and informs the search for calcium wave initiation and propagation mechanisms by showing that both expansion events fit diffusive models that are consistent with previously observed rates of calcium wave propagation *in vivo*, but are driven by different signals. Finally, this laser wounding model exhibits exaggerated, but controllable single cell damage and may be useful for future investigations at the intersection of single-cell wound healing and tissue wound healing.

CHAPTER 3

AN UNKNOWN LIGAND MEDIATES INFLUX AND PROPAGATION OF CALCIUM
VIA THE GAQ SIGNALING CASCADE

Introduction

Throughout re-epithelialization, cells distant from the wound contribute to wound closure[8,64,75,83,247,248]. Furthermore, these cells can be observed to participate in wound closure within minutes of wounding[8]. In the *Drosophila* notum, calcium dynamics have been shown to correspond with these early wound responses[8]. Our goal is to build a more complete understanding of early wound healing by determining how these calcium waves are initiated and propagated. In the previous chapter we demonstrated that cavitation-induced micro-tears permit direct calcium entry into cells. In this chapter we aim to identify the mechanisms of initiation and propagation for the larger, second calcium expansion by providing additional analysis and characterization. This second expansion seems to be a tissue-level wound response as it only occurs when a true wound, or break in the cell monolayer, is present (Figure 10B). We term the large, second expansion a wound-induced calcium wave.

Mechanisms of wound-induced calcium wave initiation and propagation are highly variable in the literature. Often, these mechanisms seem mutually exclusive. For example, gap junctions are required in some models – usually *in vivo* models[12,21,31,36] but also in cell culture models[34,37] – and not in others[25,30,32,34,37,38]. When gap junctions are not required, investigators usually find a diffusible ligand initiates the calcium wave. This diffusible ligand may, or may not, be ATP[30,32,38,42]. Tissue mechanics are often implicated in calcium wave initiation, but the mechanism of action is unclear[8,10,20,31,38-42]. Mechanical perturbations of the tissue may induce ATP release which induces the calcium influx[30,32,38,42] or mechanical perturbations may somehow promote calcium release from ER stores[31,39]. We aim to characterize the calcium wave in the notum to determine similarities and differences between the calcium wave we observe and those reported in the literature. We observe common features, and a few differences, from both *in vivo* and *in culture* calcium waves around a single wound in the *Drosophila* notum.

Like other wound-induced waves *in vivo*, the calcium wave in the notum propagates slowly: compare 0.4 to 6.9 μm/s in other models[12,31] vs 1.7 μm/s in the notum.

43

In this chapter, we show the wound-induced wave in the notum exhibits similar qualitative characteristics to other *in vivo* waves, such as oscillations and flares. We also observe some differences between our model and previous *in vivo* work. Research in worms and flies has implicated TRPM, a putative mechano-sensitive calcium channel, in wound-induced calcium influx[8,12,20]. Other research in the fly wing disc has shown that prodding the tissue is sufficient for wave formation[31,39]. Results presented in this chapter demonstrate that a wave occurs when the tissue is broken by a stab wound, but not when the tissue is mechanically distorted by prodding. Instead, we provide additional analysis suggesting formation of the wound-induced calcium wave is driven by extracellular diffusion. In this way, the expanding wave we describe is also similar to the fast propagating waves characterized in cell culture models[23,24,34,35,129]. While calcium in the notum propagates much slower than 4.6 to 49.3 µm/s as observed in culture[25,34,35], both waves seem to be driven by ligand diffusion[25,30,32,34,37,38] (see also Figure 10C and D). The estimated diffusion constant for this propagating signal (7 to 30 μm^2/s, Figure 11) indicates a triggering molecule the size of insulin (~6 kD) or larger could be responsible for wave initiation. There is precedence for molecules of various sizes serving as such ligands. DAMPs are ligands that diffuse from damaged cells and activate signal transduction cascades in the surrounding tissue and can be small molecules, metabolites, or even proteins[84,86-88]. Their release from cells can occur through exocytosis or necrosis[94,95,100]. Well characterized DAMPs include ATP, HMGB1 (~25 kD), and HSPs (~70+ kD)[84,94,100]. The observed diffusion constant calculated in Figure 11 could also indicate buffered diffusion of a smaller triggering molecule, as seen with ATP diffusion[100,152-156].

To understand the signaling cascade mediating the wound-induced calcium wave, we first targeted potential downstream effectors of the unknown ligand. There are a few canonical routes by which a ligand can induce calcium influx. The ligand could bind a ligand-gated ion channel and allow calcium entry directly from the extracellular space or it can induce calcium influx from the ER by activating GPCR or Receptor Tyrosine Kinase (RTK) signaling cascades[249]. In both of these signaling cascades, receptor activation leads to activation of Phospholipase C (GPCR signaling cascade summarized in Figure 13). The RTK pathway activates PLCγ while the GPCR pathway activates PLCβ through the Gαq G-Protein[1]. Phospholipase C (PLC) generates IP3 which binds IP3 receptors (IP3R) on the ER membrane and allows calcium release. Data from a *C. elegans* single cell wounding model describes wave induction which occurs through Gαq signaling[20],

therefore we chose to target GPCR signaling cascades first. *Drosophila* have significantly fewer GPCRs than vertebrates (flies only have 111 GPCRs while humans have over 800) and only one Gαq G-protein. This one Gαq G-protein is a bottleneck for GPCR activity. By specifically targeting the Gαq G-Protein, we can distinguish GPCR signaling from RTK signaling without yet identifying the specific ligand or receptor.

In this chapter we use a novel, internally controlled, split-expression system to reveal both nuanced and dramatic changes that occur in wave expansion as a result of inhibiting Gαq signaling cascades. Our data suggests a ligand diffuses from the wound area, binds a GPCR, and induces calcium release from internal ER stores.
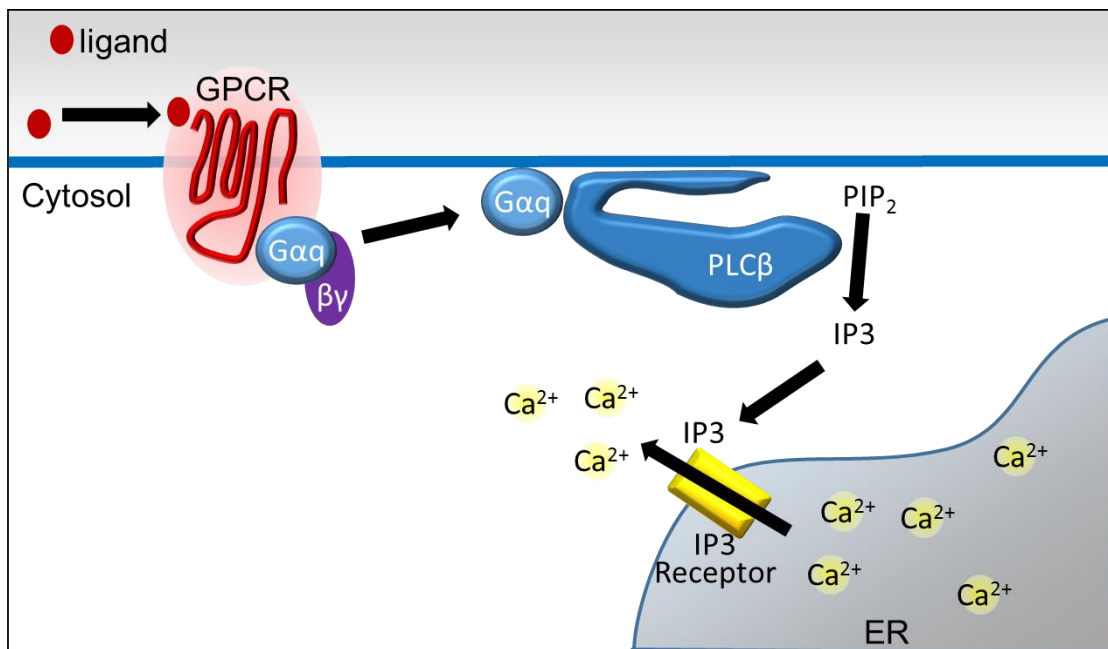
Figure 13: Simplified schematic of canonical, GPCR-activated calcium release.
A ligand diffuses extracellularly and binds a GPCR. This binding causes a conformational change in the GPCR which activates the Gαq. Gαq then dissociates from the GPCR and stimulates the activity of PLCβ. PLCβ hydrolyses PIP_2 to create IP3. IP3 diffuses through the cytosol and binds IP3 receptors located on the ER membrane. These receptors are calcium channels, and when bound to IP3, allow the passage of calcium from inside the ER to the cytosol.

Materials and Methods

Fly lines

pnr-Gal4,tub-Gal80^{ts} was used to regulate the spatial and temporal expression of UAS transgenes. *UAS-Inx2 RNAi* #1 (Fly Base ID: FBst0029306), *UAS-Inx2 RNAi* #2 (Fly

Base ID: FBst0474063), *UAS-Inx3 RNAi* (Fly Base ID: FBst0060112), *UAS-Gαq RNAi* (Fly Base ID: FBst0033765), *UAS-PLCβ #1 RNAi* (Fly Base ID: FBst0031270), *UAS-PLCβ #2 RNAi* (Fly Base ID: FBst0033719), *UAS-IP3sponge-M49[#1]* (gift from Baehrecke Lab), *UAS-IP3R RNAi #1* (NIG stock number 1063R-1), *UAS-IP3R RNAi #2* (Fly Base ID: FBst0025937), and *UAS-nucmCherry* (Fly Base ID: FBst0038424) were expressed in the notum. *Actin-GCaMP6m*, containing the complete 4 kB promoter, was used to express GCaMP6m in the dorsal epithelial tissue of the fly. For stabbing and poking experiments, *pnr-Gal4* (Fly Base ID: FBst0025758) was used to drive expression of *UAS-GCaMP6m* (Fly Base ID: FBst0042748). w^{1118} was used as wild type.

Mounting pupae, laser ablation, and live imaging

Pupae were mounted, ablated, and imaged using the protocols described in Chapter 2. For internal control split-expression experiments, the experimental region was identified prior to wounding using *UAS-nucmCherry*. Without moving the stage, laser ablation and live imaging were commenced within one minute after an image of the experimental region was saved. We targeted a point on the edge of the experimental domain for laser ablation.

Stabbing and poking pupae

Pupae were dissected from their pupal case as described in Chapter 2. A piece of double sided tape was placed on a microscope slide and pupae were mounted on the tape with their ventral side down, touching the tape. The pupae were aligned so their apical/posterior axis's pointed in the same direction. The slide was mounted on the stage of a Zeiss Axio M2 epifluorescent microscope and imaged with a 5x objective. Pupae were stabbed or poked by hand in the GCaMP6m expressing region during imaging with a chemically sharpened tungsten needle or a blunt probe (Fisher, cat. #08965A), respectively. Scans were taken every 1 second or every 2 seconds.

Image processing and analysis

Image processing and analysis was performed as described in Chapter 2. To analyze the spread of calcium over time in the internal control split-expression experiments, we used the angle feature of the ImageJ Radial Profile Angle Plot plugin. This tool allowed us to specifically select and analyze the control region only and the experimental region only. Data from this plug in was processed via the custom MATLAB script as described above.

Results

The wound-induced calcium wave expands and fades multiple times over an extended period.

From the second chapter, we know waves in the notum and waves in other *in vivo* models propagate with comparable speeds: 1.7 µm/s vs 0.4 to 6.9 µm/s[12,31], respectively. We sought to determine what other similarities the wound-induced wave in the notum has with other *in vivo* models. Other wounding models show calcium oscillates (exhibits re-occurring expansions) and flares around the wound. Waves in the *Drosophila* embryo expand and fade up to three times within twenty minutes of wounding[12]. Time lapse imaging of zebrafish tail wounds shows transient increases in cytosolic calcium levels in cells following the propagation of the wave front[9], resembling flares. Flares and oscillations also spontaneously occur in tissue that has not experienced a break in the epithelial cell layer[31,36,39].
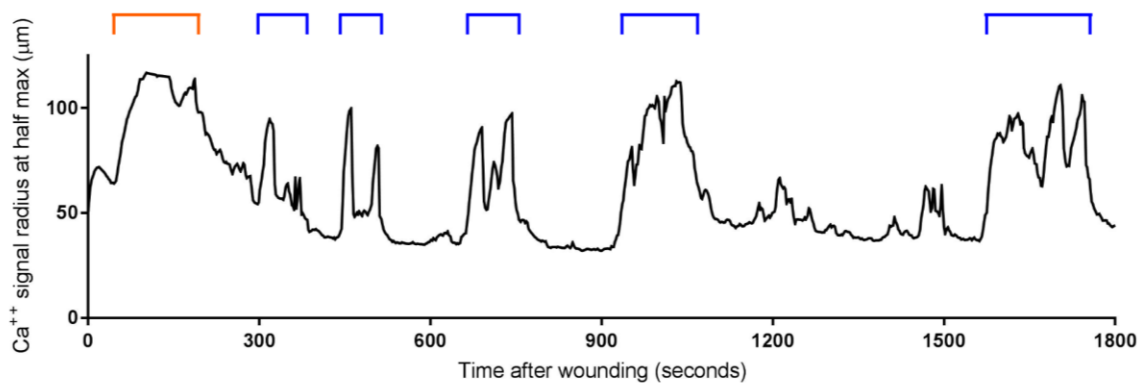
Figure 14: The wound-induced calcium wave oscillates multiple times for up to an hour after wounding.
Graph shows the expansion of calcium over time in a sample wounded using a pulsed laser. The orange bracket indicates the wound-induced second expansion described in Chapter 2 and in previous figures. The blue brackets indicate periods of oscillation that occur minutes after wounding.

To further understand the characteristics of the wound-induced calcium wave, we performed extended imaging time courses. These time courses have revealed that the wound-induced expansion propagates around the wave for approximately five minutes before fading (orange bracket in Figure 14). The wave reappears minutes later and oscillates multiple times over the course of 30 minutes (blue brackets in Figure 14). Our quantification methods use radial averaging. Therefore, the graphs accurately depict symmetrically expanding waves but not asymmetric flares. Examples of the asymmetrical

47

flares can be observed in the stills in Figure 10Av-vii. Notably, oscillations and flares are not reported in cell culture models of wounding.

A wound-induced expansion occurs when the tissue is punctured but not mechanically perturbed.

Other *in vivo* work suggests mechanically depressing tissue with a blunt tool can drive the formation of the calcium wave[31,39]. When wing discs are cultured *ex vivo*, fly lysate must be present to generate a mechanically-induced calcium wave. Furthermore, while mechanical prodding alone is not sufficient to generate a calcium wave in an *ex vivo* disc, adding fly lysate to the culture media is sufficient[31,39]. Fly lysate is the supernatant of ground up flies. It will contain all of the ligands and wound signals that can be found in cell lysate released upon wounding. It is not clear if the mechanically-induced waves require the presence of an additional wound signal to generate a calcium wave or if they simply need paracrine or endocrine factors found *in vivo*. Mechanically-induced calcium waves can be generated *in vivo*, by punching intact wing discs inside of living larvae. Cell lysate, and accompanying wound-induced signals, are not expected to be present in this system as no cells are actually damaged. We wanted to determine if cell lysate was required for calcium wave formation or if mechanical prodding in an *in vivo* environment was sufficient. To generate cell lysate we stabbed the notum with a fine needle and to mechanically perturb the tissue we prodded the notum with a blunt tool. Figure 15 shows the results of this analysis. When the tissue is stabbed a calcium wave expands around the wound (Figure 15A). This wave is qualitatively similar to waves generated via laser ablation and even exhibits stochastic flares on the wave margin. A future kinematic analysis of these waves is discussed in Appendix C. No wave appears when the tissue is vigorously poked, even after multiple attempts (Figure 15B). If the same notum is stabbed, a calcium wave does appear (Figure 15Bix and x). This data shows that mechanical perturbations alone in our *in vivo* system are not sufficient to induce a calcium wave. We have begun to expand on this work by genetically modifying tissue tension at laser ablation wounds, which generate cell lysate. Preliminary findings from these experiments can be found in Appendix B.
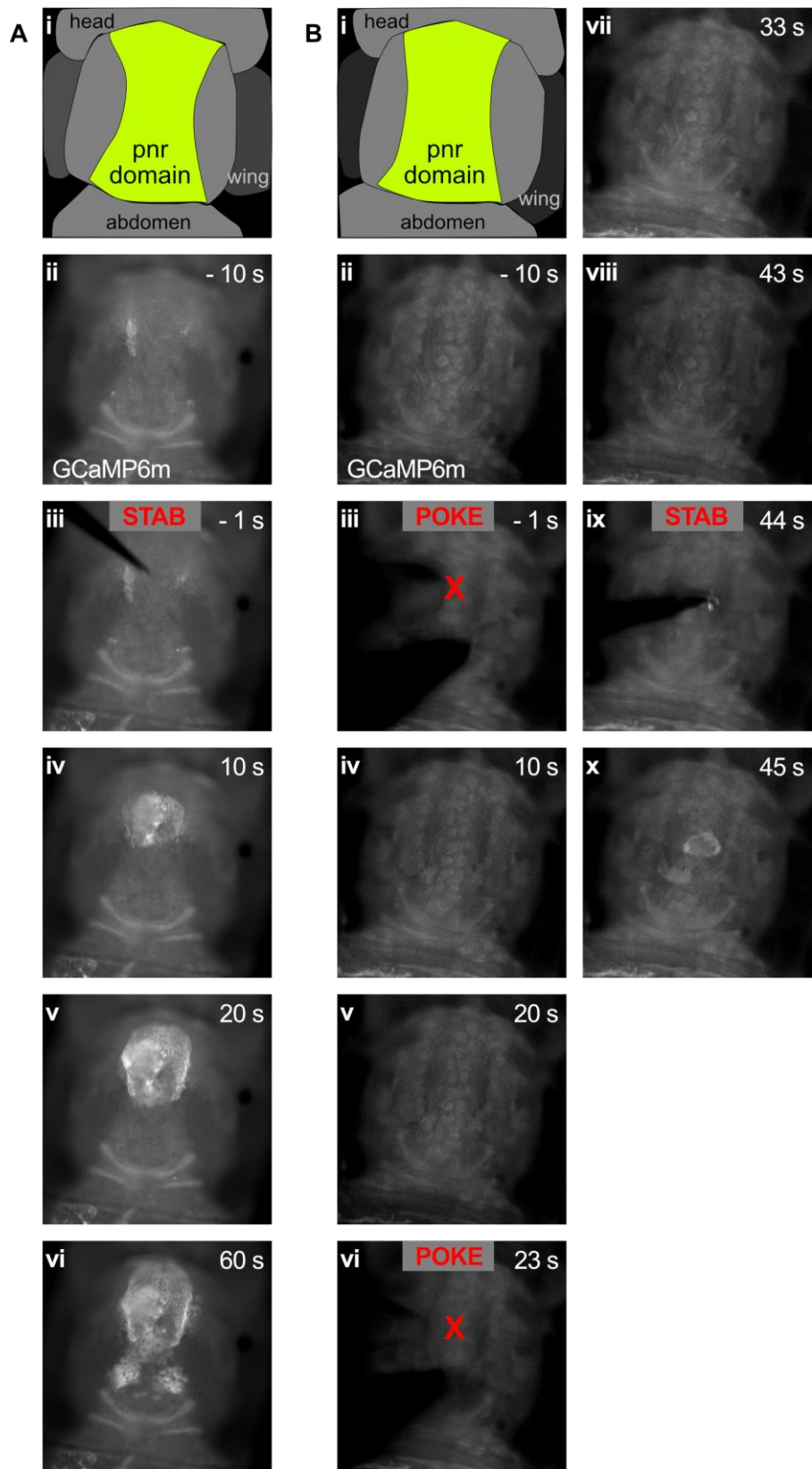
Figure 15: Calcium waves occur when the tissue is stabbed but not mechanically prodded.
A) Stills showing a stab wound over time. The general form of the pupae and the *pnr* domain, where GCaMP6m is expressed, is outlined (i). Basal fluorescence of GCaMP6m is observed in the *pnr* domain prior to wounding (ii). Upon stabbing (iii) a calcium wave expands from the wound (iv, v, vi). The calcium wave is large and spreads across the entire *pnr* domain. While it is difficult to appreciate from the stills, the edge of the calcium wave exhibits stochastic flares like those seen in laser ablation wounds. **B)** Stills from mechanical prodding over time. The general form of the pupae and the *pnr* domain, where GCaMP6m is expressed, is outlined (i). Basal fluorescence of GCaMP6m is observed in the *pnr* domain prior to wounding (ii). Upon poking with a blunt tool (iii), no calcium wave occurs (iv, v). The pupae is poked again (vi) but still no calcium wave occurs (vii, viii). To ensure the pupae was viable and capable of a calcium response the pupae was stabbed (ix). A calcium wave was observed immediately upon wounding (x). Red X's indicate the location of the poke. The needle and blunt probe are visible as black objects in the panels.

The wound-induced expansion occurs when gap junctions are knocked down, but appears qualitatively different than controls.

In Chapter 2 we reported that gap junctions are required for the first expansion of calcium but not the second, wound-induced expansion (Figure 10B). We concluded from this data that an extracellular ligand drives the wound-induced expansion. In this chapter we further characterize and discuss gap junction knockdowns and the resulting expansion patterns. Even though the wound-induced expansion occurs in gap junction knockdowns, we show they still have a role in calcium dynamics around wounds.

Gap junctions form channels between neighboring cells and allow the passage of molecules and small peptides (approx. 1 kD or smaller) from one cell to another[250]. *Drosophila*'s gap junctions are comprised of innexin proteins, which are homologous to vertebrate connexins. Three gap junction proteins are expected to be expressed in this epithelial tissue: *Inx2*, *Inx3*, and *Ogre*. These proteins form heteromeric structures so by knocking down one of these genes we expected to abolish the activity of the entire gap junction[251]. Unlike controls, unwounded gap junction RNAi samples had frequent, transient single cell calcium increases (Figure 16Bi). As expected, the micro-tear induced release of calcium occurred but did not expand to neighboring cells upon wounding (Figure 16Bii-iii). The lack of micro-tear induced expansion confirms that gap junctions have been successfully knocked down in the experiment. The wound-induced expansion spreads to distant neighboring cells over time (Figure 16Bv and vi). This expansion appears "spotty" and uneven because the calcium wave front frequently skips over cells as it expands. We expand on the "spotty" appearance of this wave in the discussion.

A control

i −15 s
GCaMP6m

ii 0 s

iii 24 s

iv 60 s

v 120 s

vi 180 s

B Inx2 RNAi #2

i −15 s
GCaMP6m

ii 0 s

iii 24 s

iv 60 s

v 120 s

vi 180 s

C Inx2 RNAi #2

wound diameter:
> 35 µm
15-35 µm
< 15 µm

Ca++ signal radius at half max (µm)

time (s)
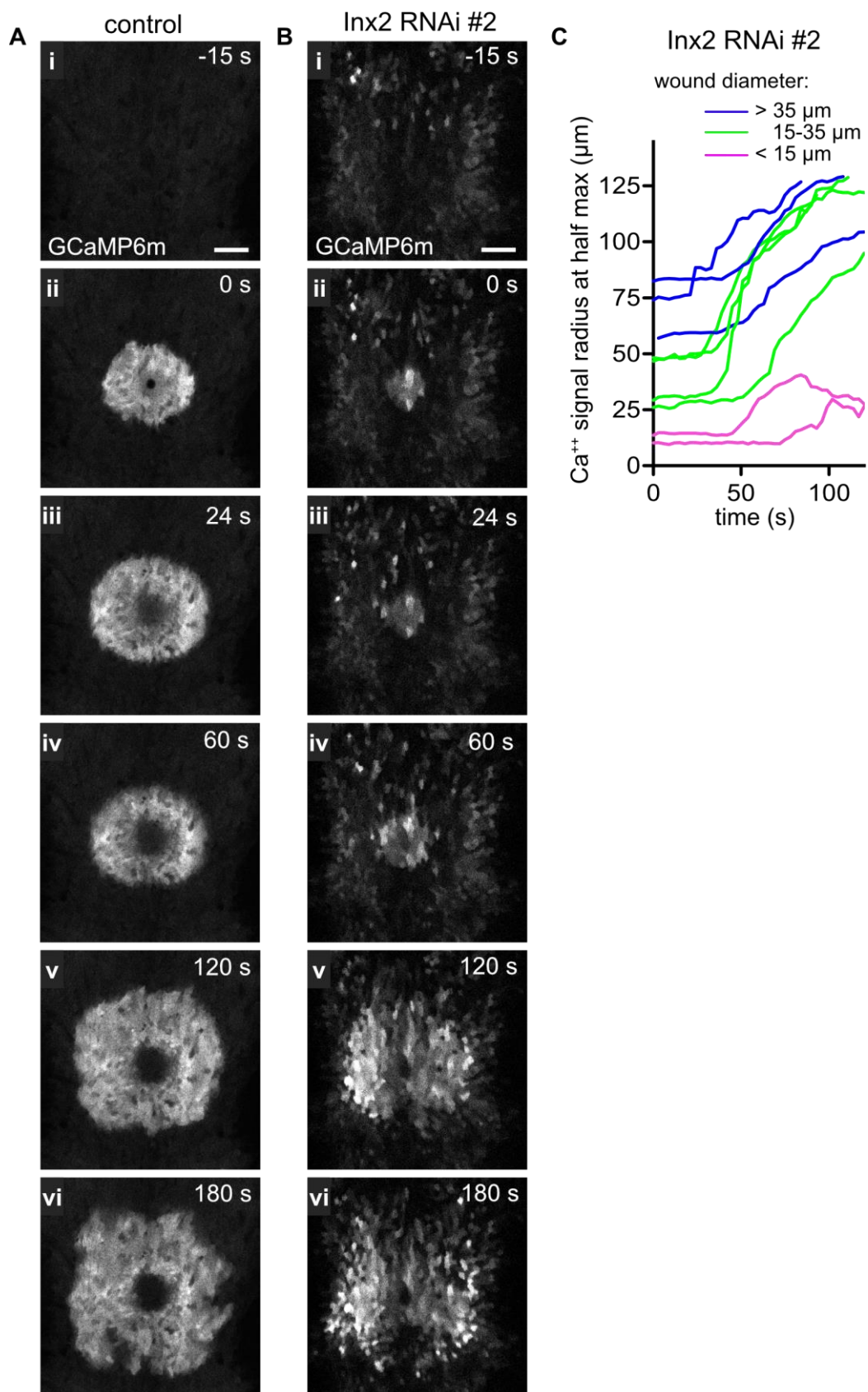
Figure 16: Gap junctions are not required for the wound-induced expansion.
A) Stills of a calcium wave visualized by GCaMP6m in wild-type tissue. There is no significant basal calcium activity prior to wounding (i). Upon wounding, cavitation-induced micro-tears allow calcium entry in the footprint of cavitation (ii) which expands to neighboring cells (iii) before fading (iv). A larger, wound-induced concentric expansion occurs (v) before breaking into calcium flares along the leading edge of the wave (vi). Scale bar is 50 µm. **B)** Stills of a calcium wave visualized by GCaMP6m in tissue expressing *Inx2 RNAi* #2. Prior to wounding we observe single cell calcium flickers throughout the tissue (i). Upon wounding, cavitation-induced micro-tears allow calcium entry in the footprint of cavitation (ii) which does not expand to neighboring cells as gap junctions are not functional (iii). A larger, wound-induced concentric expansion occurs (iv, v). Instead of propagating flares, single cells on the edge of the calcium wave flicker on and off (vi). Scale bar is 50 µm. **C)** Traces show the expansion of calcium over time for *Inx2 RNAi* #2 samples. One line represents one sample. Samples in magenta have wound diameters smaller than 15 µm, samples in green have wound diameters between 15-35 µm, and samples in blue have wound diameters larger than 35 µm. Note that the first expansion does not occur when gap junctions are knocked down.

As in Figure 10B, the occurrence of robust wound-induced calcium waves are predicted by wound size (Figure 16C). Small wounds, less than 15 µm in diameter, have small, atypical expansions while wounds larger than 15 µm in diameter have robust expansions. One interpretation of the stab vs. poke data in Figure 15 is that cell lysate is required for the wound-induced calcium expansion. When that interpretation is applied to these results, it suggests smaller wounds release less cell lysate, which results in low concentrations of ligand that cannot sustain a large expansion.

A custom built, genetic split-expression system can be used to compare experimental conditions directly to internal controls in the same wound.

Our goal is to explore the mechanism of initiation and propagation of the wound-induced calcium wave. To improve our experimental platform, we designed a split-expression system in the fly notum that enabled us to perform genetic experiments with an internal control at the same wound. Our split-expression platform allowed us to drive the expression of a gene of interest in one half of the tissue while the other half remained wild type. By wounding on the margin of the RNAi expression domain we observed how the calcium wave expanded differently into the experimental region versus the wild-type control region. With this system we can directly compare and quantify differences resulting from changing the experimental variable, which is highly advantageous. Even laser wounds can be subtlety different from sample to sample so without an internal control, it can be difficult to identify small, nuanced changes between experimental conditions.

To create this platform, we took advantage of the natural hourglass shape of the *pnr* expression domain in the notum which covers approximately one third of the dorsal epithelium. We used the *Gal4-UAS* system to drive expression of our gene of interest (GOI) and a nuclear mCherry reporter (to precisely outline domain edges) in the *pnr* domain using *pnr-Gal4*. *Tub-Gal80^{ts}* is a temperature sensitive construct that prevents Gal4 from binding UAS at the permissive temperature and thus confers temporal control of our GOI expression. We added this construct to our system so that we could turn on GOI expression after critical periods of development and before experimentation.
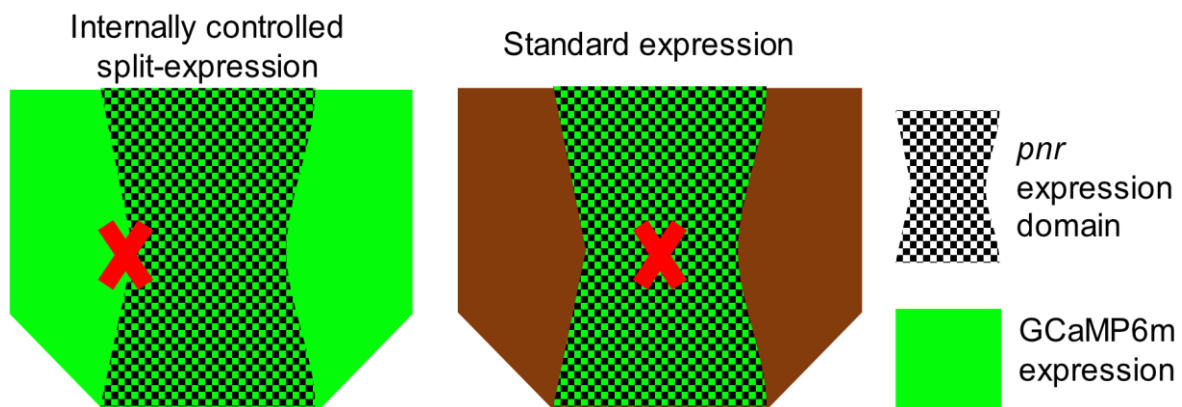
Figure 17: Diagram of internally controlled split-expression system
The panels above represent the epithelial tissue of the pupae notum. The checkered, hourglass-shaped region is the *pnr* expression domain, where nuclear mCherry reporter and GOI are expressed. In the internally controlled, split-expression system GCaMP6m is expressed throughout the tissue. Wounding on the margin of the *pnr* domain (red X) will result in calcium expansion into both the control region (left of X) and the experimental GOI region (right of X). In contrast, using a standard expression system, the GCaMP6m is expressed only in the *pnr* region. A wound is made in the center of the domain and all surrounding tissue expresses the GOI.

Because we were using the UAS-Gal4 system to generate spatial expression of our GOI, we could no longer use *UAS-GCaMP6m* to visualize the calcium wave. It was necessary to drive GCaMP6m in the entire epithelia so that we could reliably compare calcium wave expansion in control and experimental regions. After unsuccessful attempts to use an alternative driver-promoter system (the QF-QUAS system), we decided to directly drive GCaMP6m expression with an actin promoter. A key feature of this construct is that it contains the full 4.4 Kb genomic enhancer sequence of actin, and therefore contains regulatory elements that drive ubiquitous expression, instead of a

commonly used but less reliable 2.6 Kb sequence[252,253]. Despite the fact that actin is a strong promoter, it does not express GCaMP6m as strongly as the *Gal4-UAS* system, which has an amplification step. As a consequence, our *Actin-GCaMP6m* construct does not fluoresce as strongly as *UAS-GCaMP6m* constructs we have used.

The *pnr* domain we are using for this system splits the same epithelial tissue into a control domain (non-*pnr*) and an experimental (*pnr*) domain. The *pnr* domain is genetically distinct from neighboring tissue so we performed controls to determine whether this difference had any effect on calcium wave initiation and propagation. When both domains are functionally wild type, calcium wave initiation and propagation is symmetrical around the wound (Figure 18A). As a proof of principle, we used *Inx2 RNAi* to validate this system because of the clear "spotty" phenotype *Inx2 RNAi* produces. When *Inx2 RNAi* is driven in the *pnr* domain of the split-expression system, the calcium wave around the wound appears "spotty" in that region only (Figure 18B). As expected, calcium dynamics in the non-*pnr* region are consistent with a wild-type wave.

Using the Radial Angle Profile Plot Plug-in from ImageJ and custom MATLAB code, we can specifically quantify the calcium wave expansion in the experimental *pnr* domain and in the control region. We can plot the average calcium wave expansion from each domain over time on the same graph to assess how symmetrical the expansions are. Figure 18C shows that in wild-type controls, the expansions largely overlay each other in most samples. Even when atypical expansions occur, as in the bottom two traces of Figure 18C where the second expansion occurs late, the waves in each domain mirror each other. Rarely, we observe asymmetry when comparing wild type to wild type in each section (middle sample in Figure 18C).

As expected, quantification of *Inx2 RNAi* samples expressed in the split-expression system recapitulates observations from Figure 10C and Figure 16C. In the half of the tissue where gap junctions are knocked down, the micro-tear induced expansion does not occur. This analysis also reveals that the wound-induced expansion begins at the same time in gap junction knockdown conditions as in control conditions. The uneven wave front observed in the gap junction knockdown tissue results in the underestimation of the calcium radius by the MATLAB program because of its discontinuous wave front. Overall, these data demonstrates the wound-induced expansion is not mediated via calcium induced calcium release, nor any other mechanism that requires gap-junction communication.
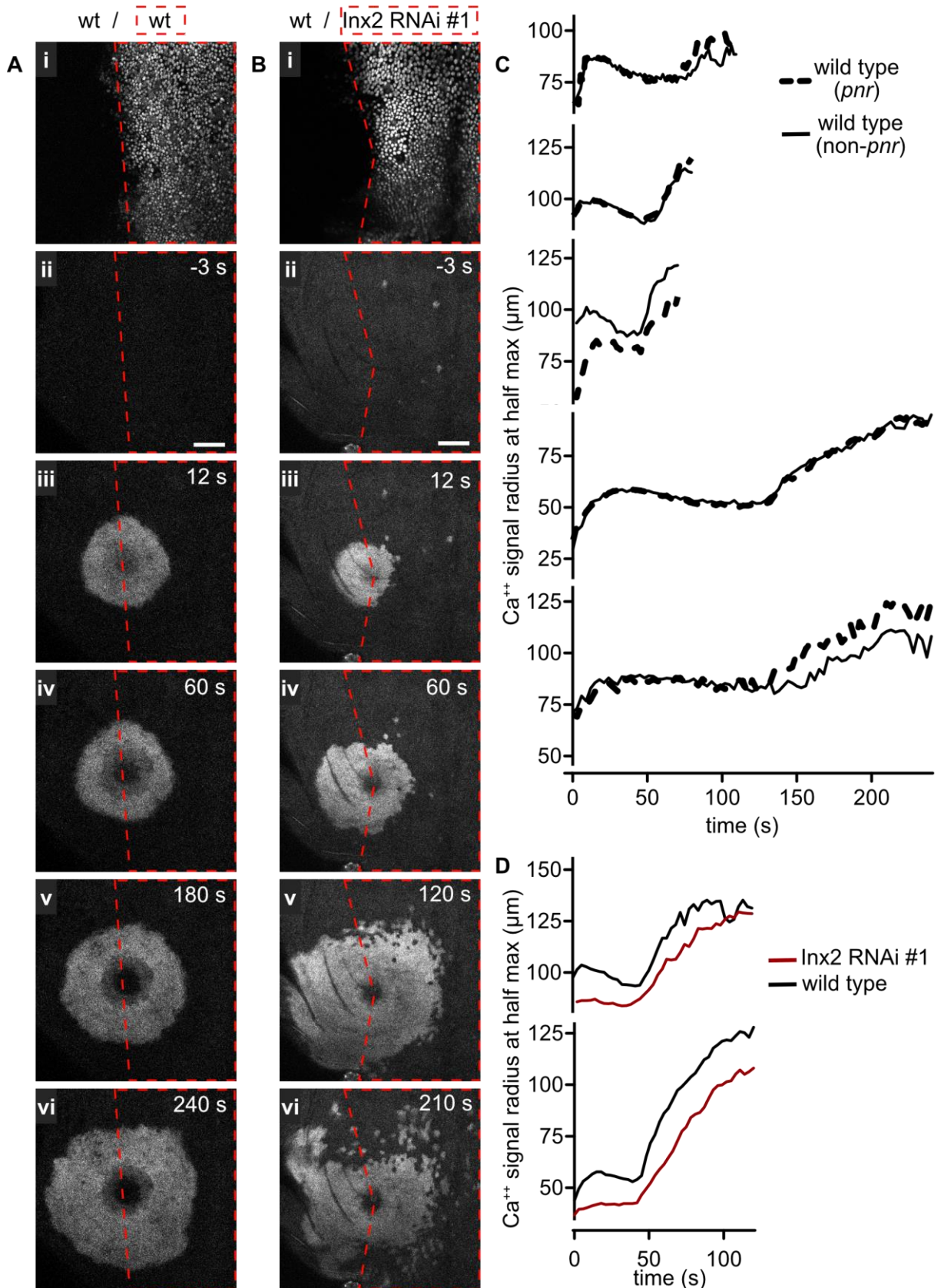
Figure 18: The internally controlled split-expression system can be used to reliably compare experimental conditions with controls at the same wound.
A) Stills comparing wild-type tissue to wild-type tissue in the split-expression system. The *pnr* domain is detected by the expression of nuclear mCherry and outlined with a dashed red line (i). Prior to wounding the basal activity of GCaMP6m is low (ii). The micro-tear induced expansion and the wound-induced wave are symmetrical around the wound (iii-vi). Scale bar = 50 µm. **B)** Stills comparing *Inx2 RNAi* #1 to an internal wild-type control in the split-expression system. A red dashed line outlines the expression of the nuclear mCherry reporter and the gap junction RNAi in the *pnr* domain (i). Single cell calcium transients occur prior to wounding only where gap junctions are knocked down. Micro-tear induced calcium influx expands in the wild-type region, but not where gap junctions are knocked down (iii). The wound-induced calcium expansion appears "spotty" in the experimental region and has a smooth wave front in the control region (iv-vi). Scale bar = 50 µm. **C)** Quantification of representative samples comparing wild type to wild type in the split-expression system. Each graph represents one sample. Data for the first three samples was provided by James O'Connor. **D)** Quantification of representative samples from our internally controlled split-expression system comparing the calcium radius over time for *Inx2 RNAi* #2 with its internal control. Note that the larger, wound-induced expansion begins at the same time for both samples.

The unknown extracellular ligand drives the wound-induced expansion of calcium via Gαq signaling cascades.

The diffusion of an extracellular ligand can promote the influx of calcium into the cytosol directly, through ligand-gated calcium channels, or indirectly, through ligand-gated G-Protein Coupled Receptor (GPCR) signaling. Figure 13 shows a common mechanism for GPCR induced calcium release where a ligand binds a GPCR, activates Gαq which then upregulates production of IP3 from PLCβ. IP3 then diffuses to the ER to bind an IP3 receptor and induce the release of calcium from the ER into the cytosol. To test whether GPCR signaling was responsible for this calcium expansion we knocked down Gαq and then PLCβ, as both are necessary for canonical GPCR induced calcium release. Using our split-expression system we found that knockdown of either Gαq or PLCβ attenuated the large expansion of calcium (Figure 19). Nuclear mCherry and the dashed red outline marks the expression domain of Gαq RNAi (Figure 19 Ai) and PLCβ RNAi #1 (Figure 19Bi). Prior to wounding, there is no basal calcium activity in the tissue (Figure 19Aii and Bii). While the micro-tear induced first expansion appears symmetrical in both samples (Figure 19A and B), the wound-induced expansion is attenuated in the experimental expression domain for both RNAis (Figure 19Aiv-vi and Bv, vi). The quantitative analysis of the calcium radius over time for additional samples shows the variation and extent of the RNAi attenuation of the second expansion (Figure 19C-E). It is possible that the Gαq RNAi line tested does not provide efficient knockdown or that Gβγ acts redundantly with

Gαq. A second RNAi line is needed to confirm these results. This data informs us that the expansion of calcium is mediated by GPCR signaling.

To further validate this mechanism, we used our internally controlled split-expression system to express an IP3 Sponge and two functional IP3 receptor (IP3R) RNAi lines to block calcium release from the ER. An IP3 Sponge is a peptide designed to sequester IP3 inside the cell. The peptide has been engineered to bind IP3 with high affinity (4.5 x 10^{-11} Kd) and competes with IP3R[254]. This construct was used by the Chisholm lab to show that epidermal wounds in *C. elegans* lead to IP3 mediated calcium release from ER stores[20]. Figure 20Ai shows the IP3 Sponge-expressing domain labeled with nuclear mCherry. No basal calcium activity is detected prior to wounding (Figure 20Aii). The micro-tear induced calcium expansion is largely symmetrical, as expected (Figure 20Aiii). The expansion of the wound-induced wave is asymmetric though. The calcium wave begins first in the wild-type tissue (Figure 20Aiv) and expands normally. The wave in the IP3 Sponge-expressing tissue expands at a slower rate than wild type (Figure 20Aiv and v) and is still expanding even when the control wave has faded (Figure 20Avi). It is likely that the IP3 sponge does not fully sequester all IP3 within cells prior to and upon wounding and therefore does not fully block the calcium wave.

Knocking down IP3R, however, does block the wound-induced expansion of calcium. Figure 20Biv-vi show a severely attenuated second expansion in the IP3R RNAi expression domain compared to a normal expansion in the control region. Quantification of the calcium radius over time using an IP3 Sponge and two different RNAi constructs supports the qualitative observations (Figure 20C-E). Together, this data reveals that an unknown ligand diffuses through extracellular space and likely binds an unknown GPCR, which then signals through canonical Gαq pathways to initiate calcium release from the ER.
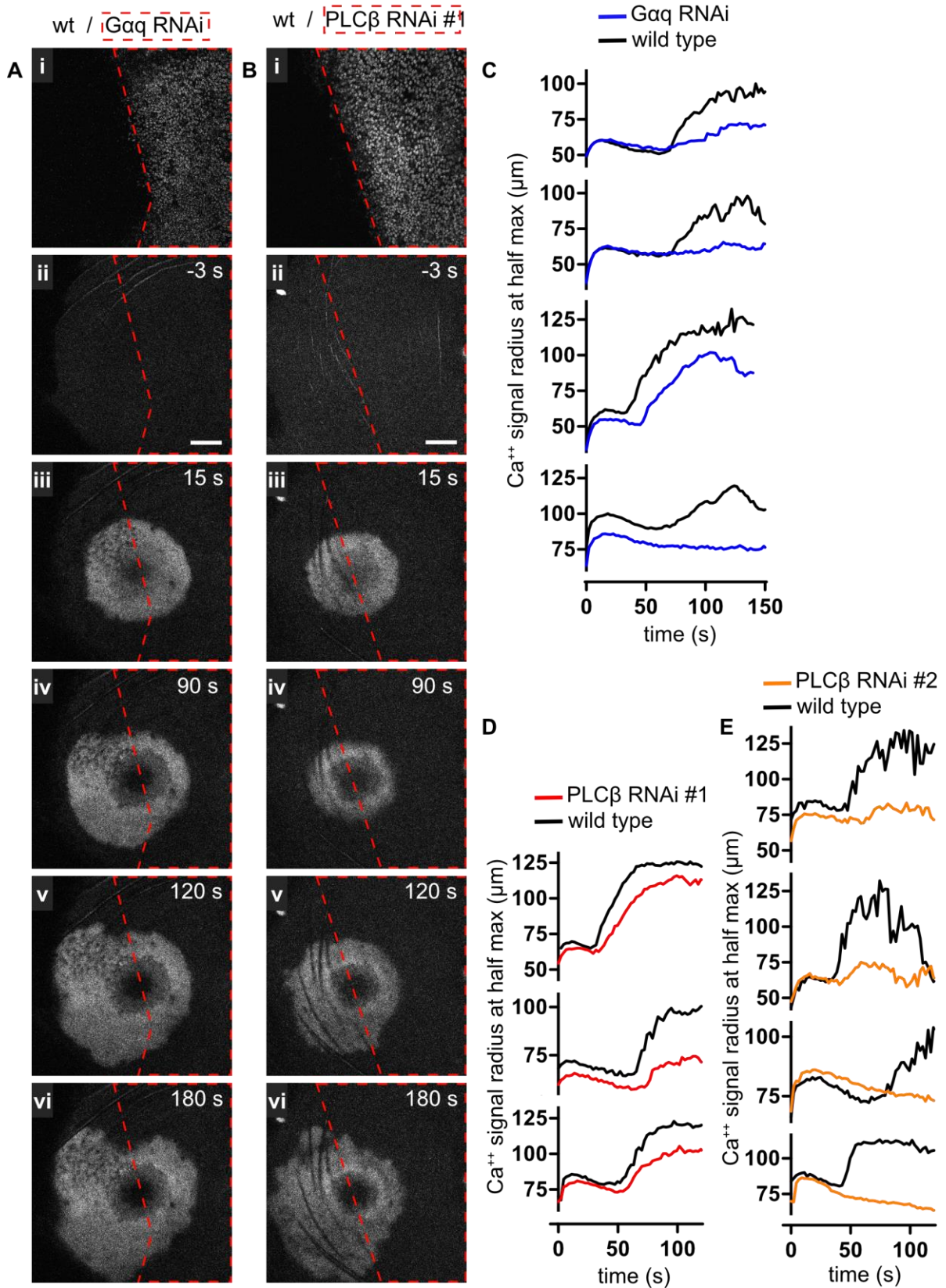
Figure 19: Gαq and PLCβ are important for the expansion of the wound-induced calcium wave.

Data gathered by James O'Connor of the Page-McCaw lab. **A)** Using our internal control split-expression system we expressed Gαq RNAi in the *pnr* domain of the *Drosophila* notum, indicated by nuclear mCherry and outlined by the red dashed line (i). Prior to wounding there is no basal calcium activity (ii). The microtear-induced calcium expansion appears similar to the wild-type control (iii). However, as the wound-induced expansion spreads, the rate of expansion is much slower in the IP3 Sponge tissue when compared to controls (iv-vi). Scale bar is 50 μm. **B)** Shows a representative sample from PLCβ RNAi knockdowns. Nuclear mCherry and the red dashed outline mark the PLCβ RNAi #1 expression domain (i). Prior to wounding there is no basal calcium activity (ii) and upon wounding the microtear-induced calcium expansion appears similar in both domains (iii). The wound-induced expansion is limited where PLCβ has been knocked down (iv-vi) but is normal in the control region (iv-vi). Scale bar is 50 μm. **C)**, **D)**, and **E)** show quantification of the calcium expansion over time for representative samples of Gαq RNAi, PLCβ RNAi #1, and PLCβ RNAi #2 genotypes, respectively. Each graph represents one sample.
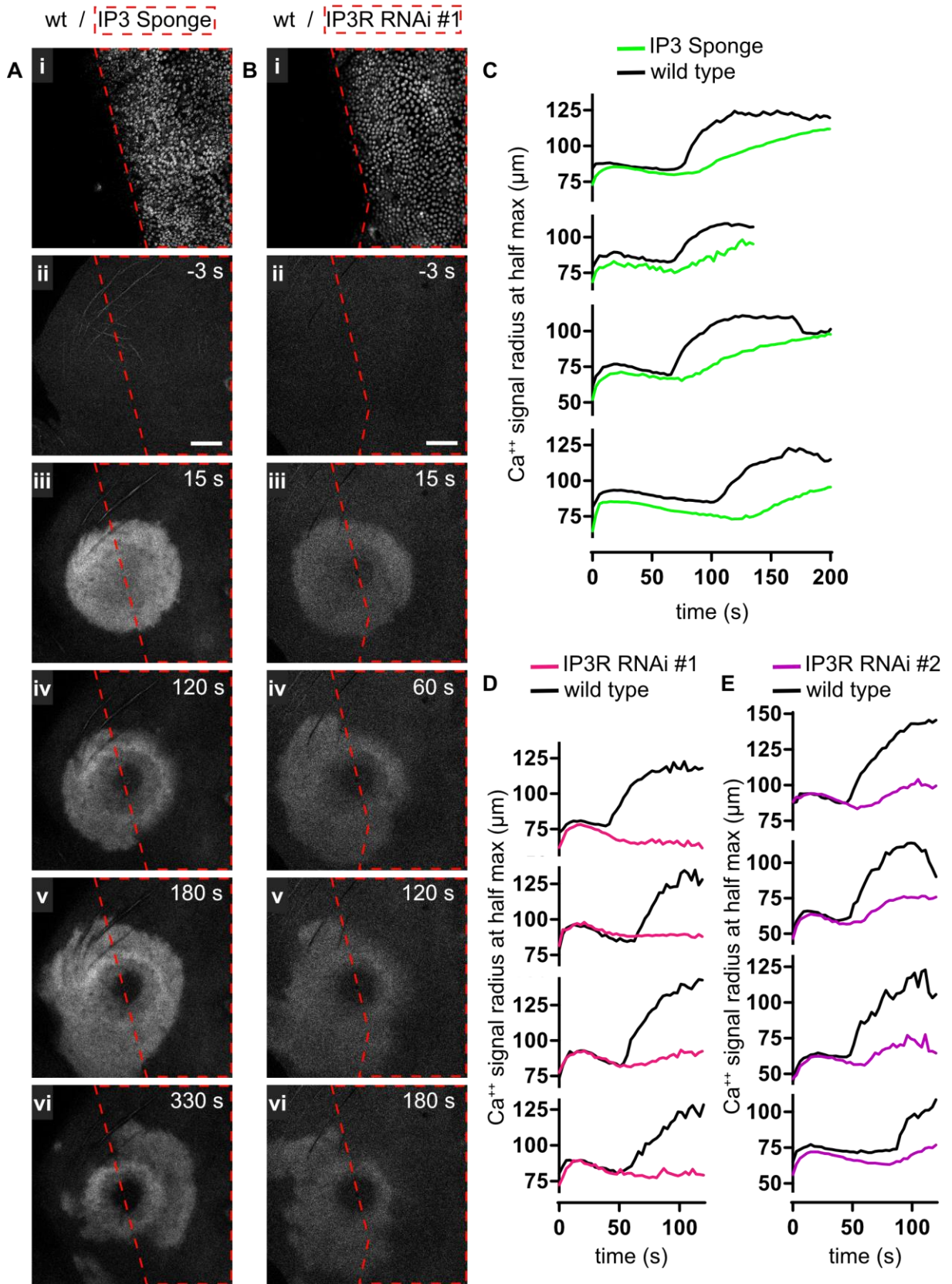
Figure 20: IP3 and the IP3R are required for the wound-induced expansion of calcium.
A) Using our internal control split-expression system we expressed an IP3 Sponge in the *pnr* domain of the *Drosophila* notum, indicated by nuclear mCherry and outlined by the red dashed line (i). Prior to wounding there is no basal calcium activity (ii). The microtear-induced calcium expansion appears similar in the IP3 Sponge domain as compared to the wild-type control (iii). However, as the wound-induced expansion spreads, the rate of expansion is much slower in the IP3 Sponge tissue when compared to controls (iv, v). By the time the expansion in the IP3 Sponge tissue reaches its maximum radius, the expansion in control tissue is flaring and fading (vi). Scale bar is 50 µm. **B)** Shows a representative sample from IP3R RNAi knockdowns using our internal control split-expression system. Nuclear mCherry and the red dashed outline mark the IP3R RNAi #1 expression domain (i). Prior to wounding there is no basal calcium activity (ii) and upon wounding the microtear-induced calcium expansion appears similar in both domains (iii). The wound-induced expansion does not occur in tissue where the IP3 Receptor has been knocked down (iv-vi). The expansion appears normal in control tissue (iv-vi). Scale bar is 50 µm. **C)**, **D)**, and **E)** show quantification of the calcium expansion over time for representative samples of IP3 Sponge, IP3R RNAi #1, and IP3R RNAi #2 genotypes, respectively. Each graph represents one sample.

Discussion and conclusions

We observe two calcium waves around wounds. The first wave is a result of micro-tears on the membrane that permeabilize cells and permit direct calcium influx. This influx of calcium spreads to neighboring cells via gap junctions and this expansion is not affected by an IP3 Sponge or IP3R RNAi. These experiments support our computational analysis from Chapter 2 and we expect that high concentrations of calcium itself is likely diffusing to neighboring cells.

Even though calcium spreads to unwounded neighbors, micro-tears are single cell wounds that cells can repair. Micro-tears alone cannot generate the second, large wave (Figure 10B, see "no wound" samples). When more catastrophic damage occurs to the tissue, a larger expansion occurs. Previous *in vivo* work has suggested that this wound-induced expansion is associated with changes in tissue mechanics. Indeed, it has been reported that mechanically prodding wing discs resulted in a calcium wave very similar to those observed here: both expand at comparable rates, both exhibit re-occurring waves (Figure 14), and both require IP3 stores (Figure 20) [31,39]. Unlike the wing disc, we find mechanical prodding is not sufficient to induce a calcium wave in notum epithelia (Figure 15). A wound-induced calcium expansion does occur when the tissue is punctured (Figure 15). The wave may be triggered by catastrophic damage caused by a stab wound. It may also be caused by cell lysate released during the course of wounding.

When added to cultured wing discs, fly lysate triggers long distant calcium waves in the tissue[36].

When considered along with our observations that the calcium wave is driven by extracellular diffusion (Figure 16), it seems likely that a component from cell lysate initiates and propagates the calcium wave. A diffusible signal can result in intercellular calcium influx by binding and activating receptors on the cell membrane. These receptors can be ligand gated ion channels, GPCRs, or RTKs. To identify the diffusible ligand and its receptor, we have targeted downstream effectors of receptor signaling. Both GPCRs and RTKs can induce calcium release from the ER via phospholipase activity[249]. However, only GPCRs require Gαq to activate this signaling cascade. Our data shows that knocking down Gαq attenuates the wound-induced expansion (Figure 19). This knockdown does not completely abolish the calcium wave, and a second RNAi has recently confirmed the observed effect (James O'Connor, unpublished data). These data suggests a GPCR mediates the initiation and propagation of the calcium wave. We further confirmed the role of this signaling cascade by knocking down PLCβ, IP3R, and expressing an IP3 Sponge (Figure 19 and Figure 20). These experiments were made possible with the use of our internally controlled split-expression system, which allows us to quantify subtle differences between conditions.

DAMPs are diffusible proteins, peptides, or metabolites which initiate wound responses and are found in cell lysates[84]. Our kinematic analysis of the second expansion indicates we are looking for a signal with a diffusion constant between 7 to 30 μm^2/s. The observed diffusion constant could suggest we are looking for a molecule about >6 kD. Large proteins have been shown to regulate calcium dynamics in previous studies[84,86-88]. In fact, data from wing disc indicates the extracellular factor driving calcium dynamics is sensitive to proteases[36].

The observed diffusion constant could also suggest the diffusing signal is a small molecule that does not freely diffuse. ATP is a DAMP that initiates calcium influx in cell culture wounding models by binding P2X and P2Y receptors. A recent cell culture study has shown that manipulating the activity of extracellular ATP degrading enzymes does not significantly alter the spread of extracellular-ATP induced calcium waves[255]. The investigators argue that ATP is released from wound sites in high concentrations and simply diffuses across the tissue to induce long distance calcium waves. ATP diffuses in water with a diffusion constant of 350 μm^2/s, which is much faster than the diffusion of the

signal measured in Chapter 2. Due to this significant difference, the calcium wave in our system is probably not driven by the free diffusion of a ligand the size of ATP. However, other investigators argue that ATP would have buffered diffusion in the extracellular space as it is readily degraded by extracellular enzymes[152-154]. If a small ligand like ATP is driving calcium influx and is buffered, then the diffusion of the ligand would appear much slower than the known diffusion of ATP in water and could potentially match our observed diffusion constant. Studies have also shown that ATP and calcium can participate in a positive feedback loop, where IP3-mediated calcium influx drives extracellular ATP release. Outside the cell, the cycle continues; ATP diffuses to neighboring cells and binds a GPCR to promote IP3 mediated calcium release. In this way, ATP signaling can participate in long distance wave propagation[100,155,156]. A positive feedback loop such as this one would also result in wave propagation much slower than the diffusion of ATP in water.

This potential mechanism could also explain how an IP3 sponge is capable of changing the rate of propagation (Figure 20C). If a positive feedback loop is propagation the wave, IP3-mediated calcium release would feedback into further ligand release. An IP3 sponge would not only delay the transduction of the extracellular signal into calcium (shifting the onset of expansion in the graphs to the right), it would delay the release and propagation of the extracellular signal (changing the rate of expansion and slope of the curve in the graphs). However, it is unclear if a positive feedback loop like the one described can result in a pattern of expansion that is capable of being fit to a diffusion equation. Typically a positive feedback loop would result in a linear expansion that would not fit a diffusion equation. Kinematic analysis is necessary to confirm or rule out this possibility. Another possible, but less exciting, explanation for the altered expansion kinetics upon IP3 Sponge expression is that the IP3 Sponge releases IP3 molecules back into the cytosol and creates artificial calcium dynamics. While we do not expect this to happen based on previous characterization of the IP3 Sponge, we have not characterized its function in the notum and cannot readily rule out this explanation.

Drosophila only have one confirmed ATP receptor, AdoR, which is a Gαq bound GPCR[256]. Future studies need to examine the role of AdoR in calcium dynamics of the notum. Future studies should also use computational methods to examine the onset and rate of expansion in different conditions in an attempt to determine if buffered diffusion of a positive feedback loop are viable mechanisms of expansion.

As ligands diffuse away from the wound site they propagate calcium expansion. The source of the re-occurring oscillations is unclear. If ligands also drive these oscillations then perhaps they are released multiple times during the course of wound healing. Alternatively, ligands could be released constantly after wounding and the refractory period between oscillations could reflect sensitization to the constant signals. It is quite possible that these oscillations are not initiated by ligands at all, and there is yet another mechanism of calcium wave initiation in this system.

When an expansion event occurs, the wave front is smooth (Figure 16A). Homogenous diffusion of an extracellular diffusion should result in an even wave front. However, when we knockdown gap junctions – which should not affect extracellular diffusion – the wave front changes from even to "spotty" (Figure 16B). We hypothesize that this is a result of altered IP3 distribution prior to wounding. Genetically identical cells within a tissue can produce heterogeneous levels of IP3[257]. When gap junctions are open, small molecules such as IP3 can diffuse to neighboring cells and establish a homogenous distribution through the epithelia. We predict that this homogenous distribution results in a smooth wave front as all cells are equally primed to respond to Gαq signaling. When gap junctions are blocked, we hypothesize that basal IP3 levels remain heterogeneous. As the Gαq signaling cascade is initiated in cells, we predict some cells do not have sufficient basal levels of IP3 to overcome the threshold needed to activate IP3 receptors while other cells do. This could result in the "spotty" appearance of calcium expansion observed. Furthermore, we would expect that when gap junctions are blocked the basal levels of IP3 in some cells would spontaneously overcome the threshold of IP3R activation and result in single cell calcium release. Indeed, we observe this in gap junction knockdowns in unwounded tissue.

Overall, our characterization of the wound-induced calcium wave expansion emphasizes many similarities with waves in previously characterized models. Our data recapitulates findings *in vivo* while also supporting the ligand-diffusion hypothesis favored by cell culture research.

CHAPTER 4

SUMMARY AND IMPLICATIONS

When a tissue is wounded via laser ablation, matter at the site of ablation is recombined into hot plasma[220]. The temperatures and pressures associated with this event create a cavitation bubble, a hot gas bubble, which expands away from the point of ablation[189]. The initial expansion and final collapse of this bubble are both so rapid that they break the sound barrier and make a popping noise that we can detect with a hydrophone[221]. The shear stresses of this rapid expansion are great enough to completely lyse cells near the point of ablation, resulting in a hole in an epithelial monolayer. The expansion rate of the bubble slows as it progresses and the cells underneath the bubble experience less shear stress[176]. While the cells adjacent to the wound aren't completely lysed, our data suggests that the cavitation bubble still rips the outer and organelle membranes. Using calcium, voltage, and dye influx assays, we showed that plasma membranes within the entire footprint of the cavitation bubble exhibit damage in the form of micro-tears (Figure 7). Based on our kinematic analysis of calcium influx into cells through micro-tears, we argue that high concentrations of calcium are pouring into these cells (Figure 6). Once inside the damaged cells, the high concentrations of calcium diffuse through gap junctions to neighboring, undamaged cells (Figure 16). Our internally controlled split-expression analysis of an IP3 Sponge and IP3R RNAi lines demonstrate that IP3 is not involved in this diffusion event (Figure 20). In the context of our studies, we have termed this micro-tear driven expansion event the "first expansion".

Laser ablation is increasingly common as a wounding model and has many advantages: it can be paired with live imaging, used to create reproducible wounds, and used to target specific sub-cellular regions[215,216]. One criticism of this model is that it does not replicate the extent of damage seen in naturally occurring wounds. Our data begins to address this concern by showing ablation wounds also exhibit complex damage profiles as a result of micro-tears. We argue that ablation wounds might be more similar to crush or puncture wounds than previously thought. Knowing this, investigators might find laser ablation to be an even more useful wounding tool. For example, we can take advantage

of the exaggerated micro-tearing caused by cavitation and use it to create a new single cell damage research model. This will be discussed further in the Future Directions section.

Depending on the laser used and the context of the study, investigators may introduce artifacts into their experiments if they are not aware of the cavitation-induced effects. We show that the cavitation bubble results in micro-tear mediated calcium influx up to 50 μm away from the wound. For those studying calcium dynamics, it is important to recognize that early events are a result of direct influx into cells and not a calcium wave propagating long distances. Our findings are also important outside of the context of calcium dynamics since calcium is a potent second messenger and can dramatically alter cell behavior. For example, sub-cellular ablation of an organelle or structure might also generate micro-tears on the cell surface and permit the entry of calcium and solutes from the extracellular environment. It will be important for investigators to control for the influx in calcium and other ions when reporting changes in cell behaviors due to the removal of a structure or organelle.

After the first expansion a larger, second expansion occurs. We term the second expansion a wound-induced expansion because it requires the presence of a primary wound. Fly lysate is required for calcium wave formation in *ex vivo* wing discs[31,36,39] and we believe a primary wound is required because it is associated with cell lysate. A wound-induced calcium wave also occurs when the tissue is mechanically stabbed or decayed with a continuous laser (Figure 15 and Appendix B). Further characterization comparing the expansion kinetics between each of these methods is required. We know that the wound-induced expansion observed at ablation wounds is driven by extracellular diffusion because it still occurs when gap junctions are blocked (Figure 16). Along with the requirement for cell lysate, this data argues for a ligand-mediated mechanism of initiation and propagation. Our quantitative analysis of ablation wounds indicates that this expansion does not initiate at the time of wounding, but is delayed (Figure 11). It may take time for nearby cells to transduce extracellular ligand binding into calcium release, causing the delay. This is especially true for metabotropic GPCRs, which are *not* ligand gated ion channels and initiate calcium influx through an IP3-dependent signaling cascade. The mechanism of this delay will be discussed further in the Future Directions.

The identity of this ligand is unknown but our computational analysis had defined parameters that describe the ligand. The signal driving the calcium wave propagates with

66

a diffusion constant of 7 to 30 um^2/s. This diffusion constant indicates 1) the signal is a molecule about the size of insulin or larger (>6 kD) and/or 2) the signal does not freely diffuse. Examples of signals which do not freely diffuse can be found in cell culture studies, where ATP is degraded[152-154] or ATP and calcium participate in a positive feedback loop to drive wave propagation[100,155,156]. These models are inconsistent with studies in the wing disc, which suggest the ligand is a protein[36]. Experiments proposed in the Future Directions section could help distinguish between diffusion and a feedback loop mechanism of propagation.

We wanted to understand the signaling cascade downstream of the ligand diffusion. Knocking down components of a GPCR/Gαq signaling cascade – Gαq, PLCβ, IP3, and IP3R – attenuates the calcium wave. We conclude from this data that the ligand driving the wound-induced expansion diffuses through the extracellular space and activates a Gαq-bound GPCR. Further analysis is needed to determine the identity of the GPCR and ligand (see Future Directions).

We know IP3 is required for the expansion of this calcium wave because sequestering IP3 with an IP3 Sponge and knocking down the IP3R attenuates the wave. Interestingly, expressing an IP3 Sponge changes the rate of wave spread. From our current data, it is not clear how this could be happening. We would expect IP3 to change the diffusion rate of the extracellular ligand if IP3 was upstream of that ligand. Previous literature indicates IP3 can be upstream of a ligand. IP3 mediated calcium release can promote ATP release in a bucket-brigade positive feedback loop. However, it is not clear whether a positive feedback loop could result in an expansion pattern characteristic of free diffusion, as we observe in wildtype conditions. Further analysis is needed to explore these results and possibilities.

We have also observed that the quality of the expansion is notably different when we express a gap junction RNAi. When gap junctions are knocked down, the wave front is no longer smooth, it is "spotty" and appears to skip cells as it advances. Prior to wounding gap-junction knockdown tissue, we also observe transient, cytosolic calcium increases within single cells. We have developed a hypothesis driven by these observations. We hypothesize that IP3 is heterogeneously produced across cells within this tissue. Such heterogeneity has also been observed in HeLa cells[257]. When gap junctions are blocked, IP3 cannot diffuse to neighboring cells and IP3 concentrations remain heterogeneous throughout the tissue. In some cells, the basal concentrations of

IP3 could be so high that they spontaneously trigger calcium release from the ER prior to wounding, as we have observed. Other cells might have such low basal concentrations of IP3 that even when the signaling cascade is initiated, the cells never produce enough IP3 to overcome the threshold for IP3R activation, as we have observed. We find this hypothesis very interesting because it suggests mechanisms by which tissue architecture can shape the wound response. Furthermore, heterogeneous calcium signaling can lead to heterogeneous cell behaviors in platelets and immune cells[258,259]. In the Future Directions, I discuss how gap junction knockdowns and other IP3 perturbations could be used to investigate IP3's role in wave expansion and tissue heterogeneity.

There is extensive variability in the literature regarding calcium wave initiation and propagation. The previous studies have contributed to the field, but the variability between them seems to generate contradictions and undermines each study's relevance and significance. Our research validates many findings from other labs in an *in vivo*, accessible, genetically tractable, and conserved wounding model. Like previous research, we find that calcium can come from the extracellular space and intracellular stores. The wave propagates via gap junctions and diffusion of an extracellular ligand. Also, we find that tissue mechanics may indeed play a role in wave dynamics. Importantly, our research takes these findings one step further by clearly demonstrating that all of these things happen *at one wound*. We show that different mechanisms of damage correspond to different calcium wave characteristics. This new understanding can help make sense of the contradictory findings in the wound healing field. When a pulsed laser is used to wound tissue, the cavitation bubble will create micro-tears. Using this wounding method, calcium influx will be at least partially derived from extracellular calcium and will likely spread through gap junctions. If the pulsed laser does not create a large enough wound, an obvious wound-induced expansion may not occur and investigators may not report a role for extracellular diffusion or ER stores (which are released upon ligand binding). These expectations could explain observations from Narciso *et. al*. 2015[43] and perhaps Razzel *et. al.* 2013[12]. Adding cell lysate to a tissue will mimic a tissue wound and ligand diffusion. Under these conditions investigators should expect to see a calcium wave expand even when gap junctions are somehow inhibited. If the ligand in their lysate binds a metabotropic receptor (as in our system) they will observe calcium release from ER stores and if it binds an ionotropic receptor they will observe calcium influx from

extracellular space. We find these expectations to be accurate for cell culture scratch assays[25,30,32,34,37,38], which generate cell lysate and but not extensive microtearing[24,34,35,130]. The expectation that the calcium wave should expand upon addition of lysate even when gap junctions are somehow inhibited could be accurate for *in vivo* studies as well, depending on how one interprets their data. Investigators report that gap junction knockdowns (or pharmacological inhibition of gap junctions) stops the expansion of a calcium wave[31,36,39]. However, this is not the only interpretation of their data. When we examine their images closely, it appears that calcium still spreads into tissues where gap junctions have been knocked down, but this wave front is no longer continuous. It is possible that the calcium wave still propagates through this region but appears "spotty", similar to our observations in Figure 16. Another interpretation of the data they present is that a calcium wave is still propagating but the gap junction perturbation creates tissue heterogeneity, so the calcium wave loses its characteristically smooth wave front. This interpretation would be consistent with the expectation we describe above.

The shear diversity of wound cues and wound healing responses tells us that wound detection is a nuanced process. Our *Drosophila* pupae laser wounding model exhibits many mechanisms of calcium wave initiation. To advance the field, future wound healing studies should focus on how the tissue integrates calcium signaling. How do cells regulate calcium and other signals? Is the concentration of calcium or wave speed and frequency important for signal integration? Must two separate wound cues be present to drive the wound healing response? Over the last twenty years growth factors have been shown to drive wound healing but have had less satisfactory clinical outcomes. Do growth factors require certain *in vivo* calcium dynamics that are not being met in clinical applications? Laser ablation in the *Drosophila* notum is a multi-dimensional model well-suited to study a multi-dimensional phenomenon. Furthermore, this model is *in vivo*, ideal for live imaging, genetically tractable, and accessible. The work presented here has contributed important findings to the wound healing field, has established the *Drosophila* notum as a strong model, and lays the foundation for future studies.

Future studies may benefit research outside of the wound healing field as well. Calcium waves propagate through epithelia during normal development. When imaging living and intact larvae, calcium waves propagate through unperturbed wing discs[31]. During *Drosophila* oogenesis, calcium waves in the follicle cell epithelia is important for fate-specification of neighboring border cells[260]. Rhythmic calcium waves have also been

suggested to drive pattern formation in zebrafish gastrulation[135,261]. But that's not all: calcium influx can occur in disease contexts too. Calcium influx occurs upon epithelial-mesenchymal transition in human breast cancer cells and blocking the calcium influx blocks the induction of EMT markers[262,263]. As calcium is important for migration[142,264-266], it is also important for migration-dependent cancer hallmarks including invasion and vascularization[141,267-269]. Characterizing the calcium wave and understanding its regulation and integration can reveal fundamental information about cell biology. Specifically, these studies may contribute to our textbook understanding of wound healing, development, migration, and cancer.

CHAPTER 5

FUTURE DIRECTIONS

Future studies should focus on early wound signals that function in parallel to the calcium wave and how multiple wound signals are regulated and integrated. Before exploring these options, I'd like to discuss other assays that should be performed to complete a comprehensive characterization of this wounding model. Validating our current findings will forge a strong foundation for future endeavors.

Further exploration and validation of the Drosophila *notum wounding model*

Permeabilization of the notum

First and foremost, expanding our methods and protocols to incorporate pharmacological assays in the *Drosophila* notum would be highly advantageous. The notum has a thin waxy cuticle overlaying the epithelial tissue[270]. While this cuticle does not impair imaging, it does make the tissue impermeable to exogenous reagents. The *Drosophila* embryo also has a waxy membrane. Protocols have been developed to permeabilize the waxy embryonic membrane while leaving the cells intact for live imaging[271,272]. If the lab can apply this protocol to *Drosophila* pupae, then we could soak pupae in pharmacological reagents prior to mounting and wounding. In situations where the genetic tools have not been developed in flies, we could turn to pharmacological tools. With the combination of genetics and drug perturbations, few experiments would be technically limiting. If this is not achievable, then the wing disc can be used instead of the notum as it is permeable to drugs and can be cultured *ex vivo*.

Release and propagation of the ligand

A diffusible ligand drives the expansion of the wound-induced calcium wave. We have mathematically determined this calcium wave does not begin at the time of wounding; it seems propagation of the wave is slightly delayed. We also know that the ligand driving wave propagation is acting through a $G\alpha q$ signaling cascade. Transducing the extracellular signal into a calcium wave by this signaling cascade takes time, which could account for the delay. We may be able to test this hypothesis by comparing data we already have to computation models of this signal transduction pathway. Perturbing the

signal transduction cascade should result in a delayed expansion because it will take longer for the cell to initiate calcium release. Indeed, when the signal transduction cascade is inhibited and the wave is not completely attenuated, a visual inspection reveals the wave appears to begin later when compared to internal controls (Figure 19 and Figure 20, the experimental traces in the graphs are shifted to the right when compared to controls). A kinematic analysis, like the one performed in Figure 11, is required for each of the samples in Figure 19 and Figure 20 to determine if the expansion actually did begin later. If a delay is occurring, it may be very slight. The data may need to be compared to a computation model of this perturbation to assess whether the slight delay is expected or whether a larger delay would be expected.

We predict the ligand is released at the time of wounding. Is the release a result of exocytosis or cell necrosis/lysis? To determine if active exocytosis of a ligand is required, the Gal4/UAS system can be used to knockdown exocytosis genes expressed in epidermis. If no second expansion occurs in a tissue where exocytosis genes have been knocked down, then we may conclude active exocytosis of a ligand is required.

If exocytosis is required, this experiment can also be used to determine if the ligand is only released from cells on the wound margin or if the ligand is released from cells distant from the wound too. Cells distant from the wound might release ligand in a situation similar to the one described by Gruenhagen *et. al.* 2004[156], where ATP and calcium participate in a positive feedback loop to propagate long distance calcium waves. Our internally controlled split-expression system could be used to knockdown exocytosis genes in one part of the tissue. A wound would then be made fully inside the wild-type region. If the calcium wave does not spread symmetrically into the region of inhibited endocytosis, the data would support a positive feedback loop mechanism of expansion. In this situation, a small molecule the size of ATP could still account for the relatively slow expansion of the calcium wave. However, we do not expect the expansion dynamics of a positive feedback loop to be fit to a diffusion equation. This possibility seems unlikely, but should be tested with a kinematic analysis or the experiments described above.

If cells are not actively releasing the ligand, then the ligand must be released as cells decay and must propagate long distances via diffusion. There are many technical challenges to quantifying when cells release their lysate and how much lysate they are releasing. Dye and luciferase assays which measure cell lysis do exist[38,170] but are optimized for assaying cells in media. When the notum is wounded it is laid flush against

a coverslip for imaging and does not have access to media. If the lab could determine how to quantify lysis, it would be advantageous to compare the extent of lysis in pulsed laser wounds, continuous laser wounds, and stab wounds. These wounds exhibit slightly different calcium dynamics and it is worth investigating whether this is a result of more or less lysate/ligand release around each type of wound.

We also want to understand how the ligand propagates after it is released. In Chapter 2 we determined the signal initiating the calcium wave spreads in a diffusive manner. It is unclear why expressing an IP3 Sponge would change the rate of expansion in such a way that causes the expansion rate to appear linear (by qualitative, visual inspection), which is not consistent with diffusion. There could be an uninteresting explanation to this – the IP3 Sponge releases IP3 back into the cytosol, creating artificial calcium dynamics. For this reason, weak IP3R RNAi constructs, which still permit attenuated IP3-mediated calcium release, may serve as better experimental tools moving forward. There is another, more exciting explanation for the change in expansion rate. The IP3 Sponge could be modulating a positive-feedback loop between a ligand and calcium, as described in the discussion of Chapter 3. One way to test this mechanism of diffusion has been described above. If the IP3 Sponge is modulating this feedback loop we would also expect the IP3R RNAi #2 to have the same effect (IP3R RNAi #2 does not completely block calcium release so a small wave can be seen). By eye, it is difficult to determine the extent of similarity between the expansion events for the IP3 Sponge and the IP3R RNAi #2. Indeed, we cannot accurately assess the characteristics of expansion (ex: linear vs diffusive, diffusion constant of signal) by eye. Therefore, a kinematic analysis should be performed on the data in Chapter 3 to determine which conditions could represent diffusion or a positive feedback mechanism of expansion.

Identifying the receptor and ligand

Before moving forward to identify the GPCR it is crucial to confirm the role of Gαq in calcium wave initiation. Our current RNAi data shows a slight attenuation of the calcium wave compared to the internal control. It is possible that Gβγ acts redundantly with Gαq to activate PLCβ and promote calcium release. Since *Drosophila* only have one Gαq G-Protein, if we can show that Gαq is fully knocked down with the RNAi then it would support a role for Gβγ. RTKs can also induce calcium release from the ER, but they do so through PLCγ activity and not PLCβ. Because we observe complete knockdown of the calcium wave with a PLCβ RNAi we are confident that a GPCR mediates this signaling cascade.

We can perform an RNAi screen to identify the GPCR mediating calcium wave expansion. *Drosophila* have 111 GPCRs according to FlyBase, a public database. Literature searches may suggest which GPCRs do not bind Gαq, and these GPCRs will be excluded from the screen or de-prioritized. We will determine which genes are likely expressed in the epithelia by searching for expression in the "adult carcass" using FlyAtlas, a public gene expression database. The RNAi lines for those genes will be prioritized in the screen. Assuming we can screen 2 RNAi lines per day, we expect this screen will take at most 3 months. AdoR, a Gαq-bound GPCR and the only ATP receptor in *Drosophila*[256], should be prioritized in this screen. Even though the diffusion constants calculated in Chapter 2 do not match known rates of ATP diffusion, previous cell culture studies show ATP is the ligand that drives calcium expansion. Wound healing is a complex and essential process and redundancy is possible. If two different ligands induce calcium influx we still may be able to detect their receptors in this screen if the ligands have different diffusion constants. We can quantify the rate of expansion in each experiment and identify RNAi lines that alter the expansion rates. If the rate of expansion is altered then it could indicate that we knocked out the receptor for the faster diffusing ligand, but there is a slower, redundant ligand present. A secondary screen, with the receptor for the fast diffusing ligand knocked down in the background, should identify the receptor for the slow diffusing ligand.

To identify the ligand, it is essential to start with a list of justifiable candidate molecules. Identifying the receptor may immediately suggest the identity of the ligand (ex: AdoR receptor and ATP). It is also possible that the receptor will not be well characterized or have no known ligand. In this situation, there are only a few practical options for moving forward. First, we may consider screening other known DAMPs and molecules that can activate Gαq-bound GPCRs. Unfortunately, we could not knockdown or deplete those molecules from the cells because most are required for viability. Instead, we could perhaps biochemically purify each molecule and add it to unwounded tissue (where no waxy cuticle is present) and determine if a calcium wave occurs. To confirm that a purified component is working through the pathway we have already identified, any effect of the molecule would be blocked when the GPCR or PLCβ is knocked down. Second, if we find that the ligand is secreted via active exocytosis, we could isolate exosomes using standard protocols and attempt to identify candidate molecules in exosomes via mass spec. We may wish to collaborate with a biochemist, who has experience fractionating,

identifying, and purifying compounds.

Identifying other early wound signals

Gβγ Activity

The development of GCaMP reporters has permitted the *in vivo* assessment of calcium around wounds. While calcium seems to play a dominant role in the wound healing response, other early wound signals exist. There may be signaling cascades occurring in parallel to calcium activation in the *Drosophila* notum. One obvious candidate is Gβγ signaling. Gβγ binds GPCRs as a heterotrimer with Gαq. When a GPCR undergoes a conformational change upon activation, Gαq and Gβγ are released from the GPCR in an active state. For many years, it was thought that Gβγ simply functioned to inactivate Gαq. However, Gβγ is actually quite active and has many downstream effectors[273]. For example, Gβγ can activate other ion channels[274-276] and regulate cytoskeletal associated proteins[277-279]. If a GPCR mediates calcium influx then we can be sure that Gβγ is activated. Does Gβγ have a functional role in the early wound response? To answer this question the lab should perform a double knockout of Gβ and Gγ as well as individual knockouts of both subunits and monitor migration and wound closure. This experiment should be performed in our internally controlled split-expression system in addition to the standard whole tissue expression. The internally controlled split-expression system might allow us to detect nuanced changes in wound healing, like impaired migration. However, if half of the tissue is still completely functional, the wild-type half might still be able to close the wound. This will not be a concern if the RNAi's are expressed in the whole tissue.

Tissue mechanics

Previous studies and our own observations hint at a role for tissue mechanics in wound healing[8,10,20,31,39] (Appendix B). Could mechanotransduction somehow regulate or modulate calcium dynamics? Our internally controlled split-expression system is ideal for these studies. We can genetically perturb cell architecture to create conditions with different tissue mechanics and then observe how calcium expansion is altered as a result. Our current observations are suggestive but not conclusive. Most of the constructs we have expressed so far will relax actomyosin networks. However, at this time in development the notum is not under much tension[280], so the constructs may not significantly change tissue tension. Through a collaboration with the Hutson lab, we are

building a fly that will allow us to quantify tissue tension using CellFIT. CellFIT can map relative tissue tensions based on cell shapes[281]. With existing genetic tools, we cannot visualize cell borders and the calcium wave in the same samples. By quantifying changes in tissue tension as a result of expressing different genetic constructs, we can identify effective constructs to use in future tension experiments.

Our IP3R RNAi data shows that calcium expansion is completely blocked upon IP3R knockdown. This tells us that a stretch activated ion channel does not directly allow calcium entry from outside the cell. If mechanics modulate calcium, they must be effecting the IP3 cascade. It is possible that a mechanosensitive GPCR acts synergistically with ligand diffusion to contribute to the production of IP3. If we are able to identify the GPCR which binds the diffusible ligand, we could knock it down and then modulate tissue tension in a way that would attenuate the calcium wave. We would expect this to synergistically attenuate the calcium wave compared to GPCR knockdown or tissue tension modulation alone.

TRPM is a putative mechanosensitive ion channel in *Drosophila* and has not been well characterized. Its mechanosensitive classification is based on weak sequence homology with the mammalian TRP channels. Other work in *Drosophila* has found that knocking down TRPM attenuates the intensity of GCaMP fluorescence upon wounding, suggesting lower concentrations of calcium influx, but it does not alter the propagation of the wave. We find that the wound-induced calcium wave is mediated solely through IP3R so it is unclear how an ion channel contributes to calcium levels. It is possible that the TRPM ion channel is not mechanosensitive, but is itself activated by intercellular calcium and serves to increase the concentration of calcium in the cell[282]. If this occurs, then knocking down TRPM should have no effect on mechanically induced calcium dynamics, like those described in Appendix B. Furthermore, IP3R knockdown should suppress any GCaMP6m intensity increase observed upon TRPM overexpression.

Understanding the regulation and integration of wound signals

Intersection of single cell wound healing and tissue wound healing

The notum wounding model presents unique opportunities to explore single-cell wound healing in the context of a tissue. By mis-targeting the laser we can generate single cell wounds without a primary, tissue wound. Calcium influx in the single cell wounds can spread to unwounded neighboring cells. Using this single-cell wounding method, we can determine if the calcium influx derived from single cells wounds is

sufficient to generate a wound response in neighboring unwounded tissue (visualized by JNK activity).

We can also determine if the single cell wounds prime the tissue for responding to subsequent multicellular wounds. By mis-targeting the laser we can generate single cell wounds to prime one population of cells. Next we would refocus the laser on a nearby population of cells to create a primary, tissue wound and observe wound response parameters in the primed cell population. Wound response parameters that we could measure are calcium level intensity and propagation rate, cytoskeleton reorganization/migration, and JNK activity.

The experiment above tests the sequential intersection of single cell and tissue level wounds. A naturally occurring puncture wound is complex; both types of damage occur at the same time. Teasing apart the interactions between single cell wounds and tissue wounds at the same wound event requires finesse. We cannot simply block the closure of single cell wounds because that would lead to cell death and would not be informative. A better approach may be to prevent the propagation of micro-tear damage signals to neighboring cells by knocking down gap junctions only in the region of cavitation damage. This could be achieved with careful laser targeting within our split-expression system. Examining calcium wave propagation, cell behavior, and JNK activity in tissue adjacent to single cells wounds 1) with blocked gap junctions and 2) without blocked gap junctions will help identify functional intersections of single cell and multicellular wound healing.

Integration and interpretation of wound signals

Here we show that different types of damage drive calcium influx with different mechanisms. Single cells wounds experience direct calcium influx from the extracellular environment while tissue surrounding primary wounds experience calcium release from the ER. Furthermore, many different types of signals can drive calcium dynamics around wounds. Can cells interpret the type of damage based on the source of calcium? How do cells distinguish developmentally induced calcium waves from damage induced calcium waves? Can the same wound response – the calcium wave – result in different cellular outcomes in different contexts? Does the calcium wave intersect with other early wound signals? These are all critically important questions that are at the forefront of the wound healing field.

Wound healing is very complex and must be highly regulated. When a wound

occurs the cells must re-activate quiescent developmental programs to drive re-epithelialization. They must only migrate and proliferate just enough to close the wound. Losing control of these programs could result in serious consequences, like cancer. The calcium wave is a master regulator of wound healing, but it is just one signal. We do not expect that binary control, calcium on vs. calcium off, can provide the necessary regulation of such powerful cellular behaviors. We expect the calcium wave is actually multi-dimensional, and cells interpret and integrate the multi-dimensional information in different ways. Perhaps cells can sense calcium concentration or propagation patterns. Or perhaps cells use a signaling circuit, where certain combinations of wound signals (for example, calcium influx and mechanical changes) result in different outcomes. Understanding how the calcium wave is integrated and interpreted by cells will advance our fundamental knowledge of wound healing and may have important clinical applications. For example, perhaps mapping out potential signaling circuits will reveal why the clinical use of growth factors in wound healing has not been overwhelmingly successful[283]. These studies may also have clinical applications in cardiac development and repair. Cardiac tissue has normal, frequent calcium oscillations. Heart failure can occur if cells do not appropriately regulate their response to calcium dynamics[284].

There is precedence for such complex interpretation and integration of calcium dynamics during wound healing. Investigators have found that platelets will aggregate, release coagulation-protein containing granules, or signal to other cells by changing the composition of their plasma membrane based on the concentration of calcium in their cytosol[259]. In T-cells, specific spatiotemporal patterns of calcium dynamics can activate specific transcription factors[258]. For example, NFAT is activated by frequent calcium transients and its sustained presence in the nucleus requires a constant level of low basal calcium. NFκB, however, can be activated with short, infrequent calcium transients.

To study the multi-dimensional interpretation and integration of the calcium wave in epithelial tissue we can take advantage of the naturally occurring cellular heterogeneity or intentionally create extreme heterogeneity. Naturally occurring heterogeneity in epithelial cells arises are a result of heterogeneous PLC isoforms and heterogeneous IP3 activity[257,285]. We can experimentally manipulate calcium dynamics around wounds using our IP3 Sponge and IP3R RNAi lines. If we develop an optogenetic gene expression system, we could regulate the activity of these constructs in very specific cell populations creating a highly controllable heterogeneous population. Otherwise we can use mitotic

clones or our internally controlled split-expression system. It may be possible to study heterogeneity and calcium wave integration in wild-type samples, without any manipulation at all. In wild-type samples, we observe flares propagating asymmetrically around the wound. This asymmetry may result in extensive heterogeneity in cells in the regions of flares. It may also cause cells in the flaring regions to integrate the calcium signal very differently than those which experience more sustained calcium influx closer to the wound. We can measure calcium intensity, propagation rates, calcium transient duration and oscillation frequency and observe cytoskeletal reorganization and transcription factor activity. These assays will require intensive quantification and mathematical modeling.

Our lab is uniquely suited to address these future directions. With our model we can dissect different mechanisms driving calcium dynamics in an *in vivo* context. Using *Drosophila* as a model organism allows us to assay calcium dynamics with a range of advanced genetic tools, like our internally controlled split-expression system. Perhaps we will soon add pharmacological tools to our repertoire. Furthermore, our established collaboration with the Hutson lab enables us to approach data analysis with robust and quantitative methods. These methods will be essential for teasing apart precise mechanisms of ligand-induced calcium release. They will also be important for determining how cells integrate and interpret calcium influx around wounds. The complementary perspectives and tool sets between our labs gives our team a powerful advantage moving forward in the wound healing field.
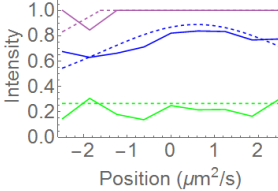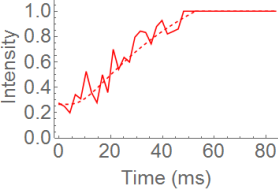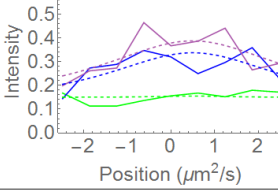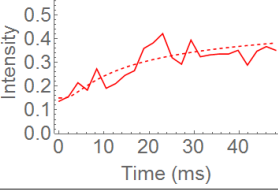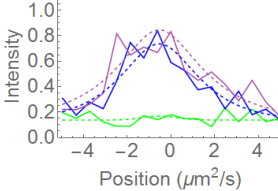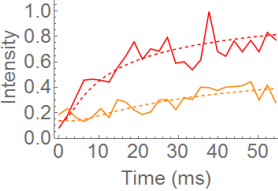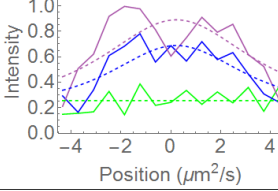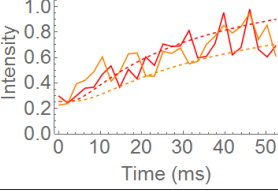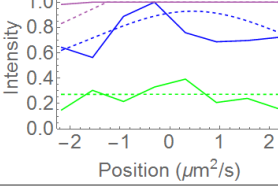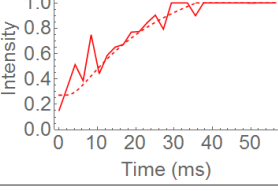
APPENDIX A

COMPLETE SET OF FITS FROM FIGURE 6 AND FIGURE 11

Number	Rocket Density Plot	Fit Densiy Plot	Intensity v. Position	Intensity v. Time	Diffusion Constant
1					32 ± 2 μm^2/s
2					34 ± 5 μm^2/s
3					51 ± 8 μm^2/s
4					52 ± 9 μm^2/s
5					68 ± 11 μm^2/s

80

Number	Rocket Density Plot	Fit Densiy Plot	Intensity v. Position	Intensity v. Time	Diffusion Constant
6					71 ± 12 $\mu m^2/s$
7					78 ± 9 $\mu m^2/s$
8					81 ± 9 $\mu m^2/s$
9					86 ± 12 $\mu m^2/s$
10					89 ± 14 $\mu m^2/s$

Number	Rocket Density Plot	Fit Densiy Plot	Intensity v. Position	Intensity v. Time	Diffusion Constant
11					$104 \pm 17\ \mu m^2/s$
12					$108 \pm 9\ \mu m^2/s$
13					$123 \pm 13\ \mu m^2/s$
14					$123 \pm 13\ \mu m^2/s$
15					$126 \pm 22\ \mu m^2/s$

Number	Rocket Density Plot	Fit Densiy Plot	Intensity v. Position	Intensity v. Time	Diffusion Constant
16					139 ± 13 μm^2/s
17					187 ± 42 μm^2/s
18					197 ± 18 μm^2/s
19					219 ± 30 μm^2/s
20					225 ± 32 μm^2/s

Number	Rocket Density Plot	Fit Densiy Plot	Intensity v. Position	Intensity v. Time	Diffusion Constant
21					$260 \pm 33\ \mu m^2/s$
22					$270 \pm 38\ \mu m^2/s$
23					$286 \pm 45\ \mu m^2/s$
24					$405 \pm 72\ \mu m^2/s$
25					$474 \pm 57\ \mu m^2/s$

Figure 21: Complete set of kymograph peak fits from Figure 6.
The complete set of 25 cropped kymograph peaks (or rockets) from Figure 6 and their diffusion model fits is sorted from smallest to largest diffusion constant. Data was fit to the diffusion of calcium continuously being released from a point source fixed in space. For the intensity vs position and intensity vs time plots, solid lines and dashed lines correspond to the data and fits respectively. The intensity vs position plots show data and fits at 2.1 ms after ablation (green), at the time half-way between the start and end of the image (blue), and at the time 4.2 ms before the end of the image (purple). The intensity vs time plots show data and fits along the midline of the image (red), and at a point half-way between the midline and the right edge of the image (orange, only shown if the image is wider than 13 pixels or 8.06 µm). Reported uncertainty for each diffusion is the standard error from the regression.
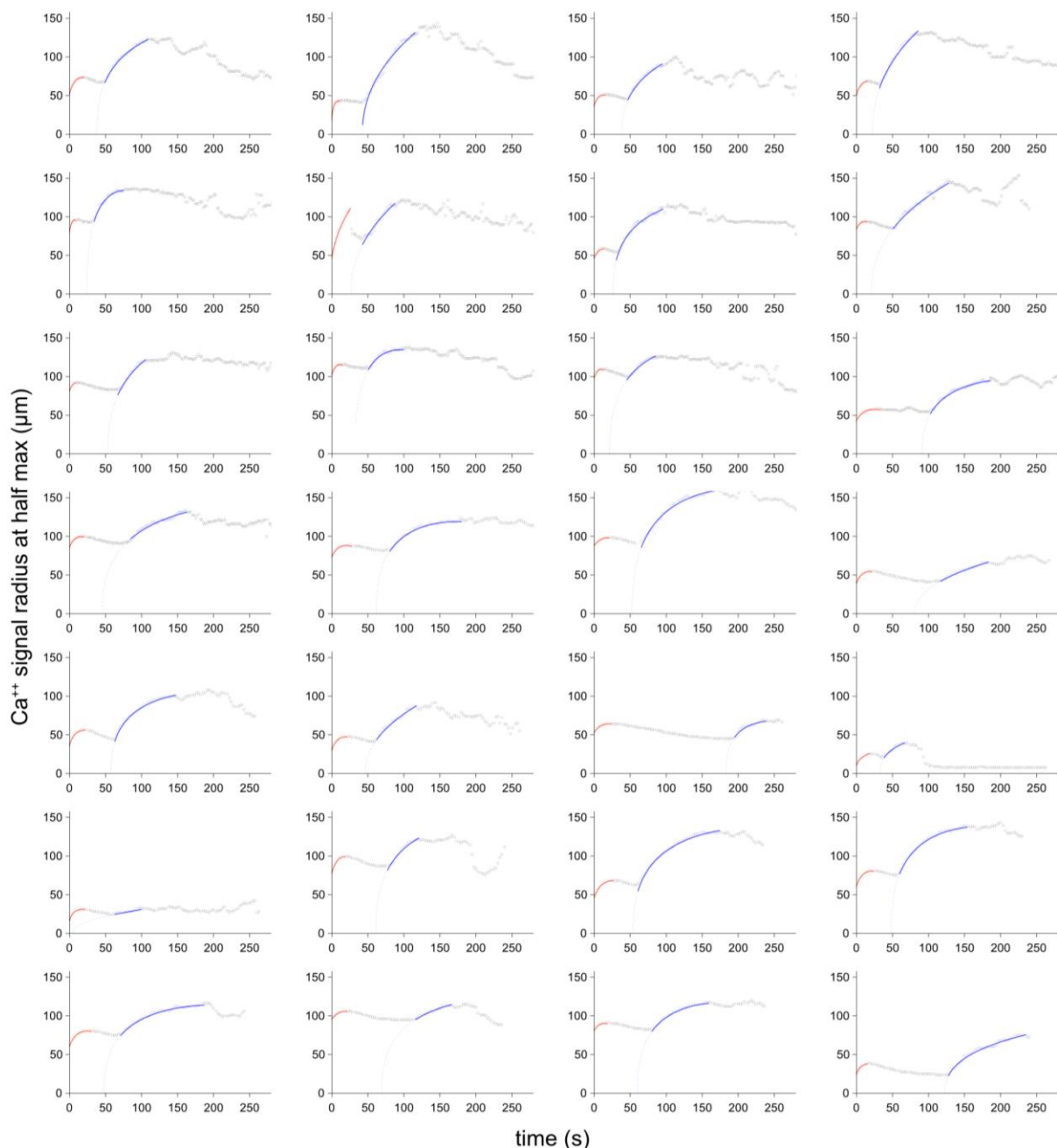
Figure 22: Fitting calcium wave expansions from Figure 11 to diffusion models. Graphs show calcium signal expansion over time for 28 individual wounds, including the four shown in Figure 11A. The first and second expansions are highlighted in red and blue respectively. The solid lines show nonlinear regression fits to each expansion using Eqn. 1 in the main text; the dashed blue lines show back-projections of fits to the second expansion. As a measure of goodness-of-fit, standard errors of the regressions for the first expansions range from 0.1 to 1.3 μm, with a median of 0.4 μm. Those for the second expansions range from 0.3 to 6.7 μm, with a median of 1.3 μm.

85

APPENDIX B

A PRELIMINARY REPORT ON THE ROLE OF TISSUE MECHANICS IN CALCIUM WAVE INITIATION AND PROPAGATION

The role of tissue mechanics is of growing interest in cell biology as it has been shown to play a role in migration, gene expression, and differentiation[157-159]. Investigators have begun to ask, what is the role of mechanotransduction at wounds? See the section titled "Tissue mechanics and mechanically gated channels" in the introduction for a review of previous work done in this area.

Through the course of our studies we have observed hints that differences in mechanical tensions throughout the tissue may somehow modulate calcium dynamics. Occasionally, we observe asymmetrically propagating waves. Regions where the calcium wave does not propagate and/or propagates slower correspond to regions with decreased mechanical tension and vice versa. For example, calcium wave propagation through the thoracic midline is attenuated around notum wounds (Figure 23A). During this stage of development, the midline is known to be under little-to-no tension, as indicated by cell morphology and ablation-recoil experiments[280]. As seen in Figure 23Aii and iii, the micro-tear induced release expands symmetrically. The wound-induced expansion, however, does not expand evenly around the midline (Figure 23Aiv-vi). We observe this trend in both wild-type tissue and under various experimental conditions. Figure 23B shows tissue where Inx3 has been knocked down. Again, wave propagation seems to be attenuated at the midline. We find it interesting that the calcium wave propagation is centered on the midline, and not the wound, which was made left of the midline.

The wave propagates faster when the notum is under tension. Occasionally the flies are mounted in such a way that creates folds in the tissue. We believe these folds indicate the tissue is under strain, as when a piece of fabric folds when one side is pulled or when matrix creases as cells apply force during migration (Ramos-Lewis, unpublished data). Figure 23C and D show examples of this. Unlike the thoracic midline, these folds are randomly generated across the tissue. The faster propagation across these randomly located folds suggests there is something intrinsic to the properties of the fold, such as actomyosin contractility, that cause this effect.
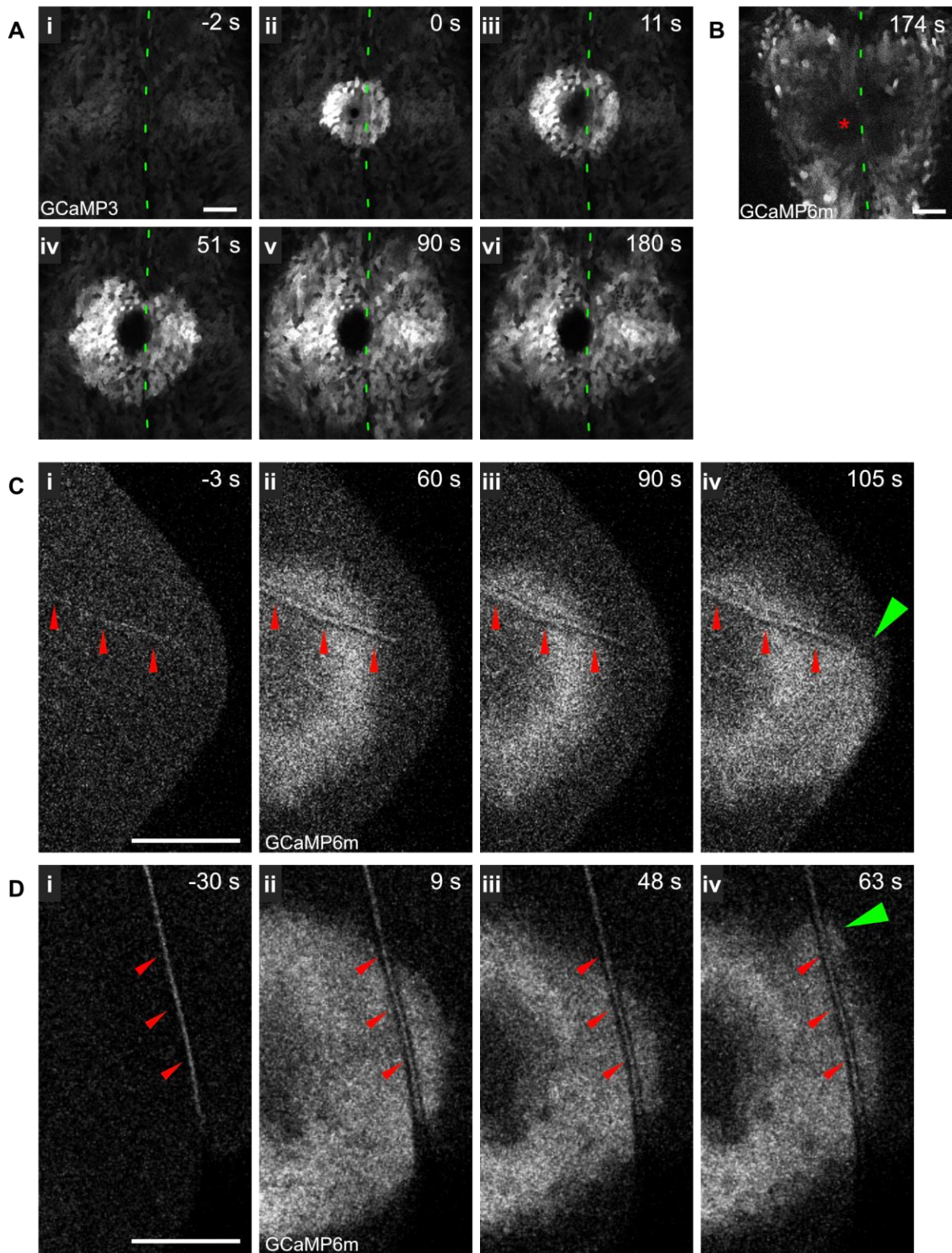
Figure 23: Asymmetric calcium wave expansion and propagation around wounds
A) Basal calcium activity is low in unwounded tissue of a fly expressing GCaMP3. Green dashed line marks the thoracic midline (i). The micro-tear induced expansion is symmetrical around the wound (ii, iii). The wound-induced expansion's propagation is

inhibited in the region of the thoracic midline creating an asymmetrical expansion (iv-vi). Scale bar is 50 µm. **B)** Asymmetrical expansion occurs in flies expressing GCaMP6m and Inx3 RNAi. The wound-induced calcium wave does not propagate symmetrically across the midline (green dashed line). However, the wave does appear to center on the midline and not the wound, which is located just left to the midline. Scale bar is 50 µm. **C and D)** A fold or crease is present in the wild-type regions of an internally controlled split-expression system flies. The region expressing IP3R RNAi is not shown. On the right of the images in C. the tissue is outside of the optically sectioned focal plane, and appears black. The fold is marked by red arrowheads. Auto-fluorescence of the thin, waxy pupae cuticle allow us to visualize the fold (i). The micro-tear induced expansion is relatively symmetric (ii and iii). In both C and D, the wound-induced expansion propagates faster along the fold than in other regions (marked by green arrowhead) (iv). Scale bar is 50 µm.

Because the first expansion event is not also affected by the midline, we conclude that our observations are not a result of altered tissue architecture along this region. As randomly located tissue folds can also effect wave propagation, this effect is not likely a result of developmental differences, like gene expression profile. We observe asymmetrical expansion even when gap junctions are blocked and the ligand driving the wound-induced expansion diffuses extracellularly. Changes in tissue tension would not affect the extracellular diffusion of a ligand; the ligand would still diffuse radially. Based on this, there are two logical explanations for these observations. First, increased tissue tension could somehow make the cell more sensitive to the ligand so the ligand's signal is translated into calcium faster. The second explanation applies to a model where calcium and the ligand participate in a feedback loop, where calcium induced the release of more ligand. Perhaps high tension and intracellular calcium are both required for the release of the ligand. Assessing the role of tissue tension is a direct, controlled manner may help us distinguish between these two possibilities.

We next aimed to directly manipulate tissue tension in a controlled fashion using our internally controlled split-expression system. Using this system, we expressed constructs that would either increase or decrease tissue tension as a result of increasing or decreasing actomyosin contraction. We found subtle differences between the time the wound-induced expansion appears in experimental and control regions. The stills in Figure 24A show the calcium wave begins earlier for the wound-induced expansion when compared to controls. This can also be seen in the graph of expansion over time in Figure 24B. By subtracting the time of expansion initiation for the experimental condition (t_{exp}) with the time of expansion initiation for the control condition (t_{con}), we can assess trends occurring over many samples.
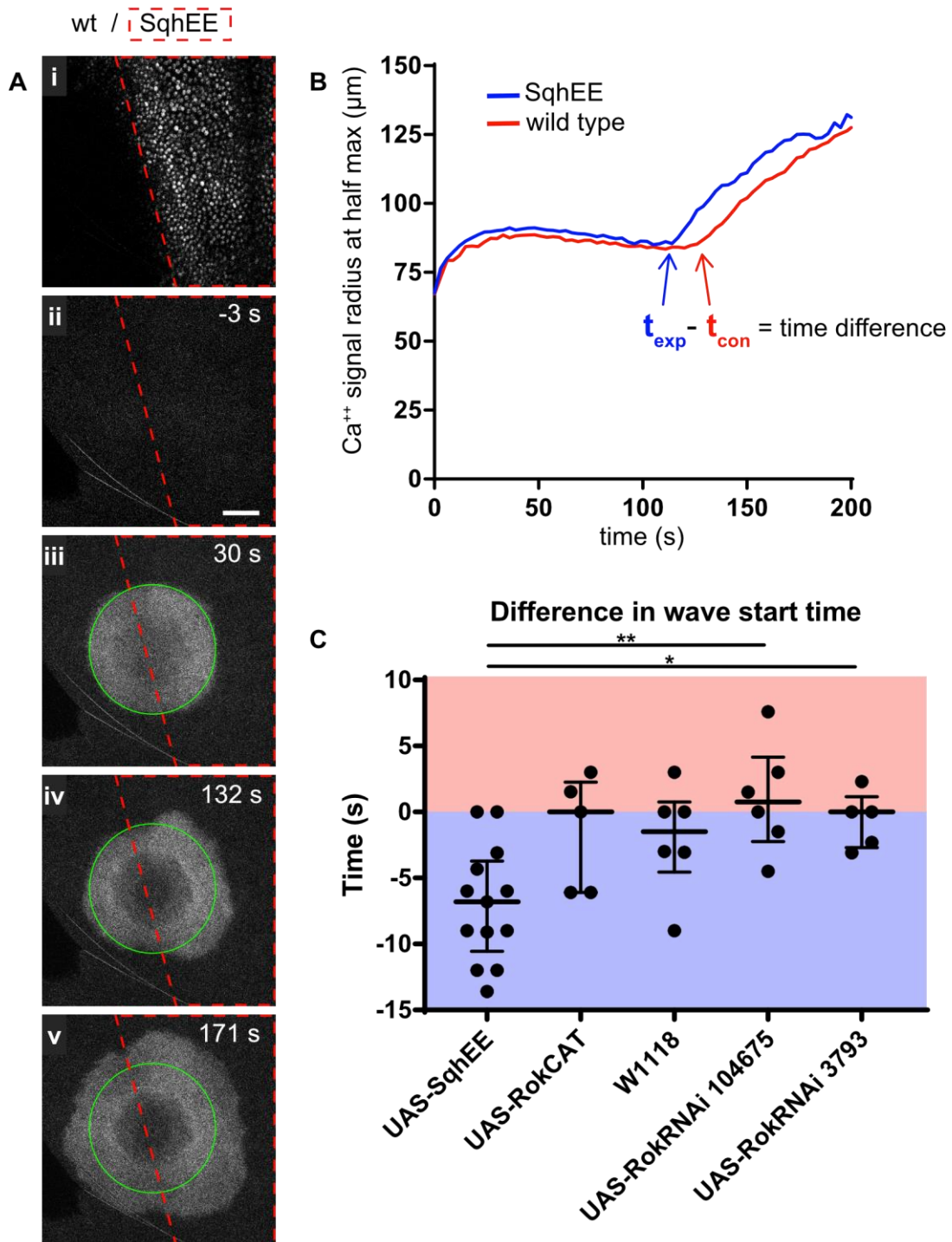
Figure 24: Calcium wave asymmetry occurs as a result of genetic perturbations to tissue tension.
A) Stills comparing wave propagation into SqhEE and wild-type regions using our internally controlled split-expression system. UAS-nucmCherry was used to identify the experimental domain, outlined in dashed red lines (i). Prior to wounding, basal calcium levels are low (ii). The micro-tear induced expansion is symmetrical (iii) but the wound-induced expansion is not (iv). The green circle is centered on the wound, overlays the

symmetrical expansion in (iii), and can be used to more easily distinguish the asymmetry in (vi and v). The wound-induced expansion begins earlier in the SqhEE region. Over time, the wave fronts even out (v). **B)** Shows the expansion over time for both domains in the stills from (A). The wound-induced calcium wave begins expanding sooner in the SqhEE region (blue line) when compared to controls (red line). Other characterisics of the calcium wave appear similar between the regions. The difference in time between the two is calculated by subtracting the experimental (t_{exp}) from control (t_{con}). **C)** James O'Connor contributed ~70% of the samples and performed the original analysis for panel C. The graph plots the time difference between the start of the wave in experimental and control regions, calculated as shown in (B). The calcium wave starts first in the experimental region if points are in the blue half of the graph and starts first in the control region if the points fall into the red half. Each point represents one wounded sample. Multiple genotypes were compared. SqhEE and RokCAT are expected to increase tissue tension while the Rok RNAi lines are expected to decrease tissue tension. *****p value is 0.0402. ******p value is 0.0031.

Figure 24C compares the time difference between the start of the visible expansion for experimental and control regions. The graph shows data from multiple samples and multiple genotypes. SqhEE and RokCAT are expected to increase tissue tension by contracting the actomyosin cytoskeleton. SqhEE is a partial phospho-mimetic for myosin regulatory light chain and RokCAT is a constitutively active kinase which phosphorylates myosin regulatory light chain[286]. RokRNAi is expected to decrease tissue tension by preventing actomyosin contraction. Like data from Figure 23, this data shows a subtle trend indicating that the calcium wave propagates earlier and/or more quickly into regions of high tension. The opposite is true for regions of low tension. This set of preliminary data suggests that the onset of expansion is altered, which is consistent with the hypothesis that the tension tunes the cell's sensitivity to a ligand. Because our data does not show the rate of expansion changes, it seems unlikely that tension plays a role in any potential calcium/ligand feedback loop mechanism of expansion.

One limitation of this analysis is that we have not confirmed how the tissue mechanics of the notum have actually changed as a result of expressing these constructs. These constructs were chosen because they all function as described in other tissues. However, this does not guarantee they will have the same effect in the notum. We can determine the effect of each construct on tissue tension using CellFIT analysis, which maps relative tissue tensions based on cell shapes and cell morphology. Our lab is currently building a fly that would allow us to visualize cell shapes and the *pnr* domain at the same time so that we can use CellFIT and strengthen these results.

APPENDIX C

ALTERNATIVE WOUNDING MECHANISMS

This appendix presents preliminary data for continuous-laser wounds and stab wounds.

Calcium influx occurs in cells around continuous laser ablation wounds as well. Figure 25 shows two examples of this. Continuous lasers do not generate a cavitation bubble and therefore are not expected to create the same extent of micro-tear damage observed around the pulsed laser ablation wounds we have previously described. Continuous lasers damage tissue with heat by decaying molecules over seconds. We observe one calcium expansion event at continuous laser wounds. When we imaged a continuous laser wound over a long time frame we found that calcium persisted in the cells near the wound margin for approximately an hour (data not shown, experiment performed by James O'Connor). Flaring is observed, but the flares propagate around the wound for seconds rather than minutes. We did not observe oscillation events as shown in Figure 14. Further analysis is required to determine if differences we observe between continuous-laser wounds and pulsed-laser wounds are a result of the different damage profiles each method creates. The different lasers could result in different amounts of lysate generated at the wound site. See the Future Directions for discussion regarding the role of lysate in calcium dynamics.

This data is quite preliminary, and without fully understanding the damage profile of continuous laser wounds it is difficult to interpret the results. Theoretically, a continuous laser wound should be quite similar to a pulsed laser wound, without cavitation. This would suggest that signals integrated by single cell wounds play a role in the tissue level wound response. If the lab chooses to build a more comprehensive understanding of the damage profile and calcium dynamics of continuous wounds we can perform similar experiments to those described in Figure 7A, Figure 10B, Figure 11, Figure 16, Figure 19, and Figure 20.
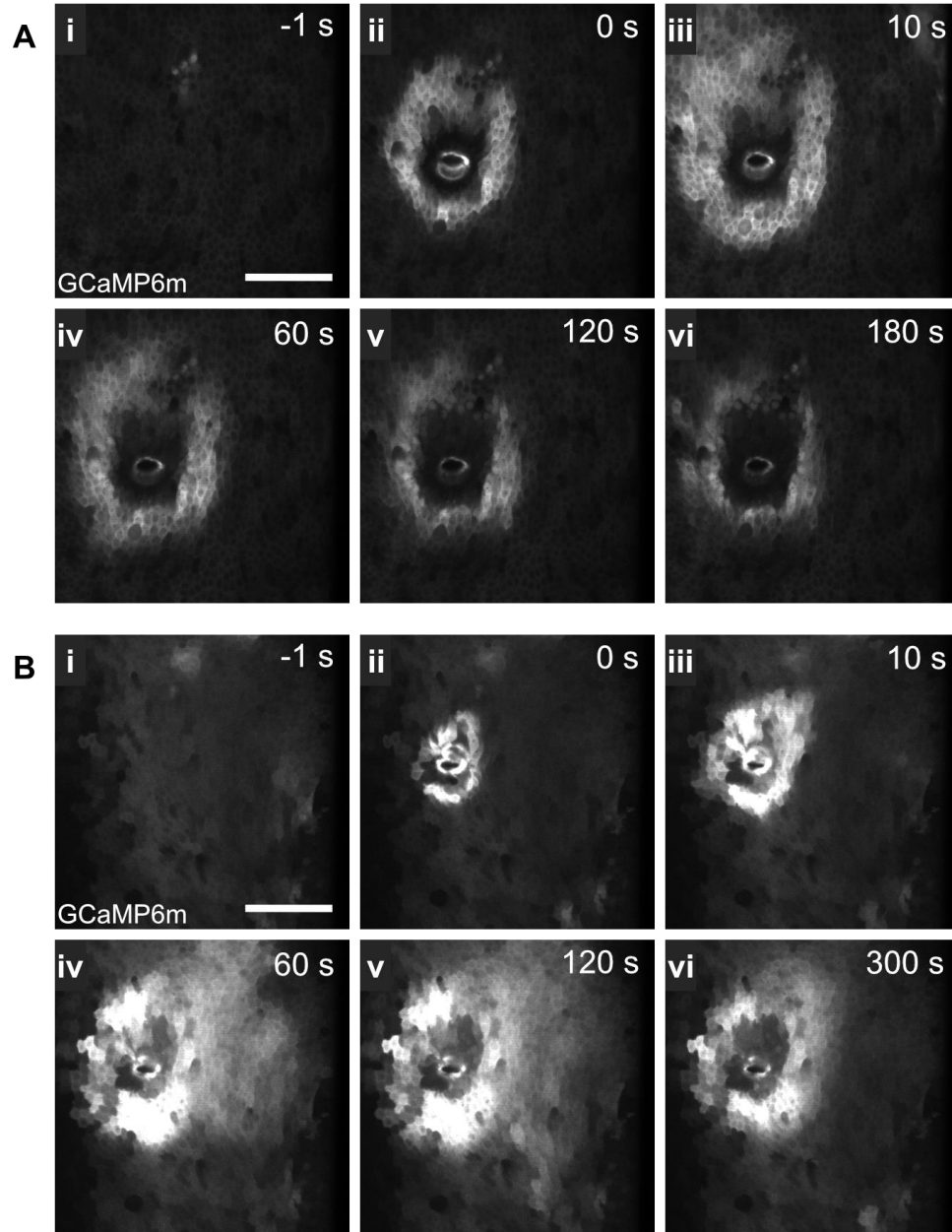
Figure 25: Calcium influx and propagation occurs around continuous laser wounds.
A) Before wounding GCaMP6m fluorescence is low in the notum (i). A wound is made by decaying the tissue with a continuous laser for ~2 seconds. We refer to the first image taken after exposure as 0 seconds. The small circle inside of the wounded region is photo-damaged, auto-fluorescent cuticle. Cytosolic calcium concentrations rise in cells near the wound over the time frame of wounding (ii). Calcium is present in neighboring cells further from the wound (iii). The calcium wave slowly fades over the course of

minutes (iv-vi). We observe some asymmetrical flaring (not shown) but not to the extent observed in pulsed laser ablation waves. Scale bar = 50 µm. **B)** A continuous laser wound was made in another sample to show normal variability. Calcium dynamics in panels Bi-vi are similar to those described in Ai-vi. Scale bar = 50 µm.

As seen in Figure 15, calcium waves also occur around stab wounds. Figure 26 shows traces for the calcium expansion over time at these wounds. The expansion events are much larger than laser ablation wounds, likely because the wound size is also much larger. Visually, it appears that only one expansion event occurs around these wounds. Based on our understanding of pulsed-laser ablation wounds, we would predict that the expansion we observe in stab wounds is similar to the wound-induced expansion. Because pulsed-laser ablation wound generate exaggerated amounts of micro-tearing, the micro-tear induced expansion is very obvious and easy to study. We wound not expect stab wounds to have exaggerated micro-tearing and therefore we do not expect to see a micro-tear induced expansion. However, in the traces we can identify inflection points in the curve. These inflection points could indicate the presence of a second expansion merging with the first.

To learn more about this expansion, we can perform a kinematic analysis as shown in Figure 11. In the analysis, we could chose to assume there are two expansion events, as in our pulsed laser wounds, and use the inflection points to break apart the first and second expansions. We could also perform the analysis where we assume there is only one expansion event. We can then compare the diffusion constants calculated from both of these scenarios to the diffusion constant calculated for the second expansion in Figure 11. If the diffusion constant for the "one wave" analysis matches the diffusion constant that we have identified for the second, wound-induced expansion, then it is likely that the calcium wave we observe at stab wounds is mechanistically similar to the wound-induced expansion at pulsed-laser ablation wounds.

We could further test the similarities between stab wounds and ablation wounds by knocking down Gαq, PLCβ, and IP3R in the *pnr* domain before stab wounding. Each of these RNAi constructs yielded significant differences from controls, therefore it should be easy to assess whether or not the calcium wave in stab wounds is attenuated without the internally controlled split-expression system.
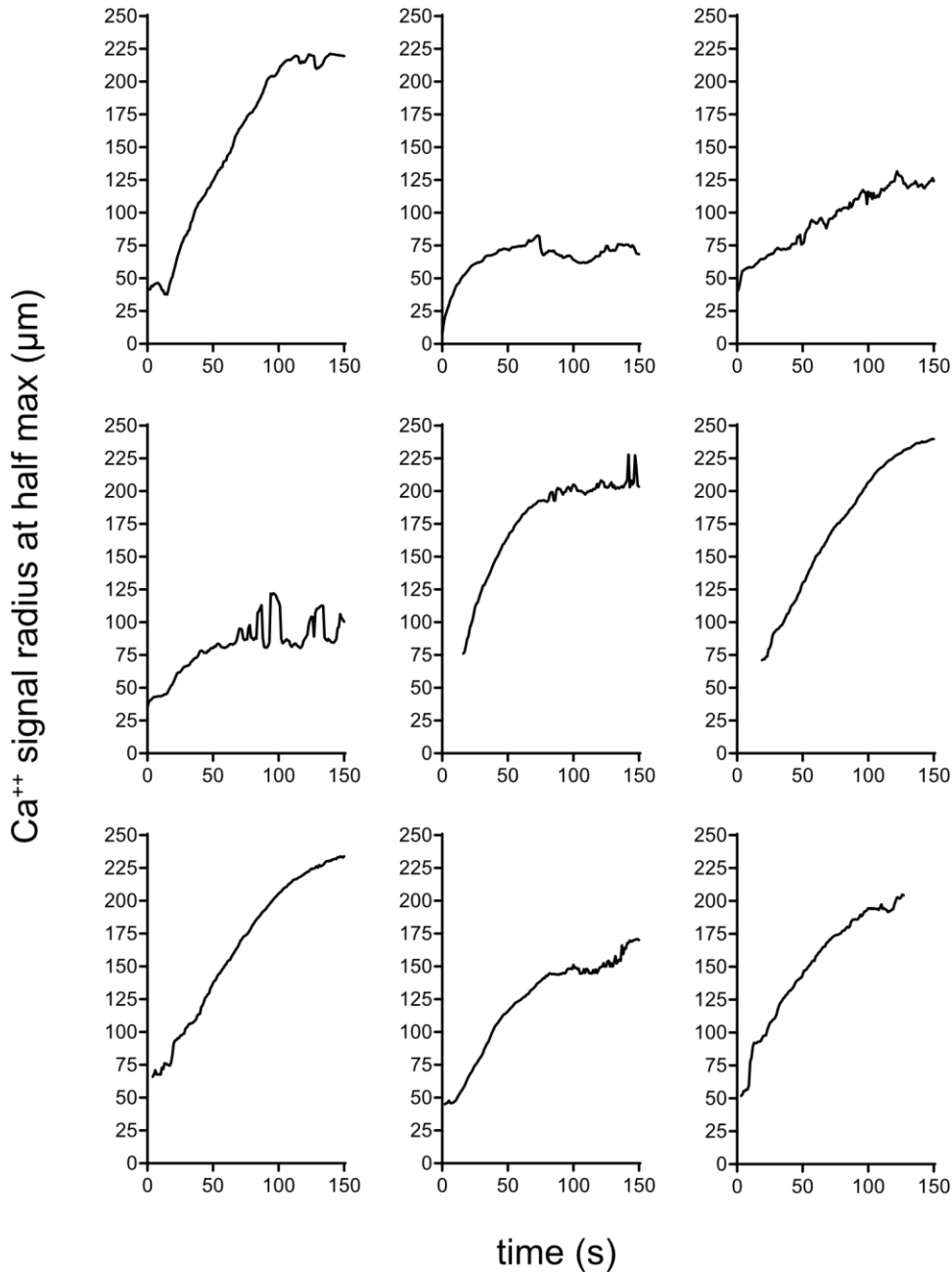
Figure 26: Calcium expansion over time in stab wounds
Graphs show the average calcium radius over time for stab wounds. Each graph represents one sample. When the notum is stabbed, hemolymph bubbles out of the wound and can obscure the wound margin. As a result, occasionally it is not possible to measure the radius of calcium until it expands away from the hemolymph bubble. We do observe calcium flares around stab wounds. However, the asymmetrical flares are not represented in this analysis due to radial averaging.

APPENDIX D

LIGHT INDUCED CALCIUM WAVES

There is at least one previous report in the literature that light can induce calcium waves in non-stimulatory cells. When chondrocytes containing a fluorescent calcium dye were exposed to intense light they exhibited spontaneous calcium transients[287]. The calcium transients were attenuated when ROS was quenched or when exposed to less intense light. These results suggest photo-bleaching of the cell was capable of producing sufficient ROS to stimulate calcium influx. This is not entirely surprising as oxidative stress is known to alter calcium metabolism[288-290].

We have observed that light induces calcium dynamics in the *Drosophila* notum. When a notum expressing GCaMP is exposed to epifluorescent light at the maximum intensity setting on our M2 Zeiss microscope for 40-60 seconds spontaneous calcium waves appear and propagate through the tissue (data not shown). This does not occur when we expose the tissue to the lowest setting of epifluorescent light, even over long periods of time. We have also confirmed that this does not occur when the tissue is exposed to the light from the scanning confocal (data not shown). We suspect photo-degradation releases sufficient ROS to activate a calcium wave. This light induced wave could also be a response to heat. However, after heat shocking the tissue in a water bath, we did not observe a calcium wave (data not shown).

It would be interesting to see if these calcium dynamics still occur when the tissue is soaked in a ROS quencher, such as catalase. It would also be interesting to determine whether these calcium dynamics are acting through the Gαq pathway we have identified in Chapter 3.

REFERENCES

1   Alberts, B., Lewis, J., Raff, M., Roberts, K. & Walter, P. Molecular Biology of the Cell. *Garland Science* (2002).

2   Martini, E., Krug, S. M., Siegmund, B., Neurath, M. F. & Becker, C. Mend Your Fences The Epithelial Barrier and its Relationship With Mucosal Immunity in Inflammatory Bowel Disease. *Cellular and Molecular Gastroenterology and Hepatology* **4**, 33-46, doi:10.1016/j.jcmgh.2017.03.007 (2017).

3   Honda, H. The world of epithelial sheets. *Development, Growth & Differentiation*, doi:10.1111/dgd.12350 (2017).

4   Gumbiner, B. M. Mini-Review Breaking through the Tight Junction Barrier. *Mini-Review Breaking through the Tight Junction Barrier* (1993).

5   Lommel, A. T. L. *From cells to organs: a histology textbook and atlas*. (Springer Science & Business Media, 2003).

6   Wood, W. Wound Healing: Calcium Flashes Illuminate Early Events. *Current Biology*, doi:10.1016/j.cub.2011.11.019 (2012).

7   Scemes, E. & Giaume, C. Astrocyte calcium waves: what they are and what they do. *Glia* **54**, 716-725, doi:10.1002/glia.20374 (2006).

8   Antunes, M., Pereira, T., Cordeiro, J., Almeida, L. & Jacinto, A. Coordinated waves of actomyosin flow and apical cell constriction immediately after wounding. *The Journal of Cell Biology* **202**, doi:10.1083/jcb.201211039.

9   Yoo, S. K., Freisinger, C. M., LeBert, D. C. & Huttenlocher, A. Early redox, Src family kinase, and calcium signaling integrate wound responses and tissue regeneration in zebrafish. *The Journal of cell biology* **199**, 225-234, doi:10.1083/jcb.201203154 (2012).

10   Bement, W. M., Mandato, C. A. & Kirsch, M. N. Wound-induced assembly and closure of an actomyosin purse string in Xenopus oocytes. *Current biology* (1999).

11   Berridge, M. J., Bootman, M. D. & Roderick, H. L. Calcium signalling: dynamics, homeostasis and remodelling. *Nat Rev Mol Cell Biol* **4**, 517-529, doi:10.1038/nrm1155 (2003).

12   Razzell, W., Evans, I. R., Martin, P. & Wood, W. Calcium flashes orchestrate the wound inflammatory response through DUOX activation and hydrogen peroxide release. *Current biology : CB* **23**, 424-429, doi:10.1016/j.cub.2013.01.058 (2013).

13   Enyedi, B. & Niethammer, P. Mechanisms of epithelial wound detection. *Trends in Cell Biology* **25**, doi:10.1016/j.tcb.2015.02.007 (2015).

14   Enyedi, B., Kala, S. & Nikolich-Zugich, T. Tissue damage detection by osmotic surveillance. *Nature cell …* (2013).

15   Wales, P. *et al.* Calcium-mediated actin reset (CaAR) mediates acute cell adaptations. *eLife* **5**, doi:10.7554/eLife.19850 (2016).

16   Abreu-Blanco, M. T., Verboon, J. M. & Parkhurst, S. M. Coordination of Rho family GTPase activities to orchestrate cytoskeleton responses during cell wound repair. *Current biology : CB* **24**, 144-155, doi:10.1016/j.cub.2013.11.048 (2014).

17   Soto, X. *et al.* Inositol kinase and its product accelerate wound healing by modulating calcium levels, Rho GTPases, and F-actin assembly. *Proceedings of the National Academy of Sciences of the United States of America* **110**, 11029-11034, doi:10.1073/pnas.1217308110 (2013).

18   Mandato, C. A. & Bement, W. M. Contraction and polymerization cooperate to assemble and close actomyosin rings around Xenopus oocyte wounds. *J Cell Biol*, doi:10.1083/jcb.200103105 (2001).

19   Godin, L. M., Vergen, J., Prakash, Y. S., Pagano, R. E. & Hubmayr, R. D. Spatiotemporal

dynamics of actin remodeling and endomembrane trafficking in alveolar epithelial type I cell wound healing. *Am J Physiol Lung Cell Mol Physiol* **300**, L615-623, doi:10.1152/ajplung.00265.2010 (2011).

20 Xu, S. & Chisholm, A. D. A Gα q-Ca 2+ signaling pathway promotes actin-mediated epidermal wound closure in C. elegans. *Current biology*, doi:10.1016/j.cub.2011.10.050 (2011).

21 Gao, K. *et al.* Traumatic scratch injury in astrocytes triggers calcium influx to activate the JNK/c-Jun/AP-1 pathway and switch on GFAP expression. *Glia* **61**, 2063-2077, doi:10.1002/glia.22577 (2013).

22 Tran, P. O. T., Hinman, L. E., Unger, G. M. & Sammak, P. J. A wound-induced [Ca 2+] i increase and its transcriptional activation of immediate early genes is important in the regulation of motility. *Experimental cell research* (1999).

23 Justet, C., Hernández, J. A., Torriglia, A. & Chifflet, S. Fast calcium wave inhibits excessive apoptosis during epithelial wound healing. *Cell and Tissue Research*, doi:10.1007/s00441-016-2388-8 (2016).

24 Chifflet, S. *et al.* Early and late calcium waves during wound healing in corneal endothelial cells. *Wound repair and regeneration : official publication of the Wound Healing Society [and] the European Tissue Repair Society* **20**, 28-37, doi:10.1111/j.1524-475X.2011.00749.x (2012).

25 Klepeis, V. E., Cornell-Bell, A. & Trinkaus-Randall, V. Growth factors but not gap junctions play a role in injury-induced Ca2+ waves in epithelial cells. *Journal of Cell Science* **114**, 4185-4195 (2001).

26 Sung, Y. J. *et al.* Intercellular calcium waves mediate preferential cell growth toward the wound edge in polarized hepatic cells. *Exp Cell Res* **287**, 209-218 (2003).

27 Leiper, L. J. *et al.* The roles of calcium signaling and ERK1/2 phosphorylation in a Pax6+/- mouse model of epithelial wound-healing delay. *BMC Biol* **4**, 27, doi:10.1186/1741-7007-4-27 (2006).

28 Lansdown, A. B. G. Calcium: a potential central regulator in wound healing in the skin. *Wound repair and regeneration*, doi:10.1046/j.1524-475X.2002.10502.x (2002).

29 Stanisstreet, M. Calcium and wound healing in Xenopus early embryos. *Development* (1982).

30 Weinger, I., Klepeis, V. E. & Trinkaus-Randall, V. Tri-nucleotide receptors play a critical role in epithelial cell wound repair. *Purinergic signalling* **1**, 281-292, doi:10.1007/s11302-005-8132-6 (2005).

31 Restrepo, S. & Basler, K. Drosophila wing imaginal discs respond to mechanical injury via slow InsP3R-mediated intercellular calcium waves. *Nature communications* **7**, 12450, doi:10.1038/ncomms12450 (2016).

32 Klepeis, V. E., Weinger, I., Kaczmarek, E. & Trinkaus-Randall, V. P2Y receptors play a critical role in epithelial cell communication and migration. *Journal of cellular biochemistry* **93**, 1115-1133, doi:10.1002/jcb.20258 (2004).

33 Benink, H. A. & Bement, W. M. Concentric zones of active RhoA and Cdc42 around single cell wounds. *The Journal of Cell Biology* **168**, doi:10.1083/jcb.200411109 (2005).

34 Sammak, P. J., Hinman, L. E., Tran, P. O., Sjaastad, M. D. & Machen, T. E. How do injured cells communicate with the surviving cell monolayer? *Journal of cell science* **110 (Pt 4)**, 465-475 (1997).

35 Shabir, S. & Southgate, J. Calcium signalling in wound-responsive normal human urothelial cell monolayers. *Cell calcium* **44**, 453-464, doi:10.1016/j.ceca.2008.02.008 (2008).

36 Balaji, R. *et al.* Calcium spikes, waves and oscillations in a large, patterned epithelial tissue. *Scientific reports* **7**, 42786, doi:10.1038/srep42786 (2017).

37 Frame, M. K. & de Feijter, A. W. Propagation of mechanically induced intercellular calcium waves via gap junctions and ATP receptors in rat liver epithelial cells. *Exp Cell Res* **230**,

197-207, doi:10.1006/excr.1996.3409 (1997).

38   Arcuino, G. *et al.* Intercellular calcium signaling mediated by point-source burst release of ATP. *Proceedings of the National Academy of Sciences of the United States of America* **99**, 9840-9845, doi:10.1073/pnas.152588599 (2002).

39   Narciso, C. E., Contento, N. M., Storey, T. J., Hoelzle, D. J. & Zartman, J. J. Release of Applied Mechanical Loading Stimulates Intercellular Calcium Waves in Drosophila Wing Discs. *Biophys J* **113**, 491-501, doi:10.1016/j.bpj.2017.05.051 (2017).

40   Clark, A. G. *et al.* Integration of single and multicellular wound responses. *Current biology : CB* **19**, 1389-1395, doi:10.1016/j.cub.2009.06.044 (2009).

41   Churchill, G. C., Atkinson, M. M. & Louis, C. F. Mechanical stimulation initiates cell-to-cell calcium signaling in ovine lens epithelial cells. *J Cell Sci* **109 (Pt 2)**, 355-365 (1996).

42   Enomoto, K., Furuya, K., Yamagishi, S., Oka, T. & Maeno, T. The increase in the intracellular Ca2+ concentration induced by mechanical stimulation is propagated via release of pyrophosphorylated nucleotides in mammary epithelial cells. *Pflugers Archiv : European journal of physiology* **427**, 533-542 (1994).

43   Narciso, C. *et al.* Patterning of wound-induced intercellular Ca(2+) flashes in a developing epithelium. *Physical biology* **12**, 56005, doi:10.1088/1478-3975/12/5/056005 (2015).

44   Zeitlinger, J. & Bohmann, D. Thorax closure in Drosophila: involvement of Fos and the JNK pathway. *Development (Cambridge, England)* **126**, 3947-3956 (1999).

45   Clark, R. A. F. Regulation of fibroplasia in cutaneous wound repair. *The American journal of the medical sciences* (1993).

46   Clark, R. A. F. Wound repair. Overview and general considerations. *The molecular and cellular biology of wound repair* (1994).

47   Werner, S. & Grose, R. Regulation of wound healing by growth factors and cytokines. *Physiological reviews* (2003).

48   Martin, P. Wound healing--aiming for perfect skin regeneration. *Science* (1997).

49   Riches, D. W. H. Macrophage involvement in wound repair, remodeling, and fibrosis. *The molecular and cellular biology of wound repair* (1988).

50   Eriksson, A., Siegbahn, A., Westermark, B., Heldin, C. H. & Claesson-Welsh, L. PDGF alpha- and beta-receptors activate unique and common signal transduction pathways. *EMBO J* **11**, 543-550 (1992).

51   Nanney, L. B., Ellis, D. L., Levine, J. & King, L. E. Epidermal growth factor receptors in idiopathic and virally induced skin diseases. *Am J Pathol* **140**, 915-925 (1992).

52   Frank, S., Madlener, M. & Werner, S. Transforming growth factors beta1, beta2, and beta3 and their receptors are differentially regulated during normal and impaired wound healing. *J Biol Chem* **271**, 10188-10193 (1996).

53   Hübner, G., Brauchle, M., Smola, H. & Madlener, M. Differential regulation of pro-inflammatory cytokines during wound healing in normal and glucocorticoid-treated mice. *Cytokine* (1996).

54   Shaw, T. J. & Martin, P. Wound repair at a glance. *J Cell Sci* **122**, 3209-3213, doi:10.1242/jcs.031187 (2009).

55   Michopoulou, A. & Rousselle, P. How do epidermal matrix metalloproteinases support re-epithelialization during skin healing? *Eur J Dermatol* **25 Suppl 1**, 33-42, doi:10.1684/ejd.2015.2553 (2015).

56   Cavani, A. *et al.* Distinctive integrin expression in the newly forming epidermis during wound healing in humans. *J Invest Dermatol* **101**, 600-604 (1993).

57   Breuss, J. M. *et al.* Expression of the beta 6 integrin subunit in development, neoplasia and tissue repair suggests a role in epithelial remodeling. *J Cell Sci* **108 (Pt 6)**, 2241-2251 (1995).

58   Haapasalmi, K. *et al.* Keratinocytes in human wounds express alpha v beta 6 integrin. *J*

Invest Dermatol **106**, 42-48 (1996).

59   Garlick, J. A. & Taichman, L. B. Fate of human keratinocytes during reepithelialization in an organotypic culture model. *Lab Invest* **70**, 916-924 (1994).

60   Ito, M., Liu, Y., Yang, Z., Nguyen, J. & Fan, L. Stem cells in the hair follicle bulge contribute to wound repair but not to homeostasis of the epidermis. *Nature …* (2005).

61   Hertle, M. D., Kubler, M. D., Leigh, I. M. & Watt, F. M. Aberrant integrin expression during epidermal wound healing and in psoriatic epidermis. *J Clin Invest* **89**, 1892-1901, doi:10.1172/JCI115794 (1992).

62   Compton, C. C. *et al.* Skin regenerated from cultured epithelial autografts on full-thickness burn wounds from 6 days to 5 years after grafting. A light, electron microscopic and immunohistochemical study. *Lab Invest* **60**, 600-612 (1989).

63   Singer, A. J. & Clark, R. A. F. Cutaneous wound healing. *New England journal of medicine* (1999).

64   Sonnemann, K. J. & Bement, W. M. Wound repair: toward understanding and integration of single-cell and multicellular wound responses. *Annual review of cell and developmental biology* **27**, 237-263, doi:10.1146/annurev-cellbio-092910-154251 (2011).

65   Martin, P. & Lewis, J. Actin cables and epidermal movement in embryonic wound healing. *Nature* (1992).

66   Martin, P. & Parkhurst, S. M. Parallels between tissue repair and embryo morphogenesis. *Development*, doi:10.1242/dev.01253 (2004).

67   McCluskey, J. & Martin, P. Analysis of the tissue movements of embryonic wound healing--DiI studies in the limb bud stage mouse embryo. *Dev Biol* **170**, 102-114, doi:10.1006/dbio.1995.1199 (1995).

68   Brock, J., Midwinter, K., Lewis, J. & Martin, P. Healing of incisional wounds in the embryonic chick wing bud: characterization of the actin purse-string and demonstration of a requirement for Rho activation. *J Cell Biol* **135**, 1097-1107 (1996).

69   Larson, B. J., Longaker, M. T. & Lorenz, H. P. Scarless fetal wound healing: a basic science review. *Plastic and reconstructive …* (2010).

70   Belacortu, Y. & Paricio, N. Drosophila as a model of wound healing and tissue regeneration in vertebrates. *Developmental Dynamics*, doi:10.1002/dvdy.22753 (2011).

71   Danjo, Y. & Gipson, I. K. Actin 'purse string'filaments are anchored by E-cadherin-mediated adherens junctions at the leading edge of the epithelial wound, providing coordinated cell …. *Journal of cell science* (1998).

72   Gurtner, G. C., Werner, S., Barrandon, Y. & Longaker, M. T. Wound repair and regeneration. *Nature* (2008).

73   Hopkinson-Woolley, J., Hughes, D., Gordon, S. & Martin, P. Macrophage recruitment during limb development and wound healing in the embryonic and foetal mouse. *J Cell Sci* **107 (Pt 5)**, 1159-1167 (1994).

74   Leavitt, T., Hu, M. S., Marshall, C. D. & Barnes, L. A. Scarless wound healing: finding the right cells and signals. *Cell and tissue …* (2016).

75   Galko, M. J. & Krasnow, M. A. Cellular and genetic analysis of wound healing in Drosophila larvae. *PLoS biology* **2**, doi:10.1371/journal.pbio.0020239 (2004).

76   Arwert, E. N., Hoste, E. & Watt, F. M. Epithelial stem cells, wound healing and cancer. *Nat Rev Cancer* **12**, 170-180, doi:10.1038/nrc3217 (2012).

77   Grice, E. A. & Segre, J. A. The skin microbiome. *Nat Rev Microbiol* **9**, 244-253, doi:10.1038/nrmicro2537 (2011).

78   Wood, W., Faria, C. & Jacinto, A. Distinct mechanisms regulate hemocyte chemotaxis during development and wound healing in Drosophila melanogaster. *J Cell Biol* **173**, 405-416, doi:10.1083/jcb.200508161 (2006).

79   Grose, R. & Werner, S. Wound-healing studies in transgenic and knockout mice. *Mol*

Biotechnol **28**, 147-166, doi:10.1385/MB:28:2:147 (2004).

80   Dvorak, H. F. Tumors: wounds that do not heal. Similarities between tumor stroma generation and wound healing. *N Engl J Med* **315**, 1650-1659, doi:10.1056/NEJM198612253152606 (1986).

81   Schafer, M. & Werner, S. Cancer as an overhealing wound: an old hypothesis revisited. *Nat Rev Mol Cell Biol* **9**, 628-638, doi:10.1038/nrm2455 (2008).

82   Gonda, T. A., Tu, S. & Wang, T. C. Chronic inflammation, the tumor microenvironment and carcinogenesis. *Cell Cycle* **8**, 2005-2013, doi:10.4161/cc.8.13.8985 (2009).

83   Stevens, L. J. & Page-McCaw, A. A secreted MMP is required for reepithelialization during wound healing. *Molecular biology of the cell* **23**, 1068-1079, doi:10.1091/mbc.E11-09-0745 (2012).

84   Bianchi, M. E. DAMPs, PAMPs and alarmins: all we need to know about danger. *Journal of Leukocyte Biology* **81**, 1-5, doi:10.1189/jlb.0306164 (2007).

85   Cordeiro, J. V. & Jacinto, A. The role of transcription-independent damage signals in the initiation of epithelial wound healing. *Nature reviews. Molecular cell biology* (2013).

86   Janeway, C. A. Approaching the asymptote? Evolution and revolution in immunology. *Cold Spring Harbor symposia on quantitative …*, doi:10.1101/SQB.1989.054.01.003 (1989).

87   Matzinger, P. Tolerance, danger, and the extended family. *Annual review of immunology*, doi:10.1146/annurev.iy.12.040194.005015 (1994).

88   Rock, K. L., Latz, E. & Ontiveros, F. The sterile inflammatory response. *Annual review of …* (2009).

89   Kono, H. & Rock, K. L. How dying cells alert the immune system to danger. *Nature Reviews Immunology* **8**, 279-289, doi:10.1038/nri2215 (2008).

90   Kono, H., Onda, A. & Yanagida, T. Molecular determinants of sterile inflammation. *Current opinion in immunology* **26**, 147-156 (2014).

91   Srinivasan, N., Gordon, O., Ahrens, S. & Franz, A. Actin is an evolutionarily-conserved damage-associated molecular pattern that signals tissue injury in Drosophila melanogaster. *Elife* (2016).

92   Ahrens, S., Zelenay, S., Sancho, D., Hanč, P. & Kjær, S. F-actin is an evolutionarily conserved damage-associated molecular pattern recognized by DNGR-1, a receptor for dead cells. *Immunity* (2012).

93   Adair-Kirk, T. L. & Atkinson, J. J. A site on laminin α5, AQARSAASKVKVSMKF, induces inflammatory cell production of matrix metalloproteinase-9 and chemotaxis. *The Journal of …*, doi:10.4049/jimmunol.171.1.398 (2003).

94   Müller, S., Scaffidi, P., Degryse, B. & Bonaldi, T. The double life of HMGB1 chromatin protein: architectural factor and extracellular signal. *The EMBO …* (2001).

95   Andersson, U. *et al.* High mobility group 1 protein (HMG-1) stimulates proinflammatory cytokine synthesis in human monocytes. *J Exp Med* **192**, 565-570 (2000).

96   Scaffidi, P., Mistell, T. & Bianchi, M. E. Release of chromatin protein HMGB1 by necrotic cells triggers inflammation. *Nature* (2002).

97   Seong, S.-Y. & Matzinger, P. Opinion: Hydrophobicity: an ancient damage-associated molecular pattern that initiates innate immune responses. *Nature Reviews Immunology* **4**, 469-478, doi:10.1038/nri1372 (2004).

98   Binder, R. J., Anderson, K. M. & Basu, S. Cutting edge: heat shock protein gp96 induces maturation and migration of CD11c+ cells in vivo. *The Journal of …* (2000).

99   Elliott, M. R., Chekeni, F. B., Trampont, P. C. & Lazarowski, E. R. Nucleotides released by apoptotic cells act as a find-me signal for phagocytic clearance. *Nature* (2009).

100   Praetorius, H. A. & Leipziger, J. ATP release from non-excitable cells. *Purinergic signalling* (2009).

101   Burnstock, G. Introductory overview of purinergic signalling. *Frontiers in bioscience (Elite*

edition) (2011).

102   Burnstock, G., Knight, G. E. & Greig, A. V. H. Purinergic signaling in healthy and diseased skin. *Journal of Investigative Dermatology* (2012).

103   Burnstock, G. Purinergic nerves. *Pharmacological reviews* (1972).

104   Fountain, S. J. & Burnstock, G. An evolutionary history of P2X receptors. *Purinergic signalling* **5**, 269-272, doi:10.1007/s11302-008-9127-x (2009).

105   Perregaux, D. & Gabel, C. A. Interleukin-1 beta maturation and release in response to ATP and nigericin. Evidence that potassium depletion mediated by these agents is a necessary and common …. *Journal of Biological Chemistry* (1994).

106   Gault, W. J., Enyedi, B. & Niethammer, P. Osmotic surveillance mediates rapid wound closure through nucleotide release. *The Journal of Cell Biology* **207**, 767-782, doi:10.1083/jcb.201408049 (2014).

107   Boucher, I., Rich, C., Lee, A., Marcincin, M. & Trinkaus-Randall, V. The P2Y2 receptor mediates the epithelial injury response and cell migration. *AJP: Cell Physiology* **299**, doi:10.1152/ajpcell.00100.2009 (2010).

108   Yin, J., Xu, K., Zhang, J., Kumar, A. & Yu, F. S. X. Wound-induced ATP release and EGF receptor activation in epithelial cells. *Journal of Cell Science* **120**, 815-825, doi:10.1242/jcs.03389 (2007).

109   Sham, D., Wesley, U. V., Hristova, M. & van der Vliet, A. ATP-mediated transactivation of the epidermal growth factor receptor in airway epithelial cells involves DUOX1-dependent oxidation of Src and ADAM17. *PloS one* **8**, doi:10.1371/journal.pone.0054391 (2013).

110   Wesley, U. V., Bove, P. F., Hristova, M., McCarthy, S. & van der Vliet, A. Airway epithelial cell migration and wound repair by ATP-mediated activation of dual oxidase 1. *The Journal of biological chemistry* **282**, 3213-3220, doi:10.1074/jbc.M606533200 (2007).

111   Boucher, I., Yang, L., Mayo, C., Klepeis, V. & Trinkaus-Randall, V. Injury and nucleotides induce phosphorylation of epidermal growth factor receptor: MMP and HB-EGF dependent pathway. *Experimental Eye Research* **85**, 130-141, doi:10.1016/j.exer.2007.03.009 (2007).

112   Block, E. R. & Klarlund, J. K. Wounding sheets of epithelial cells activates the epidermal growth factor receptor through distinct short- and long-range mechanisms. *Molecular biology of the cell* **19**, 4909-4917, doi:10.1091/mbc.E08-01-0097 (2008).

113   Niethammer, P., Grabher, C., Look, T. A. & Mitchison, T. J. A tissue-scale gradient of hydrogen peroxide mediates rapid wound detection in zebrafish. *Nature*, doi:10.1038/nature08119 (2009).

114   Aruoma, O. I., Grootveld, M. & Bahorun, T. Free radicals in biology and medicine: from inflammation to biotechnology. *Biofactors* **27**, 1-3 (2006).

115   Hurd, T. R., DeGennaro, M. & Lehmann, R. Redox regulation of cell migration and adhesion. *Trends Cell Biol* **22**, 107-115, doi:10.1016/j.tcb.2011.11.002 (2012).

116   Veal, E. A., Day, A. M. & Morgan, B. A. Hydrogen peroxide sensing and signaling. *Mol Cell* **26**, 1-14, doi:10.1016/j.molcel.2007.03.016 (2007).

117   Essex, D. W. & Li, M. Redox control of platelet aggregation. *Biochemistry* **42**, 129-136, doi:10.1021/bi0205045 (2003).

118   Sen, C. K. & Roy, S. Redox signals in wound healing. *Biochimica et Biophysica Acta (BBA)-General Subjects* (2008).

119   de Oliveira-Marques, V., Cyrne, L., Marinho, H. S. & Antunes, F. A quantitative study of NF-kappaB activation by H2O2: relevance in inflammation and synergy with TNF-alpha. *J Immunol* **178**, 3893-3902 (2007).

120   Junn, E. *et al.* Requirement of hydrogen peroxide generation in TGF-beta 1 signal transduction in human lung fibroblast cells: involvement of hydrogen peroxide and Ca2+ in TGF-beta 1-induced IL-6 expression. *J Immunol* **165**, 2190-2197 (2000).

121   Babior, B. M. Phagocytes and oxidative stress. *Am J Med* **109**, 33-44 (2000).

122   Tang, D. *et al.* Hydrogen peroxide stimulates macrophages and monocytes to actively release HMGB1. *J Leukoc Biol* **81**, 741-747, doi:10.1189/jlb.0806540 (2007).

123   Ranjan, P. *et al.* Redox-dependent expression of cyclin D1 and cell proliferation by Nox1 in mouse lung epithelial cells. *Antioxid Redox Signal* **8**, 1447-1459, doi:10.1089/ars.2006.8.1447 (2006).

124   Nishio, E. & Watanabe, Y. The involvement of reactive oxygen species and arachidonic acid in alpha 1-adrenoceptor-induced smooth muscle cell proliferation and migration. *Br J Pharmacol* **121**, 665-670, doi:10.1038/sj.bjp.0701171 (1997).

125   Kuribayashi, K. *et al.* Essential role of protein kinase C zeta in transducing a motility signal induced by superoxide and a chemotactic peptide, fMLP. *J Cell Biol* **176**, 1049-1060, doi:10.1083/jcb.200607019 (2007).

126   Hober, S., Lundstrom Ljung, J., Uhlen, M. & Nilsson, B. Insulin-like growth factors I and II are unable to form and maintain their native disulfides under in vivo redox conditions. *FEBS Lett* **443**, 271-276 (1999).

127   Nelson, K. K. *et al.* Redox-dependent matrix metalloproteinase-1 expression is regulated by JNK through Ets and AP-1 promoter motifs. *J Biol Chem* **281**, 14100-14110, doi:10.1074/jbc.M601820200 (2006).

128   Wenk, J. *et al.* Stable overexpression of manganese superoxide dismutase in mitochondria identifies hydrogen peroxide as a major oxidant in the AP-1-mediated induction of matrix-degrading metalloprotease-1. *J Biol Chem* **274**, 25869-25876 (1999).

129   Gomes, P., Srinivas, S. P., Vereecke, J. & Himpens, B. ATP-dependent paracrine intercellular communication in cultured bovine corneal endothelial cells. *Investigative ophthalmology & visual science* **46**, 104-113, doi:10.1167/iovs.04-0846 (2005).

130   Chifflet, S., Hernández, J. A. & Grasso, S. A possible role for membrane depolarization in epithelial wound healing. *American journal of physiology. Cell physiology* **288**, 30, doi:10.1152/ajpcell.00259.2004 (2005).

131   Hansen, M., Boitano, S. & Dirksen, E. R. Intercellular calcium signaling induced by extracellular adenosine 5′-triphosphate and mechanical stimulation in airway epithelial cells. *Journal of Cell …* (1993).

132   Berra-Romani, R. *et al.* Ca2+ signaling in injured in situ endothelium of rat aorta. *Cell calcium* **44**, 298-309, doi:10.1016/j.ceca.2007.12.007 (2008).

133   Enyedi, B., Jelcic, M. & Niethammer, P. The cell nucleus serves as a mechanotransducer of tissue damage-induced inflammation. *Cell* (2016).

134   Berridge, M. J. Elementary and global aspects of calcium signalling. *The Journal of physiology*, doi:10.1113/jphysiol.1997.sp021927 (1997).

135   Berridge, M. J., Lipp, P. & Bootman, M. D. The versatility and universality of calcium signalling. *Nat Rev Mol Cell Biol* **1**, 11-21, doi:10.1038/35036035 (2000).

136   Xu, S. & Chisholm, A. D. C. elegans epidermal wounding induces a mitochondrial ROS burst that promotes wound repair. *Developmental cell* **31**, 48-60, doi:10.1016/j.devcel.2014.08.002 (2014).

137   Gustavsson, N., Wu, B. & Han, W. Calcium sensing in exocytosis. *Advances in experimental medicine and biology* **740**, 731-757, doi:10.1007/978-94-007-2888-2_32 (2012).

138   Penuela, S., Gehi, R. & Laird, D. W. The biochemistry and function of pannexin channels. *Biochim Biophys Acta* **1828**, 15-22, doi:10.1016/j.bbamem.2012.01.017 (2013).

139   Bosch, M., Serras, F., Martín-Blanco, E. & Baguñà, J. JNK signaling pathway required for wound healing in regenerating Drosophila wing imaginal discs. *Developmental biology* (2005).

140   Losick, V. P., Jun, A. S. & Spradling, A. C. Wound-Induced Polyploidization: Regulation by Hippo and JNK Signaling and Conservation in Mammals. *PloS one* **11**, doi:10.1371/journal.pone.0151251 (2016).

141   Prevarskaya, N., Skryma, R. & Shuba, Y. Calcium in tumour metastasis: new roles for known actors. *Nat Rev Cancer* **11**, 609-618, doi:10.1038/nrc3105 (2011).

142   Wei, C., Wang, X., Zheng, M. & Cheng, H. Calcium gradients underlying cell migration. *Curr Opin Cell Biol* **24**, 254-261, doi:10.1016/j.ceb.2011.12.002 (2012).

143   Kass, G. E. & Orrenius, S. Calcium signaling and cytotoxicity. *Environ Health Perspect* **107 Suppl 1**, 25-35 (1999).

144   Jewell, S. A., Bellomo, G., Thor, H., Orrenius, S. & Smith, M. Bleb formation in hepatocytes during drug metabolism is caused by disturbances in thiol and calcium ion homeostasis. *Science* **217**, 1257-1259 (1982).

145   Orrenius, S., Burkitt, M. J., Kass, G. E., Dypbukt, J. M. & Nicotera, P. Calcium ions and oxidative cell injury. *Ann Neurol* **32 Suppl**, S33-42 (1992).

146   Trump, B. F. & Berezesky, I. K. The role of altered [Ca2+]i regulation in apoptosis, oncosis, and necrosis. *Biochim Biophys Acta* **1313**, 173-178 (1996).

147   Gomes, P., Srinivas, S. P., Van Driessche, W., Vereecke, J. & Himpens, B. ATP release through connexin hemichannels in corneal endothelial cells. *Investigative ophthalmology & visual science* **46**, 1208-1218, doi:10.1167/iovs.04-1181 (2005).

148   Sherwood, C. L., Lantz, R. C., Burgess, J. L. & Boitano, S. Arsenic alters ATP-dependent Ca²+ signaling in human airway epithelial cell wound response. *Toxicological sciences : an official journal of the Society of Toxicology* **121**, 191-206, doi:10.1093/toxsci/kfr044 (2011).

149   Ljubimov, A. V. & Saghizadeh, M. Progress in corneal wound healing. *Progress in Retinal and Eye Research* **49**, 17-45, doi:10.1016/j.preteyeres.2015.07.002 (2015).

150   Adams, D. S., Masi, A. & Levin, M. H+ pump-dependent changes in membrane voltage are an early mechanism necessary and sufficient to induce Xenopus tail regeneration. *Development (Cambridge, England)* **134**, 1323-1335, doi:10.1242/dev.02812 (2007).

151   Baroja-Mazo, A. & Barberà-Cremades, M. The participation of plasma membrane hemichannels to purinergic signaling. *Biochimica et Biophysica …* (2013).

152   Zimmermann, B. The mechanism mediating regenerative intercellular Ca2+ waves in the blowfly salivary gland. *The EMBO Journal* **18**, 3222-3231, doi:10.1093/emboj/18.12.3222 (1999).

153   Zimmermann, H. & Braun, N. Extracellular metabolism of nucleotides in the nervous system. *Autonomic and Autacoid …*, doi:10.1111/j.1474-8673.1996.tb00062.x (1996).

154   Lu, D. & Insel, P. A. Hydrolysis of extracellular ATP by ectonucleoside triphosphate diphosphohydrolase (ENTPD) establishes the set point for fibrotic activity of cardiac fibroblasts. *Journal of Biological Chemistry*, doi:10.1074/jbc.M113.466102 (2013).

155   Liu, G. J., Kalous, A., Werry, E. L. & Bennett, M. R. Purine release from spinal cord microglia after elevation of calcium by glutamate. *Molecular pharmacology*, doi:10.1124/mol.105.021436 (2006).

156   Gruenhagen, J. A. & Yeung, E. S. Investigation of G protein-initiated, Ca2+-dependent release of ATP from endothelial cells. *Biochimica et biophysica acta* **1693**, 135-146, doi:10.1016/j.bbamcr.2004.06.004 (2004).

157   Pelham, R. J., Jr. & Wang, Y. Cell locomotion and focal adhesions are regulated by substrate flexibility. *Proc Natl Acad Sci U S A* **94**, 13661-13665 (1997).

158   Guilluy, C. *et al.* Isolated nuclei adapt to force and reveal a mechanotransduction pathway in the nucleus. *Nat Cell Biol* **16**, 376-381, doi:10.1038/ncb2927 (2014).

159   Swift, J. *et al.* Nuclear lamin-A scales with tissue stiffness and enhances matrix-directed differentiation. *Science* **341**, 1240104, doi:10.1126/science.1240104 (2013).

160   Lynch, H. *et al.* Cellular mechanics of germ band retraction in Drosophila. *Developmental biology* **384**, doi:10.1016/j.ydbio.2013.10.005.

161   Liang, X. *et al.* A NOMPC-dependent membrane-microtubule connector is a candidate for the gating spring in fly mechanoreceptors. *Curr Biol* **23**, 755-763, doi:10.1016/j.cub.2013.03.065 (2013).

162   Chubinskiy-Nadezhdin, V. I., Negulyaev, Y. A. & Morachevskaya, E. A. Functional coupling of ion channels in cellular mechanotransduction. *Biochemical and biophysical research communications* **451**, 421-424, doi:10.1016/j.bbrc.2014.07.131 (2014).

163   Ranade, S. S., Syeda, R. & Patapoutian, A. Mechanically Activated Ion Channels. *Neuron* **87**, 1162-1179, doi:10.1016/j.neuron.2015.08.032 (2015).

164   Sethi, K., Cram, E. J. & Zaidel-Bar, R. in *Stretch-induced actomyosin contraction in epithelial tubes: Mechanotransduction pathways for tubular homeostasis.* (Elsevier).

165   Bae, Y. *et al.* A FAK-Cas-Rac-Lamellipodin Signaling Module Transduces Extracellular Matrix Stiffness into Mechanosensitive Cell Cycling. *Science Signaling* **7**, doi:10.1126/scisignal.2004838.

166   Case, L. B. & Waterman, C. M. Integration of actin dynamics and cell adhesion by a three-dimensional, mechanosensitive molecular clutch. *Nature cell biology* **17**, 955-963, doi:10.1038/ncb3191 (2015).

167   Kenny, F. N. & Connelly, J. T. Integrin-mediated adhesion and mechano-sensing in cutaneous wound healing. *Cell and Tissue Research* (2014).

168   Fiore, V. F. *et al.* Conformational coupling of integrin and Thy-1 regulates Fyn priming and fibroblast mechanotransduction. *The Journal of cell biology* **211**, 173-190, doi:10.1083/jcb.201505007 (2015).

169   Takada, H., Furuya, K. & Sokabe, M. Mechanosensitive ATP release from hemichannels and Ca^{2+} influx through TRPC6 accelerate wound closure in keratinocytes. *Journal of cell science* **127**, 4159-4171, doi:10.1242/jcs.147314 (2014).

170   Maroto, R. & Hamill, O. P. Brefeldin A Block of Integrin-dependent Mechanosensitive ATP Release from Xenopus Oocytes Reveals a Novel Mechanism of Mechanotransduction. *Journal of Biological Chemistry* **276**, 23867-23872, doi:10.1074/jbc.M101500200 (2001).

171   Kim, T.-J. *et al.* Distinct mechanisms regulating mechanical force-induced Ca2+ signals at the plasma membrane and the ER in human MSCs. *eLife*, doi:10.7554/elife.04876 (2015).

172   Mason, F. M., Tworoger, M. & Martin, A. C. Apical domain polarization localizes actin-myosin activity to drive ratchet-like apical constriction. *Nat Cell Biol* **15**, 926-936, doi:10.1038/ncb2796 (2013).

173   Bansal, D. *et al.* Defective membrane repair in dysferlin-deficient muscular dystrophy. *Nature* **423**, 168-172, doi:10.1038/nature01573 (2003).

174   McNeil, P. L. & Steinhardt, R. A. Loss, restoration, and maintenance of plasma membrane integrity. *The Journal of cell biology* **137**, 1-4 (1997).

175   Draeger, A., Monastyrskaya, K. & Babiychuk, E. B. Plasma membrane repair and cellular damage control: the annexin survival kit. *Biochem Pharmacol* **81**, 703-712, doi:10.1016/j.bcp.2010.12.027 (2011).

176   Compton, J. L., Hellman, A. N. & Venugopalan, V. Hydrodynamic determinants of cell necrosis and molecular delivery produced by pulsed laser microbeam irradiation of adherent cells. *Biophysical journal* **105**, 2221-2231, doi:10.1016/j.bpj.2013.09.027 (2013).

177   Hellman, A. N., Rau, K. R., Yoon, H. H. & Venugopalan, V. Biophysical Response to Pulsed Laser Microbeam-Induced Cell Lysis and Molecular Delivery. *Journal of Biophotonics* **1**, 24-35, doi:10.1002/jbio.200710010 (2008).

178   Venugopalan, V., Guerra, A., Nahen, K. & Vogel, A. Role of Laser-Induced Plasma Formation in Pulsed Cellular Microsurgery and Micromanipulation. *Physical Review Letters* **88**, doi:10.1103/PhysRevLett.88.078103 (2002).

179   Shapiro, M. G., Homma, K., Villarreal, S., Richter, C. P. & Bezanilla, F. Infrared light excites cells by changing their electrical capacitance. *Nat Commun* **3**, 736, doi:10.1038/ncomms1742 (2012).

180   Cayce, J. M. *et al.* Infrared neural stimulation of primary visual cortex in non-human primates. *Neuroimage* **84**, 181-190, doi:10.1016/j.neuroimage.2013.08.040 (2014).

181   Wells, J. *et al.* Biophysical mechanisms of transient optical stimulation of peripheral nerve.

Biophys J **93**, 2567-2580, doi:10.1529/biophysj.107.104786 (2007).

182   Jaiswal, J. K. *et al.* S100A11 is required for efficient plasma membrane repair and survival of invasive cancer cells. *Nature communications* **5**, 3795, doi:10.1038/ncomms4795 (2014).

183   Cheng, X., Zhang, X., Yu, L. & Xu, H. Calcium signaling in membrane repair. *Seminars in cell & developmental biology* **45**, 24-31, doi:10.1016/j.semcdb.2015.10.031 (2015).

184   McNeil, P. L., Miyake, K. & Vogel, S. S. The endomembrane requirement for cell surface repair. *Proceedings of the National Academy of Sciences of the United States of America* **100**, 4592-4597, doi:10.1073/pnas.0736739100 (2003).

185   McNeil, P. L. & Steinhardt, R. A. Plasma membrane disruption: repair, prevention, adaptation. *Annual review of cell and …*, doi:10.1146/annurev.cellbio.19.111301.140101 (2003).

186   McNeil, P. L. & Terasaki, M. Coping with the inevitable: how cells repair a torn surface membrane. *Nature cell biology* **3**, 9, doi:10.1038/35074652 (2001).

187   McNeil, P. L. & Ito, S. Gastrointestinal cell plasma membrane wounding and resealing in vivo. *Gastroenterology* (1989).

188   McNeil, P. L. & Ito, S. Molecular traffic through plasma membrane disruptions of cells in vivo. *Journal of cell science* (1990).

189   Vogel, A., Busch, S. & Parlitz, U. Shock wave emission and cavitation bubble generation by picosecond and nanosecond optical breakdown in water. *The Journal of the Acoustical Society …*, doi:10.1121/1.415878 (1996).

190   Tsukamoto, A. *et al.* Stable cavitation induces increased cytoplasmic calcium in L929 fibroblasts exposed to 1-MHz pulsed ultrasound. *Ultrasonics* **51**, 982-990, doi:10.1016/j.ultras.2011.05.014 (2011).

191   Fan, Z., Kumon, R. E., Park, J. & Deng, C. X. Intracellular delivery and calcium transients generated in sonoporation facilitated by microbubbles. *Journal of controlled release : official journal of the Controlled Release Society* **142**, 31-39, doi:10.1016/j.jconrel.2009.09.031 (2010).

192   Kumon, R. E., Aehle, M., Sabens, D. & Parikh, P. Ultrasound-induced calcium oscillations and waves in Chinese hamster ovary cells in the presence of microbubbles. *Biophysical journal* (2007).

193   Juffermans, L. J. M. & Dijkmans, P. A. Transient permeabilization of cell membranes by ultrasound-exposed microbubbles is related to formation of hydrogen peroxide. *American Journal of …*, doi:10.1152/ajpheart.01120.2005 (2006).

194   Stevenson, D. J. & Gunn-Moore, F. J. Single cell optical transfection. *… Society Interface* (2010).

195   Stracke, F., Rieman, I. & König, K. Optical nanoinjection of macromolecules into vital cells. *Journal of Photochemistry and Photobiology …* (2005).

196   Clark, I. B., Hanania, E. G. & Stevens, J. Optoinjection for efficient targeted delivery of a broad range of compounds and macromolecules into diverse cell types. *Journal of …*, doi:10.1117/1.2168148 (2006).

197   Rhodes, K., Clark, I., Zatcoff, M., Eustaquio, T. & Hoyte, K. L. Cellular laserfection. *Methods in cell …* (2007).

198   Baumgart, J., Bintig, W. & Ngezahayo, A. Fs-laser-induced Ca 2+ concentration change during membrane perforation for cell transfection. *Optics …* (2010).

199   Tao, W., Wilkinson, J. & Stanbridge, E. J. Direct gene transfer into human cultured cells facilitated by laser micropuncture of the cell membrane. *Proceedings of the …* (1987).

200   Michelangeli, F. & East, J. M. A diversity of SERCA Ca2+ pump inhibitors. *Biochem Soc Trans* **39**, 789-797, doi:10.1042/BST0390789 (2011).

201   Blaustein, M. P. & Golovina, V. A. Structural complexity and functional diversity of endoplasmic reticulum Ca(2+) stores. *Trends Neurosci* **24**, 602-608 (2001).

202   Streb, H., Irvine, R. F., Berridge, M. J. & Schulz, I. Release of Ca2+ from a nonmitochondrial intracellular store in pancreatic acinar cells by inositol-1,4,5-trisphosphate. *Nature* **306**, 67-69 (1983).

203   Hagar, R. E., Burgstahler, A. D., Nathanson, M. H. & Ehrlich, B. E. Type III InsP3 receptor channel stays open in the presence of increased calcium. *Nature* **396**, 81-84, doi:10.1038/23954 (1998).

204   Mak, D. O., McBride, S. & Foskett, J. K. Inositol 1,4,5-trisphosphate [correction of tris-phosphate] activation of inositol trisphosphate [correction of tris-phosphate] receptor Ca2+ channel by ligand tuning of Ca2+ inhibition. *Proc Natl Acad Sci U S A* **95**, 15821-15825 (1998).

205   Foskett, J. K., White, C., Cheung, K. H. & Mak, D. O. Inositol trisphosphate receptor Ca2+ release channels. *Physiol Rev* **87**, 593-658, doi:10.1152/physrev.00035.2006 (2007).

206   Iino, M. Molecular basis of spatio-temporal dynamics in inositol 1,4,5-trisphosphate-mediated Ca2+ signalling. *Jpn J Pharmacol* **82**, 15-20 (2000).

207   Van Petegem, F. Ryanodine receptors: structure and function. *J Biol Chem* **287**, 31624-31632, doi:10.1074/jbc.R112.349068 (2012).

208   Smith, J. S., Coronado, R. & Meissner, G. Single channel measurements of the calcium release channel from skeletal muscle sarcoplasmic reticulum. Activation by Ca2+ and ATP and modulation by Mg2+. *J Gen Physiol* **88**, 573-588 (1986).

209   Fry, T., Evans, J. H. & Sanderson, M. J. Propagation of intercellular calcium waves in C6 glioma cells transfected with connexins 43 or 32. *Microsc Res Tech* **52**, 289-300, doi:10.1002/1097-0029(20010201)52:3<289::AID-JEMT1014>3.0.CO;2-0 (2001).

210   Thore, S., Dyachok, O., Gylfe, E. & Tengholm, A. Feedback activation of phospholipase C via intracellular mobilization and store-operated influx of Ca2+ in insulin-secreting beta-cells. *J Cell Sci* **118**, 4463-4471, doi:10.1242/jcs.02577 (2005).

211   Ryan, M. J., Gross, K. W. & Hajduczok, G. Calcium-dependent activation of phospholipase C by mechanical distension in renin-expressing As4.1 cells. *Am J Physiol Endocrinol Metab* **279**, E823-829 (2000).

212   Derler, I., Jardin, I. & Romanin, C. Molecular mechanisms of STIM/Orai communication. *Am J Physiol Cell Physiol* **310**, C643-662, doi:10.1152/ajpcell.00007.2016 (2016).

213   Abreu-Blanco, M. T., Verboon, J. M., Liu, R., Watts, J. J. & Parkhurst, S. M. Drosophila embryos close epithelial wounds using a combination of cellular protrusions and an actomyosin purse string. *Journal of cell science* **125**, 5984-5997, doi:10.1242/jcs.109066 (2012).

214   Matsubayashi, Y. & Millard, T. H. Analysis of the Molecular Mechanisms of Reepithelialization in Drosophila Embryos. *Advances in Wound Care*, doi:10.1089/wound.2014.0549 (2014).

215   Colombelli, J., Reynaud, E. G., Rietdorf, J., Pepperkok, R. & Stelzer, E. In vivo Selective Cytoskeleton Dynamics Quantification in Interphase Cells Induced by Pulsed Ultraviolet Laser Nanosurgery. *Traffic* **6**, 1093-1102, doi:10.1111/j.1600-0854.2005.00334.x (2005).

216   Khodjakov, A., Cole, R. W., Oakley, B. R. & Rieder, C. L. Centrosome-independent mitotic spindle formation in vertebrates. *Current Biology* (2000).

217   Abreu-Blanco, M. T., Verboon, J. M. & Parkhurst, S. M. Cell wound repair in Drosophila occurs through three distinct phases of membrane and cytoskeletal remodeling. *The Journal of cell biology* **193**, 455-464, doi:10.1083/jcb.201011018 (2011).

218   Greulich, K. O. *et al.* Micromanipulation by laser microbeam and optical tweezers: from plant cells to single molecules. *Journal of Microscopy* **198**, 182-187, doi:10.1046/j.1365-2818.2000.00698.x (2000).

219   Berns, M. W., Wright, W. H. & Steubing, R. Laser microbeam as a tool in cell biology. *International review of cytology* **129**, 1-44 (1991).

220   Vogel, A. Nonlinear absorption: intraocular microsurgery and laser lithotripsy. *Physics in*

medicine and biology (1997).

221 Hutson, S. M. & Ma, X. Plasma and Cavitation Dynamics during Pulsed Laser Microsurgeryin vivo. *Physical Review Letters* **99**, doi:10.1103/PhysRevLett.99.158104 (2007).

222 Rau, K. R., Quinto-Su, P. A., Hellman, A. N. & Venugopalan, V. Pulsed laser microbeam-induced cell lysis: time-resolved imaging and analysis of hydrodynamic effects. *Biophysical journal* **91**, 317-329, doi:10.1529/biophysj.105.079921 (2006).

223 Tian, L. *et al.* Imaging neural activity in worms, flies and mice with improved GCaMP calcium indicators. *Nature methods* **6**, 875-881, doi:10.1038/nmeth.1398 (2009).

224 Ding, J., Luo, A., Hu, L., Wang, D. & Shao, F. Structural basis of the ultrasensitive calcium indicator GCaMP6. *Science China Life Sciences* **57**, doi:10.1007/s11427-013-4599-5.

225 Chen, T.-W. *et al.* Ultrasensitive fluorescent proteins for imaging neuronal activity. *Nature* **499**, doi:10.1038/nature12354.

226 Allbritton, N. L., Meyer, T. & Stryer, L. Range of messenger action of calcium ion and inositol 1,4,5-trisphosphate. *Science (New York, N.Y.)* **258**, 1812-1815 (1992).

227 Dijkink, R. *et al.* Controlled cavitation-cell interaction: trans-membrane transport and viability studies. *Physics in medicine and biology* **53**, 375-390, doi:10.1088/0031-9155/53/2/006 (2008).

228 Yuan, F., Yang, C. & Zhong, P. Cell membrane deformation and bioeffects produced by tandem bubble-induced jetting flow. *Proceedings of the National Academy of Sciences of the United States of America* **112**, 47, doi:10.1073/pnas.1518679112 (2015).

229 Wright, S. H. Generation of resting membrane potential. *Advances in Physiology Education*, doi:10.1152/advan.00029.2004 (2004).

230 Cao, G. *et al.* Genetically Targeted Optical Electrophysiology in Intact Neural Circuits. *Cell* **154**, 904-913, doi:10.1016/j.cell.2013.07.027 (2013).

231 Jin, L. *et al.* Single action potentials and subthreshold electrical events imaged in neurons with a fluorescent protein voltage probe. *Neuron* **75**, 779-785, doi:10.1016/j.neuron.2012.06.040 (2012).

232 Davenport, N. R., Sonnemann, K. J., Eliceiri, K. W. & Bement, W. M. Membrane dynamics during cellular wound repair. *Molecular biology of the cell* **27**, 2272-2285, doi:10.1091/mbc.E16-04-0223 (2016).

233 Li, X. *et al.* Cell membrane damage is involved in the impaired survival of bone marrow stem cells by oxidized low-density lipoprotein. *J Cell Mol Med* **18**, 2445-2453, doi:10.1111/jcmm.12424 (2014).

234 Escoffre, J. M. *et al.* Membrane disorder and phospholipid scrambling in electropermeabilized and viable cells. *Biochim Biophys Acta* **1838**, 1701-1709, doi:10.1016/j.bbamem.2014.02.013 (2014).

235 McDade, J. R., Archambeau, A. & Michele, D. E. Rapid actin-cytoskeleton-dependent recruitment of plasma membrane-derived dysferlin at wounds is critical for muscle membrane repair. *FASEB J* **28**, 3660-3670, doi:10.1096/fj.14-250191 (2014).

236 Thompson, G. L., Roth, C. C., Dalzell, D. R., Kuipers, M. & Ibey, B. L. Calcium influx affects intracellular transport and membrane repair following nanosecond pulsed electric field exposure. *J Biomed Opt* **19**, 055005, doi:10.1117/1.JBO.19.5.055005 (2014).

237 Defour, A., Sreetama, S. C. & Jaiswal, J. K. Imaging cell membrane injury and subcellular processes involved in repair. *J Vis Exp*, doi:10.3791/51106 (2014).

238 Clementi, E. A., Marks, L. R., Roche-Hakansson, H. & Hakansson, A. P. Monitoring changes in membrane polarity, membrane integrity, and intracellular ion concentrations in Streptococcus pneumoniae using fluorescent dyes. *J Vis Exp*, e51008, doi:10.3791/51008 (2014).

239 Cheng, J. P. *et al.* Caveolae protect endothelial cells from membrane rupture during increased cardiac output. *J Cell Biol* **211**, 53-61, doi:10.1083/jcb.201504042 (2015).

240   Corrotte, M., Castro-Gomes, T., Koushik, A. B. & Andrews, N. W. Approaches for plasma membrane wounding and assessment of lysosome-mediated repair responses. *Methods Cell Biol* **126**, 139-158, doi:10.1016/bs.mcb.2014.11.009 (2015).

241   Marquez-Curtis, L. A., Sultani, A. B., McGann, L. E. & Elliott, J. A. Beyond membrane integrity: Assessing the functionality of human umbilical vein endothelial cells after cryopreservation. *Cryobiology* **72**, 183-190, doi:10.1016/j.cryobiol.2016.05.005 (2016).

242   Meyers, J. R. *et al.* Lighting up the senses: FM1-43 loading of sensory cells through nonselective ion channels. *J Neurosci* **23**, 4054-4065 (2003).

243   Li, D., Herault, K., Oheim, M. & Ropert, N. FM dyes enter via a store-operated calcium channel and modify calcium signaling of cultured astrocytes. *Proc Natl Acad Sci U S A* **106**, 21960-21965, doi:10.1073/pnas.0909109106 (2009).

244   Leybaert, L. & Sanderson, M. J. Intercellular Ca(2+) waves: mechanisms and function. *Physiol Rev* **92**, 1359-1392, doi:10.1152/physrev.00029.2011 (2012).

245   Compton, J. L., Luo, J. C., Ma, H., Botvinick, E. & Venugopalan, V. High-throughput optical screening of cellular mechanotransduction. *Nature Photonics* **8**, 710-715, doi:10.1038/nphoton.2014.165 (2014).

246   Minns, M. S., Teicher, G., Rich, C. B. & Trinkaus-Randall, V. Purinoreceptor P2X7 Regulation of Ca(2+) Mobilization and Cytoskeletal Rearrangement Is Required for Corneal Reepithelialization after Injury. *The American journal of pathology* **186**, 285-296, doi:10.1016/j.ajpath.2015.10.006 (2016).

247   Lesch, C., Jo, J., Wu, Y., Fish, G. S. & Galko, M. J. A Targeted UAS-RNAi Screen in Drosophila Larvae Identifies Wound Closure Genes Regulating Distinct Cellular Processes. *Genetics* **186**, 943-957, doi:10.1534/genetics.110.121822 (2010).

248   Kwon, Y.-C. C., Baek, S. H., Lee, H. & Choe, K.-M. M. Nonmuscle myosin II localization is regulated by JNK during Drosophila larval wound healing. *Biochemical and biophysical research communications* **393**, 656-661, doi:10.1016/j.bbrc.2010.02.047 (2010).

249   Rhodes, J. D. & Sanderson, J. The mechanisms of calcium homeostasis and signalling in the lens. *Exp Eye Res* **88**, 226-234, doi:10.1016/j.exer.2008.10.025 (2009).

250   Bauer, R. *et al.* Intercellular Communication: the Drosophila Innexin Multiprotein Family of Gap Junction Proteins. *Chemistry & Biology* **12**, 515-526, doi:10.1016/j.chembiol.2005.02.013 (2005).

251   Stebbings, L. A., Todman, M. G., Phelan, P., Bacon, J. P. & Davies, J. A. Two Drosophila innexins are expressed in overlapping domains and cooperate to form gap-junction channels. *Mol Biol Cell* **11**, 2459-2470 (2000).

252   Bond-Matthews, B. & Davidson, N. Transcription from each of the Drosophila act5C leader exons is driven by a separate functional promoter. *Gene* **62**, 289-300 (1988).

253   Chung, Y. T. & Keller, E. B. Regulatory elements mediating transcription from the Drosophila melanogaster actin 5C proximal promoter. *Mol Cell Biol* **10**, 206-216 (1990).

254   Usui-Aoki, K. *et al.* Targeted expression of Ip3 sponge and Ip3 dsRNA impaires sugar taste sensation in Drosophila. *Journal of neurogenetics* **19**, 123-141, doi:10.1080/01677060600569713 (2005).

255   Handly, N. L. & Wollman, R. Wound-induced Ca2+ wave propagates through a simple release and diffusion mechanism. *Molecular Biology of the Cell* **28**, 1457-1466, doi:10.1091/mbc.E16-10-0695 (2017).

256   Dolezelova, E., Nothacker, H.-P. P., Civelli, O., Bryant, P. J. & Zurovec, M. A Drosophila adenosine receptor activates cAMP and calcium signaling. *Insect biochemistry and molecular biology* **37**, 318-329, doi:10.1016/j.ibmb.2006.12.003 (2007).

257   Ishida, S., Matsu-Ura, T., Fukami, K., Michikawa, T. & Mikoshiba, K. Phospholipase C-β1 and β4 contribute to non-genetic cell-to-cell variability in histamine-induced calcium signals in HeLa cells. *PloS one* **9**, doi:10.1371/journal.pone.0086410 (2014).

258   Christo, S. N. & Diener, K. R. The functional contribution of calcium ion flux heterogeneity

in T cells. *Immunology and cell …* (2015).

259   Sveshnikova, A. N., Ataullakhanov, F. I. & Panteleev, M. A. Compartmentalized calcium signaling triggers subpopulation formation upon platelet activation through PAR1. *Molecular bioSystems* **11**, 1052-1060, doi:10.1039/c4mb00667d (2015).

260   Sahu, A., Ghosh, R., Deshpande, G. & Prasad, M. A Gap Junction Protein, Inx2, Modulates Calcium Flux to Specify Border Cell Fate during Drosophila oogenesis. *PLoS genetics* **13**, doi:10.1371/journal.pgen.1006542 (2017).

261   Webb, S. E. & Miller, A. L. Calcium signalling during zebrafish embryonic development. *Bioessays* **22**, 113-123, doi:10.1002/(SICI)1521-1878(200002)22:2<113::AID-BIES3>3.0.CO;2-L (2000).

262   Davis, F. M. *et al.* Induction of epithelial-mesenchymal transition (EMT) in breast cancer cells is calcium signal dependent. *Oncogene* **33**, 2307-2316, doi:10.1038/onc.2013.187 (2014).

263   Stewart, T. A., Azimi, I., Thompson, E. W., Roberts-Thomson, S. J. & Monteith, G. R. A role for calcium in the regulation of ATP-binding cassette, sub-family C, member 3 (ABCC3) gene expression in a model of epidermal growth factor-mediated breast cancer epithelial-mesenchymal transition. *Biochem Biophys Res Commun* **458**, 509-514, doi:10.1016/j.bbrc.2015.01.141 (2015).

264   Yang, S. & Huang, X. Y. Ca2+ influx through L-type Ca2+ channels controls the trailing tail contraction in growth factor-induced fibroblast cell migration. *J Biol Chem* **280**, 27130-27137, doi:10.1074/jbc.M501625200 (2005).

265   Howe, A. K. Cross-talk between calcium and protein kinase A in the regulation of cell migration. *Curr Opin Cell Biol* **23**, 554-561, doi:10.1016/j.ceb.2011.05.006 (2011).

266   Brundage, R. A., Fogarty, K. E., Tuft, R. A. & Fay, F. S. Calcium gradients underlying polarization and chemotaxis of eosinophils. *Science* **254**, 703-706 (1991).

267   Stewart, T. A., Yapa, K. T. & Monteith, G. R. Altered calcium signaling in cancer cells. *Biochim Biophys Acta* **1848**, 2502-2511, doi:10.1016/j.bbamem.2014.08.016 (2015).

268   Patton, A. M., Kassis, J., Doong, H. & Kohn, E. C. Calcium as a molecular target in angiogenesis. *Curr Pharm Des* **9**, 543-551 (2003).

269   Fiorio Pla, A., Avanzato, D., Munaron, L. & Ambudkar, I. S. Ion channels and transporters in cancer. 6. Vascularizing the tumor: TRP channels as molecular targets. *Am J Physiol Cell Physiol* **302**, C9-15, doi:10.1152/ajpcell.00280.2011 (2012).

270   Fristrom, J., Doctor, J., Fristrom, D., Logan, W. & Silvert, D. The formation of the pupal cuticle by Drosophila imaginal discs in vitro. *Developmental Biology* **91**, doi:10.1016/0012-1606(82)90040-9.

271   Rand, M. D. A method of permeabilization of Drosophila embryos for assays of small molecule activity. *Journal of visualized experiments : JoVE*, doi:10.3791/51634 (2014).

272   Rand, M. D., Kearney, A. L., Dao, J. & Clason, T. Permeabilization of Drosophila embryos for introduction of small molecules. *Insect Biochemistry and Molecular Biology* **40**, 792-804, doi:10.1016/j.ibmb.2010.07.007 (2010).

273   Smrcka, A. V. G protein betagamma subunits: central mediators of G protein-coupled receptor signaling. *Cell Mol Life Sci* **65**, 2191-2214, doi:10.1007/s00018-008-8006-5 (2008).

274   Logothetis, D. E., Kurachi, Y., Galper, J., Neer, E. J. & Clapham, D. E. The beta gamma subunits of GTP-binding proteins activate the muscarinic K+ channel in heart. *Nature* **325**, 321-326, doi:10.1038/325321a0 (1987).

275   Clapham, D. E. & Neer, E. J. G protein beta gamma subunits. *Annu Rev Pharmacol Toxicol* **37**, 167-203, doi:10.1146/annurev.pharmtox.37.1.167 (1997).

276   Wickman, K. D. *et al.* Recombinant G-protein beta gamma-subunits activate the muscarinic-gated atrial potassium channel. *Nature* **368**, 255-257, doi:10.1038/368255a0 (1994).

277   Popova, J. S. & Rasenick, M. M. G beta gamma mediates the interplay between tubulin dimers and microtubules in the modulation of Gq signaling. *J Biol Chem* **278**, 34299-34308, doi:10.1074/jbc.M301748200 (2003).

278   Roychowdhury, S. & Rasenick, M. M. G protein beta1gamma2 subunits promote microtubule assembly. *J Biol Chem* **272**, 31576-31581 (1997).

279   Niu, J., Profirovic, J., Pan, H., Vaiskunaite, R. & Voyno-Yasenetskaya, T. G Protein betagamma subunits stimulate p114RhoGEF, a guanine nucleotide exchange factor for RhoA and Rac1: regulation of cell shape and reactive oxygen species production. *Circ Res* **93**, 848-856, doi:10.1161/01.RES.0000097607.14733.0C (2003).

280   Marinari, E. *et al.* Live-cell delamination counterbalances epithelial growth to limit tissue overcrowding. *Nature* **484**, 542-545, doi:10.1038/nature10984 (2012).

281   Brodland, G. *et al.* CellFIT: a cellular force-inference toolkit using curvilinear cell boundaries. *PLOS ONE* **9**, doi:10.1371/journal.pone.0099116.

282   Veldhuis, N. A., Poole, D. P., Grace, M. & McIntyre, P. The G Protein–Coupled Receptor–Transient Receptor Potential Channel Axis: Molecular Insights for Targeting Disorders of Sensation and Inflammation. *Pharmacological …*, doi:10.1124/pr.114.009555 (2015).

283   Mudge, E. J. Recent accomplishments in wound healing. *Int Wound J* **12**, 4-9, doi:10.1111/iwj.12230 (2015).

284   Parra, V. & Rothermel, B. A. Calcineurin signaling in the heart: The importance of time and place. *Journal of molecular and cellular cardiology* **103**, 121-136 (2017).

285   Yao, J., Pilko, A. & Wollman, R. Distinct cellular states determine calcium signaling response. *Molecular systems biology* (2016).

286   Vasquez, C. G., Heissler, S. M., Billington, N., Sellers, J. R. & Martin, A. C. Drosophila non-muscle myosin II motor activity determines the rate of tissue folding. *Elife* **5**, doi:10.7554/eLife.20828 (2016).

287   Knight, M. M., Roberts, S. R. & Lee, D. A. Live cell imaging using confocal microscopy induces intracellular calcium transients and cell death. *American Journal of …*, doi:10.1152/ajpcell.00276.2002 (2003).

288   Chang, C.-T. *et al.* Oxidative stress disruption of receptor-mediated calcium signaling mechanisms. *Journal of biomedical science* **20**, doi:10.1186/1423-0127-20-48.

289   Gorlach, A., Bertram, K., Hudecova, S. & Krizanova, O. Calcium and ROS: A mutual interplay. *Redox Biol* **6**, 260-271, doi:10.1016/j.redox.2015.08.010 (2015).

290   Tabet, F., Savoia, C., Schiffrin, E. L. & Touyz, R. M. Differential calcium regulation by hydrogen peroxide and superoxide in vascular smooth muscle cells from spontaneously hypertensive rats. *J Cardiovasc Pharmacol* **44**, 200-208 (2004).